TU Delft

TU Delft EEMCS
Intelligent Electrical Power Grids

Frequency support of Non-Synchronous Generation in the Nordic Power System in 2030

N.A. van Wageningen

Frequency support of Non-Synchronous Generation in the Nordic Power System in 2030
Fast active power control of VSC-HVDC links and Fully Rated Converter Wind Turbines

Master Thesis
June, 2022

By
N.A. van Wageningen

Cover photo: Roan Wind Farm, Ole Martin Wold, 2018
Published by: TU Delft, Intelligent Electrical Power Grids, P.O. Box 5031, 2600 GA Delft, The Netherlands

Preface

This thesis is written in order to obtain the master degree Sustainable Energy Technology of the Delft University of Technology. The work presented in this thesis is a continuation on the model presented by Even Strand Aas in 2016 [1]. While writing this thesis I assumed the reader to have basic knowledge in modeling and computer aided scripting and simulation (under root mean square perspective) of power system dynamics.

I would like to thank my parents for their patience and support, Nina for her help during difficult conversations, and all my friends who contributed in coffee, spell check and advice.

N.A. van Wageningen
Delft, August 2022

Abstract

The Nordic Power System is developing in the next decade; more High Voltage Direct Current (HVDC) links are being built, and the Nordic countries are investing in Renewable Energy Source (RES) generation with the goal to work toward carbon net neutrality [2]. The increase in Non-Synchronous Generation (NSG) penetration, such as HVDC import and wind generation is expected to affect the frequency stability of the grid or the ability of the grid to stay within frequency limits after being subject to a disturbance.

Frequency stability is associated with the active power balance of a system due to electromechanical coupling and the predominance of synchronous generators used in conventional power plants (like hydro and thermal). The bulk of utility-scaled Non-Synchronous Generation is decoupled from the grid and does not contribute inertia and limited short circuit current to the grid. Therefore, power discrepancies lead to larger frequency deviations which unlike in the synchronous generator dominated system can happen in a shorter time frame. This aspect challenges the way primary frequency control shall react to quickly arrest high Rate of Change of Frequency (RoCoF) and maximum frequency deviation (MFD) values.

Limited short circuit currents lead to a diminished system strength, which means that the voltage will react more sensitive to disturbances. The control system of Voltage Source Converters, present in both type 4 wind turbines and VSC-HVDC links, relies on the ability of the Phase Lock Loop to track the voltage angle of the grid. In systems with low system strength, tracking the voltage angle by the Phase Lock Loop can be a problem.

NSG also offers possibilities for Fast Frequency Response (FFR) that work quicker and with lower droop values than the primary response of synchronous generation.

This thesis aims to investigate the change in frequency performance of the Nordic Power System in 2030 caused by the replacement of synchronous generation by NSG. To do this, the Nordic Power System is modeled in the simulation software DIgSILENT PowerFactory 2022 SP1 for modeling and simulation. For the Nordic Power system, periods of low demand and high penetration of wind-generated power and HVDC import are expected to have the lowest amount of inertia. An operational scenario of 60% NSG is therefore developed.

To find the critical disturbance in the Nordic Power System, each power supplying unit, that is the WT, VSC-HVDC links, and synchronous generations is subject to an outage event simulation. The critical disturbance is the outage of the HVDC link NSN2, which leads to a Maximum Frequency Deviation of 0.4 Hz and a RoCoF of 3 Hz in Feda. The MDF is within the limits set by the Nordic TSOs, but the RoCoF is higher than admissible.

The investigation into the critical disturbances also shows that the system voltage in the North of the Nordic Power System is sensitive to changes in the load. Voltage sensitivity can be described by the system strength. One way to quantify system strength is the Short Circuit Ratio at the point of common coupling for NSG. Finmmark has the lowest Short Circuit Ratio, which can be explained by the fact that it has high impedance because of long transmission lines, transformers, and proximity to other NSG.

Two FFR control blocks are added to the system: The Emulated Inertia (EI) control by ENERCON [3], is added to the Wind Turbines. The EI supplies active power to the grid when a frequency trigger is exceeded. The amount of extra power supplied to the grid is proportional to the frequency deviation. The Synthetic Inertia (SI) control is added to the VSC-HVDC links, which supplies active power inversely proportional to the RoCoF. The

abilities to mitigate large frequency deviations and large values of RoCoF of the two FFR blocks are evaluated for the critical disturbance of the outage of the NSN2 link. The worst frequency deviation is found in Feda.

Application of the EI control block of the Wind turbines leads to low improvement of the MFD. The EI control of the WTs acts only starts after the trigger frequency is reached, and reaches its maximum not directly. The EI mostly improves the frequency after 3 seconds, when the extra power supplied by the wind turbines increases the frequency compared to the case with no FFR support. The frequency at FED also reaches the quasi steady state quicker. The SI control of the VSC-HVDC links improves the MDF and the RoCoF. Unlike the EI control of the wind turbines, it acts instantaneously and supplies a large amount of active power at the beginning of the outage when the absolute value of RoCoF is highest. If only three VSC-HVDC links employ synthetic inertia, the value of RoCoF is decreased to admissible values. The SI control also dampens the frequency swings in the system.

Simulation results show that the two FFR control blocks complement each other. The EI blocks improve the recovery time and the overall frequency response whereas Synthetic Inertia decreases the MFD and the absolute RoCoF. Furthermore, if the NSG employing FFR is close to the critical node, the FFR has the best effect. This is because this node has low inertia, so SI will effectively mitigate high RoCof levels, whereas IE blocks are triggered quicker, and therefore supply power to parts of the grid where it is necessary.

Contents

Acronyms

The acronyms that have been used throughout this thesis are listed in alphabetical order:

SCADA	Supervisory Control And Data Acquisition
EMT	Electromagnetic Transients
ENTSO-E	European Network of Transmission System Operators of Electricity
FCR-D	Frequency Containment Reserve for Disturbances
FCR-N	Frequency Containment Reserve for Normal operation
FFR	Fast Frequency Response
FRTI	Frequency Recovery Time Index
HVDC	High Voltage Direct Current
IEEE	Institute of Electrical and Electronics Engineers
IGBT	Insulated Gate Bipolar Transistors
LCC	Line Commutated Converter
MFD	Maximum Frequency Deviation
MFDI	Maximum Frequency Deviation Index
NSG	Non-Synchronous Generation
PCC	Point of Common Coupling
PEI	Power Electronic Interfaced
PID	Proportional-Integral-Derivative
PLL	Phase Lock Loop
PSSSE	Power System Simulator for Engineering
PWM	Pulse Width Modulation
RES	Renewable Energy Source
RMS	Electromechanical Transients
RoCoF	Rate of Change of Frequency
SCMVA	Short Circuit Apparent Power
SCR	Short Circuit Ratio
TFDI	Total Frequency Deviation Index
TSO	Transmission System Operator
VSC	Voltage Source Converter
WT	Wind Turbine

1 Introduction

In November 2019, the prime ministers of the Nordic countries declared to work toward carbon net neutrality [2]. To achieve this, the Nordic countries are investing in Renewable Energy Source (RES) generation. Specifically, wind energy is expected to increase in the northern parts of Norway and Sweden in the next decade [4].

Another development is an increased use of High Voltage Direct Current (HVDC) links in the Nordic Power System. These links make it possible to trade more electricity with other countries in Europe. New links are being built which increases the capacity of the HVDC links to 18 GW in 2030 [1].

Both wind generation and HVDC imports are categorized as Non-Synchronous Generation (NSG) because they are decoupled from the grid. The replacement of synchronous generation by NSG decreases the inertia of the system. System inertia also varies over time and becomes more heterogeneous, i.e. with different inertia values in different areas [5]. For the Nordic Power system, periods of low demand and high penetration of wind generated power and HVDC import are expected to have the lowest amount of inertia. This could be the case at night during a dry hydrological year, with strong winds in Denmark and on the North Sea [6].

The inertia of the system is linked with its frequency performance, because of electromechanical coupling. For a sudden loss in load, generators will store the surplus of active power by accelerating the rotating masses. In case of a deficit of power, for example caused by an outage of a nearby generator, the rotors of the generators decelerate and this energy is supplied to the grid. This causes the frequency to change when the active power supply is not equal to the demand.

The decrease in inertia will have a considerable impact on the frequency quality and operational security. For example, there is a higher occurrence of maximum frequency deviations and high values of Rate of Change of Frequency. This is recognized by the Transmission System Operators (TSOs) of the Nordic countries as one of the main challenges leading towards 2025 [7]. However, the penetration of NSG is only expected to increase in the next decade. Therefore, there is an urgent need to investigate the impact of lower inertia in the Nordic Power System.

1.1 Research questions

The thesis aims to investigate the change in frequency performance of the Nordic Power System caused by the replacement of synchronous generation by non-synchronous generation.

Main question
To what extent will frequency performance of the Nordic Power System of 2030 be affected by Non-Synchronous Generation?

To answer the main question, a dynamic model of the Nordic Power System needs to be developed. This model should represent the power grid as expected in 2030.

Subquestion 1
What generic dynamic models can be used to represent the generators of the Nordic Power System in 2030? The models for the synchronous generators and the wind turbines

and HVDC links need to me modelled in time domain simulation models, using guidelines from the Institute of Electrical and Electronics Engineers (IEEE). Furthermore, the turbine requirements of the Nordic TSO's should be taken into account.

Subquestion 2
What are the critical disturbances in the Nordic Power System in 2030?

The frequency performance can be analyzed by evaluating the response of the generators to various disturbance events. Disturbance events include sudden load increases, and outage events of various elements. The weak points in the grid are identified.

Subquestion 3
How can Fast Frequency Response of Non-Synchronous Generation be used to improve the frequency performance?

The rapidly developing technology of NSG also offers possibilities. Voltage Source Converters (VSC) that connect NSG with the grid are able to rapidly change the power output and contribute to the frequency response of the system. This control system is defined as Fast Frequency Response (FFR).

1.2 Method

The study conducted is exploratory in nature. Its starting point is the model of the Nordic Power System of 2030 as it was developed by Even Strand Aas in 2016 [1]. First, the model of Aas is modified and upgraded. Second, the frequency performance of the system is inspected for multiple disturbance scenarios. Third, Fast Frequency Response (FFR) control blocks are added to the NSG in the system to evaluate the improvement of the frequency performance by FFR.

1. The base model is modified to include wind generation and to better represent the dynamic response of the system. An operational scenario of 60% NSG is developed. The model is then upgraded to include the dynamic models for two types of synchronous generators, wind turbines and VSC-HVDC links. For each dynamic model, initialisation and calibration of the tuning parameters is done.
2. To analyse the frequency performance of the model with 60% NSG, all potential generation outage events are simulated to find the critical disturbance. This is compared to the current dimensional incidents of the Nordic Power System.
3. The Fast Frequency Response (FFR) control blocks are evaluated for the capability to benefit the frequency response of the Nordic Grid to this critical disturbance. This includes a sensitivity analysis of the control parameters. The FFR control blocks are analyzed to determine how they affect the Maximum Frequency Deviation (MFD), the Rate of Change of Frequency (RoCoF), and the recovery time T_{rec}.

This study uses the simulation software PowerFactory 2021 by DIgSILENT 2022 SP1. For the dynamic simulations, RMS-simulations are used. Python version 3.8 is used to access and direct PowerFactory and for the acquisition of the loadflow and time domain data.

1.3 Assumptions and limitations

The Nordic Power System is presented as an aggregated model at transmission voltage; the demand and supply is summed at each node. This is a simplification of the grid and the model should therefore be used to investigate system-wide phenomena rather than specific local operations.

There are some limitations regarding RMS-simulation. There are two options for dynamic analysis in power systems; RMS and EMT dynamic studies. The RMS simulation uses a steady state phasor network model as a starting point. It is suitable for electromechanical, or mid-term to long-term transients [8]. EMT uses a dynamic model and is suited for electromagnetic, or short-term transients [8]. Because frequency stability issues are in the mid-term to long term-time frame, RMS simulation is used in this study. Part of the converter controls operates in a smaller time frame; for example the switching transients. Issues related to resonance stability and fast interaction, converter-driven stability are therefore out of scope of this study.

1.4 Thesis Outline

The report is presented in the following structure:

Chapter 2.1 starts with a theoretical background examination to get a better understanding on frequency stability. Chapter 2.2 continues with a general control of frequency in power systems. In chapter 2.3 the frequency control is specified for the Nordic Power System. The frequency response of HVDC-links is presented in chapters 2.4. Chapter 2.5 describes the frequency response of wind turbines. Since stability has changed with the introduction of NSG in the system, Section 2.6 focuses on the effect of NSG on power system stability.

Chapter 3 continues with an explanation of the development of the model, having in mind the first sub question. Chapter 3.1 starts with an introduction to the simulation software PowerFactory. Chapter 3.2 introduces the base model of [1]. Because each power plant type has a specific dynamic response, a distribution per power plant type is proposed in chapter 3.3. This results in an operational scenario of 60% NSG. The modifications to the base model to reach the 60% NSG are presented in chapter 3.4. Finally, the model of the Nordic Power Syste is subjected to a small frequency event in chapter 3.4 to confirm if the chapter shows typical frequency behaviour.

Chapter 4 continues with the subquestions ‘What are the critical disturbances in the Nordic Power System in 2030?’ and ‘How Non-Synchronous Generation can be used to improve the frequency performance?’. Chapter 4.1 presents the procedure and the findings of the critical disturbance development. Chapter 4.2 then presents a proposal for the FFR control blocks of the wind and VSC-HVDC links. In chapter 4.3 the parameters of the control blocks are optimized. Chapter 4.4 concludes with the results of the FFR blocks.

Chapter 5 lays out the lessons learned and provides conclusions. Section 5.1 answers the main question and subquestions. Section 5.2 closes with recommendations for further study.

2 Theoretical background related to frequency stability and control

In this chapter, the theoretical background on frequency stability and the response of the power system is described. First, frequency stability is introduced in section 2.1 as part of the power system stability. The definition of system inertia and its effect on the system frequency is described with the swing equation. Second, the response of a power system frequency is described in section 2.2. This includes the performance indicators of frequency response and the control structure of frequency response. The specific frequency control policy of the Nordic Power System is described in section 2.3. The frequency response of Non-Synchronous Generation (NSG) differs significantly from the response of synchronous machines, section 2.4 and section 2.5 provide the frequency response of HVDC and wind turbines respectively. Finally, the information from previous sections comes together in section 2.6, where the dynamics of a system with low inertia are explained.

2.1 Frequency stability, power balance and inertia

2.1.1 Frequency stability as part of power system stability

Power system stability is defined by Kundur as ”the ability of an electric power system, for a given initial operating condition to regain a state of operating equilibrium after being subject to a physical disturbance, with most system variables bounded so that practically the entire system remains intact”[26, p1388].

Stability is therefore a system property rather than a property of its components. A generator can lose synchronism with the rest of the system, and the system can find a new equilibrium state without this generator. In an unstable system, the loss of one component can have a detrimental, cascading, effect on the other components. The definition also specifies that stability is specific to a disturbance.

In order to analyse the different phenomena associated with system stability, The IEEE and CIGRE distinguished three different categories of stability; rotor angle stability, voltage stability and frequency stability in 2004 [9]. This division is based on the variable in which the instability problem is observed and the type of forces that react to the disturbance. There is also a distinction based on the time frame at which it occurs. In 2020 IEEE expanded this classification to take into account the development of Power Electronic Interfaced (PEI) generation in the power system [10]. Two more categories are added; resonance stability and converter driven stability. Furthermore, because of the speed of the control system and the switching of PEI generation, the time scale of the stability analysis is also enlarged to include electromagnetic phenomena [10].

Figure 2.1 shows the categorization of power system stability. What follows is a brief explanation of the different categories with a special interest in frequency stability.

- **Rotor angle instability** relates to whether the generators in a system stay in synchronism after a disturbance and is related to the opposing torques in each synchronous machine. Of influence is the power-rotor angle relationship of the system, which is nonlinear. After a disturbance, the speed of the individual machines differ from each other. Because of this, the difference between rotor angle will change. This results in a shift in the power flow between these machines. Up until a certain

point, this has a damping effect, and the difference in rotor angle is decreased by this power shift. Loss of synchronism occurs when the resulting electromechanic torque of a machine cannot be met with the torque in the stator resulting in a pole slip. As can be seen in the figure 2.1 rotor angle stability occurs in a short time frame.

- **Voltage stability** describes the ability of a system to remain within the voltage limits and is connected to load dynamics. It is unstable when the power requested by the loads can not be delivered by the system. It is a local problem but can have consequences for the the rest of the system.
- **Frequency stability** is associated with the active power balance of a system due to electro-mechanical coupling. A surplus of energy, e.g. a loss of a load, will be stored in the rotating masses of the generators, and to a lesser extent, in the masses of dynamic loads. As a result of this, the rotors of the machines and the frequency will accelerate. Generator and machines are protected against excessive levels of frequencies and will consequently shut down or trip resulting in load shedding or blackouts.
- **Resonance stability** is caused by resonance between series compensation and either the frequencies in the electrical components of a PEI (electrical) or the turbine of a synchronous generator (torsional) [10].
- **Converter driven stability** is the dynamic performance of PEI generation in the power system. The different control loops present in the converter have different time scales, which can interact with the electromechanical modes of the synchronous machines or the the electromagnetic transients of the passive electrical components. Instabilities can be characterized as fast in which case there are oscillations due to interaction with each other or the power system. Slow stability has to do with the strength of the system, and is exhibited in voltage problems.

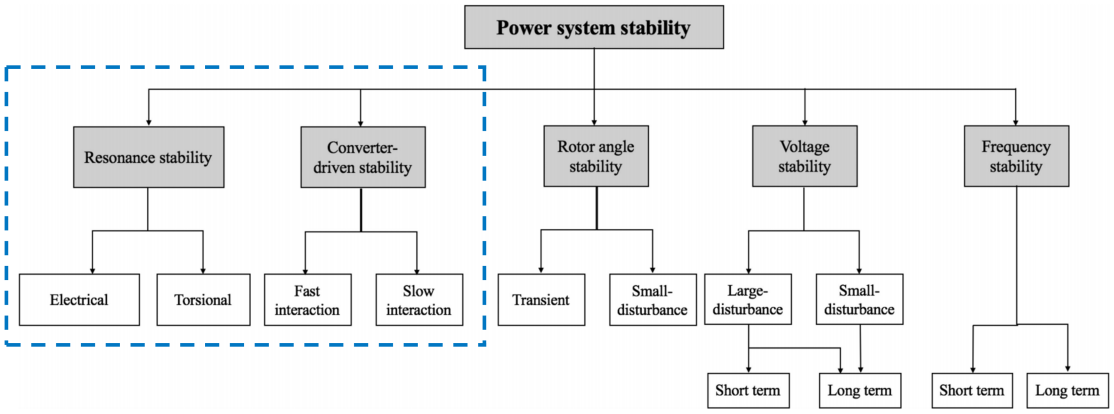

Figure 2.1: IEEE Power system stability classification by [9] in 2004 with the extension of [11] in 2020 outlined in blue

Note that instability problems can be difficult to categorize, as loss of stability in one class can lead to stability problems in other class. Rotor Angle instability, for example, leads to a loss of synchronism which leads to a voltage drop in adjoining busses [9].

2.1.2 Inertia and swing equation

For a single generator, the dynamics of power imbalance resulting in frequency change is known as the swing equation. Described by [12] and [13] , it defines the frequency

change caused by the difference of the electrical power of the load and the mechanical power of the rotor. The electro-magnetic torque (T_e [Nm]) can change rapidly after an disturbance. The mechanical torque of the rotor (T_r [Nm]) cannot . This results in an accelerating torque (T_a [Nm]) as seen in the swing equation (2.1);

$$\mathsf{J}\frac{d\omega_m}{dt} = T_r - T_e = T_a \tag{2.1}$$

With J [kg m^2] as the moment of inertia of the rotor and ω_m [rad/s] as the initial rotational mechanical velocity of the rotor. Multiplying with the rotor velocity gives:

$$\omega_m \mathsf{J}\frac{d\omega_m}{dt} = P_m - P_e \tag{2.2}$$

P_m [W] is the mechanical power and P_e [W] is the electrical (active) power. It is common practise to use the inertia constant H [s] in favour of the moment of inertia. The inertia constant is the stored energy at rated speed (ω_r [rad/s]) divided by the rated apparent power of the generator ($\mathsf{S_r}$ [VA]):

$$\mathsf{H} = \frac{\frac{1}{2}\mathsf{J}\omega_r}{\mathsf{S_r}} \tag{2.3}$$

Thus, the inertia constant signifies the resistance of a generator against a change of velocity proportional to its size. The inertia constant H is given in seconds and describes the duration for which the rotational masses can be used to supply their total rated power without mechanical input. Combining equation 2.2 and 2.3 gives:

$$2\mathsf{H}\frac{d\omega_m}{dt} = \frac{\omega_r(P_m - P_e)}{\omega_m \mathsf{S_r}} \tag{2.4}$$

With the assumption that the generator is initially operating at the rated speed, $\frac{\omega_r}{\omega_m} \approx 1$, the remaining equation is the normalized swing equation. Normalized units are presented with a bar given in per unit values [p.u.]:

$$2\mathsf{H}\frac{d\bar{\omega_m}}{dt} = \bar{P_m} - \bar{P_e} \tag{2.5}$$

Note that the system frequency relates proportionally to the rotor speed.The frequency at different machines is not uniform after a disturbance; proximity to the disturbance and system topology result in different electromechanical torques and different inertia will result in different individual rotor speed. In order to apply the swing equation of a single machine for a system, an aggregated swing model is used by [5]. For this purpose a Centre Of Inertia system frequency (f_{COI} [Hz]) is defined, a frequency to represent a system of n generators;

$$f_{COI} = \frac{\sum_{i=1}^{\mathsf{n}} \mathsf{H_i S_i} f_i}{\sum_{i=1}^{\mathsf{n}} \mathsf{H_i S_i}} \tag{2.6}$$

System inertia ($\mathsf{H_{sys}}$ [s]) is defined as the weighted average of the individual generators:

$$\mathsf{H_{sys}} = \frac{\sum_{i=1}^{\mathsf{n}} \mathsf{H_{iS_i}}}{\sum_{i=1}^{\mathsf{n}} \mathsf{S_i}} \tag{2.7}$$

To evaluate the frequency, F_{COI} can be used. An alternative is to evaluate all, or an arbitrary chosen frequencies.

2.2 Frequency control in the power system

Because of the relationship between frequency and active power balance, control of frequency stability is ultimately a process of keeping the generation and demand in balance. Control actions are taken continuously to ensure a good active power balance in the system. Control is done locally at the machines and centrally by the Automatic Generation Control (AGC) [13], which adjusts the power output of the individual generators. Because power consumption and RES generation are not fully predictable, small power unbalances occur regularly. The power system perceives this as noise in the frequency. To reduce wear and tear of the turbine vaults, synchronous machines may operate with a deadband. The frequency control strategy consists of three stages, with ascending time frames [13];

1. **Primary control**
   The first control system to react to the deviation of frequency is done at distributed, local components of the power system. For synchronous machines the governors of the individual turbines engage in frequency control. The generators and, to a lesser extent, the loads will adjust their power output proportional to the change in frequency. The applicable control parameter is the droop (R) of the governor, which is the inverse of the power gain per frequency difference;

   $$\mathrm{R} = \frac{\Delta f}{\Delta \mathrm{P}}$$

   All individual turbines have different values for R. For a system, the effect of these different values for R can be summed up. The time frame of the primary control depends on the switching valves of the turbines and is usually provided within a few seconds. The primary response after a considerable power imbalance will not result in a steady state at nominal frequency. Instead, a new quasi steady state will form with a deviation from the situation prior to the fault.

2. **Secondary control** The system can not return to the initial frequency without a centralized control system. This is the function of the secondary control and is carried out by the Automatic Generation Control (AGC). It will do so by sending new reference values for power and thus frequency to the different generating units.

3. **Tertiary control** After retaining the correct frequency in the secondary control, the AGC will find the most economic dispatch, and sends these to the generation turbines.

To evaluate the performance of a power system, performance indicators are used. A typical frequency response of a generator (*i*) after a disturbance can be seen in figure 2.2.

In this case, there is deficit of electrical power, resulting in under-frequencies. The system starts at *nominal frequency* ($\mathrm{f_{nom}}$). Directly after the disturbance, the frequency decelerates. This is the inertial, or *natural response* of the system. This value of *Rate of Change of Frequency* (*df/dt*) is abbreviated to RoCoF. The frequency will decrease until *primary control* of the generators start after response time. The control systems of the generator supply power to the grid to make up for the deficit. The Maximum Frequency Deviation ($|\Delta \mathrm{f_{i,max}}|$) is reached. The Maximum Frequency Deviation (MFD) results in an under- frequency which is defined as the *Nadir* or an over- frequency defined as the *Zenith*. The frequency reaches a value that is below the prefault frequency in a quasi steady state. The different between the prefault, nominal frequency and the recovery frequency is the frequency recovery deviation ($\Delta \mathrm{f_{i,\,rec}}$). The time that is needed to reach the quasi steady

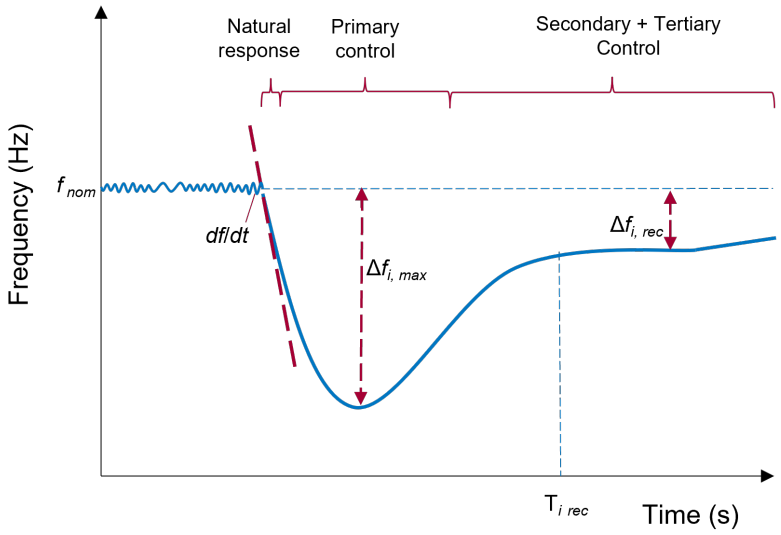

Figure 2.2: Typical generator frequency response after a disturbance with performance indicators

state is the recovery time ($T_{i,\,rec}$) of generator *i*. The MFD is typically reached between 5 and 10 seconds, whereas $T_{i,\,rec}$ is in the order of 20-30 seconds [14]

A number of factors are know to determine the size of the MFD. These are the magnitude of the power disturbance, the amount of inertia in the power system and the response time and effectiveness of the primary control [6]. As the maximum RoCoF transpires at the beginning of a frequency response, RoCoF depends only on the amount of inertia and the size of the disturbance. $\Delta f_{i,\,rec}$ is influenced by the size of the disturbance, the droop of the governors and the frequency characteristic of the loads [15]. The European Network of Transmission System Operators for Electricity (ENTSO-E) defines maximum admissible values for RoCoF, MFD and the recovery time. Furthermore, the nominal operating band for which the frequency is considered to be recovered is also defined. For the Nordic Power System, these values can be found in section 2.3.

Frequency performance indices can be calculated to assess the frequency response of a generator. The Maximum Frequency Deviation Index (MFDI), Total Frequency Deviation Index (TFDI) and the Frequency Recovery Time Index (FRTI) are presented in equations 2.8, 2.9 and 2.10:

$$\text{MFDI} = \min\left\{1, \max\left(\frac{|\Delta f_{i,max}|}{\Delta f_{max,adm}}\right)\right\} \tag{2.8}$$

$$\text{TFDI} = \min\left\{1, \max\left(\frac{\int_0^{T_s} |\Delta f_i(t)|dt}{\Delta f_{max,adm} \cdot T_s}\right)\right\} \tag{2.9}$$

$$\text{FRTI} = \min\left\{1, \max\left(\frac{T_{i,\,rec}}{T_{rec,\,adm}}\right)\right\} \tag{2.10}$$

With $\Delta f_{max,\,adm}$ as the maximum admissible frequency deviation, T_s as the total simulation time and $T_{rec,\,adm}$ as the maximum admissible recovery time. The indices evaluate the frequency compared to the maximum admissible limits, with 0 being far from the limits, and 1 having crossed the limits.

2.3 Frequency containment policy in the Nordic Power System

2.3.1 Frequency quality target parameters and control requirements

The primary response in the Nordic grid is defined as Frequency Containment and is divided into two categories; The Frequency Containment Reserve for Normal operation (FCR-N) and the Frequency Containment Reserve for Disturbances (FCR-D). The distinction between these categories is based on the operating limits; FCR-N is the control that functions between 49.9 Hz and 50.1 Hz, whereas FCR-D operates around this dead-band between 49.0 Hz and 51.0 Hz [16].

The Nordic System Operation Agreement defines the frequency target parameters in the System Operation Guideline [17]. Table 2.1 gives an overview of these parameters. Only if the frequency deviation is bigger than the normal operating deviation, the fault can be classified as a frequency event. Furthermore, [17] states that the voltage should be maintained between 0.9 and 1.05 p.u.. All machines in the Nordic power grid need to be able to withstand frequency and voltage fluctuations within these limits. When the frequency surpasses the lower limit of 48.8 Hz or when the absolute RoCoF is higher than 2 Hz/s, loads start to shed in order to avoid further frequency collapse [16].

Table 2.1: Frequency target parameters from the Nordic System Operation Agreement [17]. Deviations are are from 50 Hz. RoCoF and deviations are absolute.

Target requirement	Abbreviation	Value	Unit
Normal frequency operating deviation		100	mHz
Maximum admissible frequency deviation	$\Delta f_{max,\ adm}$	1000	mHz
Maximum admissible frequency recovery deviation	$\Delta f_{i,\ rec}$	500	mHz
Maximum admissible recovery time	$T_{rec,\ adm}$	30	s
Maximum admissible Rate of Change of Frequency	$RoCoF_{max,\ adm}$	2	Hz/s

In case of under-frequencies, the synchronous machines need to provide extra power to balance the deficit of electrical power. Therefore, the synchronous machines do not operate on full output. The extra power that needs to be available to a generator or specific area is defined as the spinning reserve. The requirements for these reserves are defined in the Nordic Grid Code. For thermal power plants the spinning reserve needs to be 5% and for nuclear power plant 5%. The governors of all connected synchronous generators are required to have a droop between 2 and 8 % [18].

2.3.2 Current frequency containment policy

The current policy of the Nordic Transmission System Operators (TSOs) is preventive; it mitigates frequency instability risks by assuring that the possible power events will not result in MDF higher than the maximum admissible frequency deviation [6]. As mentioned in section 2.2, the size of the MDF is determined by the size of the disturbance, the reaction time and droop of the individual control systems of the generators and the inertia of the system. Therefore, to assess the potential MFD, the inertia and possible power outages need to be known. The Nordic TSOs have developed a tool that estimates the available stored kinetic energy in each bidding zone as described in [19]. The available kinetic energy E_{kin} [Ws] is related to the inertia constant as can be seen from 2.11:

$$E_k = \sum_{i=1}^{n} H_i S_i \tag{2.11}$$

With H_i [s] as the inertia constant of an individual synchronous generator and S_i [VA] as the rated apparent power. Breaker measurements from SCADA (Supervisory Control And Data Acquisition) indicate if a generator is in synchronism with the grid and consequently contributes to the total kinetic energy. If breaker positions are not known, power measurements are used. The rated apparent power of the generators is known and the kinetic energy is approximated. Using the current system frequency measurements, the tool subsequently estimates the potential MFD following all disturbances that lead to a change in active power of 300 MW or more, using a linear regression model [19]. This is done by fitting the linear equation relating the frequency deviation, the kinetic energy, and the change in electrical active power with historical data for frequency events in the Nordic grid. In 2017, the largest difference between the estimated frequency deviation and the actual frequency deviation of an event was less than 0.03 Hz [19].

If the computed MDF reaches the maximum admissible frequency deviation of 0.1 Hz, mitigation measures are taken by the relevant TSO. The possible disturbance size is avoided by decommissioning part of the generated power. The producer is compensated and the omitted power has to be procured which leads to high costs for the TSO [6]. The single largest possible active power disturbance is known as the dimensioning incident. In the Nordic Power System this is the nuclear plant Oskarhamn 3 which has a rated active power of 1450 MW. [6] found that in the summer of 2018 on three low inertia occasions, the output of Oskarhamn 3 was reduced by 100 MW as a preventive measurement.

2.4 Frequency response of VSC HVDC links

High Voltage Direct Current (HVDC) transmits power between two separate synchronous areas or over a long distance with fewer electrical losses than AC lines. The growth in HVDC links is attributed to an increase in off shore wind farms and improvements in the technology. This section lays out the difference between the two current HVDC technologies, Line-Commutated Converters (LCCs) and Voltage Source Converters (VSCs). The technology of the VSC is then further explained with a particular focus on the frequency response.

HVDC links are classified according to the converter technology into a LCC and VSC. LCC was the prevailing technology for HVDC links, until development in switching device technologies led to the rise of VSC technology. LCC-HVDC utilizes thyristors for the switching device in the converters. A signal can switch the thyristor on, but can only be turned off by a reverse bias in the voltage. Consequently, the current lags the ac voltage, and the converters exclusively consume reactive power. The switching devices used in a VSC are fully controlled semi-conductors i.e. Insulated Gate Bipolar Transistors (IGBTs). IGBTs can be switched on and off and therefore the direction of the voltage and the current can be controlled. Pulse Width Modulation (PWM) delivers the switching signals. The main advantages of VSC over LCC are [20] , [21], [22] :

- Independent control of reactive power
- Higher quality of voltage wave which reduces the need of harmonic filters
- Blackstart capability
- Fast dynamic response
- Fast reversal of power flow

However, LCC technology has superiour efficiency compared to VSC and higher power ratings [22].

In the VSC-HVDC link, active and reactive power can be regulated by changing the voltage of the converter with respect to the grid voltage. The relationship between the converter voltage (V_c), the grid voltage (V_g) and the active (P) and reactive power (Q) is defined in 2.12 and 2.13 respectively:

$$P = \frac{V_c \sin \delta}{X_L} V_g \tag{2.12}$$

$$Q = \frac{V_c \cos \delta - V_g}{X_L} V_g \tag{2.13}$$

With X_L as the (ideal) phase reactor and δ as the phase angle between V_c and V_g. It is assumed that the frequency is at the nominal value. One of the converters controls the DC voltage, while the other controls the active power.

The control structure of a VSC is shown in figure 2.3. In this case, the converter controls the DC voltage and the reactive power. The control structure of a VSC is hierarchical; The outer controller accepts the dispatch values and generates the reference current values. The inner current controller then translates these into three phase voltage references which is achieved using the PWM. The inner current controller acts faster than the outer controller.

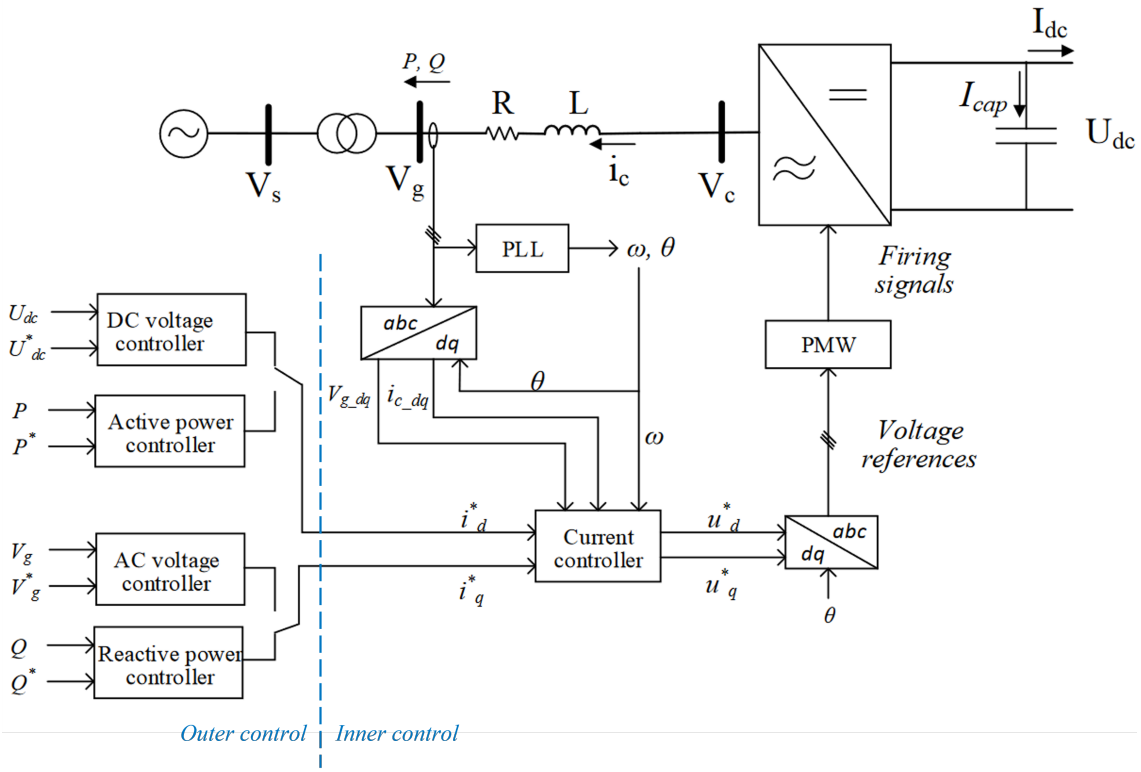

Figure 2.3: Control structure VSC adapted from [23]. In the outer control, the reference values for the reactive and active current are generated. In the inner controller, the inner controller translates thesse into three phase voltage references which relates to the active and reactive power setpoints in equation 2.12 and 2.13

The Clarke and Park transformations convert the time variant three phase currents values into two constant vectors in a rotating frame with the same frequency as the original values. This process is visualized in 2.4. When the phase angle of the grid is known, these two constants can be matched to two vectors resembling the active and reactive currents. The Phase Lock Loop (PLL) is responsible for tracking the phase angle of the adjacent power grid. Control actions can than adjust the reference values for the reactive power and the active power separately with proportional-integral-derivative (PID) control.

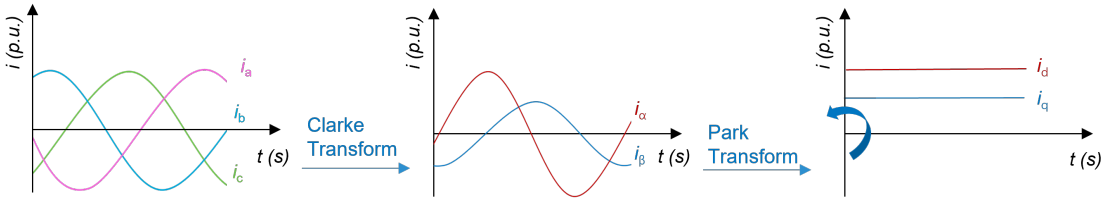

Figure 2.4: Clarke and Park transformation. Measured three phase current values are transformed with the clarke transform to a 2 phase current values before being transformed with Park to two constants in a rotating reference frame

Unlike the governors in synchronous machines, VSCs do not adjust the power output automatically to changes in frequency. Instead, a supplementary control loop is necessary. The power supplied for this frequency response can originate from the stored energy in the DC shunt capacitors or can be delivered by the asynchronous grid or the wind power farm connected by the HVDC link. [24] and [25] describe the first control approach, i.e. using the energy from the DC capacitors, as emulated inertia control. It is based on the

assumption that energy stored in the capacitor resembles the rotational energy in a synchronous generator as the DC capacitor energy is proportional to the square of the DC voltage. By changing the DC voltage, energy is discharged or charged. The capacity of the HVDC DC link is, however, limited [26], [27].

The second approach involves modification of the power set-points during a frequency event. This is achieved by adding a control loop as an input for the DC voltage or power outer controller. The control mode is defined as droop control if the change in power is proportional to the change in frequency. Typical droop values are between 3 and 5 % [27]. Control methods where the power output is proportional to the RoCoF are defined as derivative control methods. Such methods also have the characteristics of inertia. Comparative studies [23] and [22] found that frequency response method using the DC voltage-frequency control and power-frequency control both improve the frequency response, but the latter showing the best performance in the grid that experiences a frequency event.

Adjusting the power flow during a frequency event in one area has an effect on the area delivering (or consuming) the power. Consequently, agreements need to be made about the capacity and the market valuation of frequency containment services to other synchronous grids [28].

2.5 Frequency response wind turbines

The frequency performance of Wind Turbines (WTs) differs considerably from that of synchronous generators described in section 2.2. WECC Working Group on Dynamic Performance of Wind Power Generation & IEEE Working Group on Dynamic Performance of Wind Power Generation recognize four different types of wind turbines [29]. The classification is as follows:

- **Type 1:** Fixed speed, induction generator
- **Type 2:** Variable speed, induction generator with variable rotor resistance
- **Type 3:** Variable speed with doubly fed induction generator
- **Type 4:** Variable speed with Full Rated Converter (FCR) interface

Type 1 and Type 2 are coupled to the grid and provide inertial support, but have less system inertia compared to synchronous generators. Type 1 can also deliver primary frequency response.

Modern WT types 3 and 4 are connected to the grid with PEI. For type 3, only the rotor is decoupled and the stator is coupled to the grid. Type 4 WTs are completely interconnected with a converter and their operation can be compared to the VSC-HVDC converter explained in section 2.4. As these types are decoupled from the grid they do not deliver natural inertia. The PEI makes it possible to adjust the power quickly in response of a frequency event. In a typical wind power park with type 3 or type 4 wind turbines, the wind turbines have individual control systems which regulates the speed-torque, the pitch angle of the blades and the converter and there is an overall control system for the park [30].

An additional control loop adjust the power output during frequency events. Frequency Response is already a proven technology in new wind turbines. Power output can be either proportional to the RoCoF, proportional to the change in frequency or constant. Different names for these control loops exist such as synthetic, artificial or emulated inertia. In this thesis, the term ”Fast Frequency Response” (FFR) is used. This term is defined by [31] as an umbrella description for all ”controlled contribution of electrical torque from a unit which responds quickly to changes in frequency in order to counteract the effect of reduced inertial response’ [13, p509]. Synthetic inertia is specified as a subgroup of fast frequency response which is proportional to the RoCoF.

Figure 2.5 shows the power output (P) in relation to speed (v [m/s]) for a variable speed WT. The turbine starts to generate power if the wind is higher than the cut in wind speed ($v_{cut\ in}$). The WT controls the output to the maximum possible power output if the wind speed is between the cut in wind speed and the rated wind speed (v_{rated}). In the operational area between rated wind speed and cut out wind speed ($v_{cut\ out}$), the power output is controlled by adjusting the pitch angle to create a constant power output. If the wind speed exceeds the cut out wind speed, the wind turbine will stop producting power to prevent oscillations. Typical values for ($v_{cut\ in}$), (v_{rated}) and ($v_{cut\ out}$) are 3 m/s, 10 m/s and 20 m/s.

The operational point of the wind turbines determines where the required energy for the FFR of wind turbines is drawn from. If the turbine operates at rated power (P_{rated}) with a wind speed higher than rated wind speed (v_{rated}), pitch angle control changes the blade pitch angle to keep the power output constant. During a frequency event, the wind turbine is overloaded for a short period of time by reducing the pitch angle; the energy for the FFR

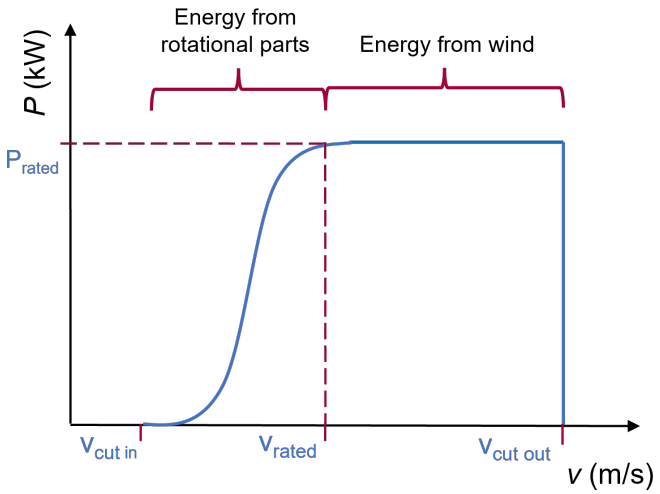

Figure 2.5: Relationship between the power output of a variable wind speed turbine and the wind speed. In the operation points before the rated speed, the energy for the FFR is supplied by the rotational energy, after the rated speed energy is subtracted from the wind by adjusting pitch control

comes from the wind. For operational points below rated speed, the energy comes from the rotational parts of the wind turbine, i.e. the blades and the rotor. This causes the rotor to decelerate. In the *recovery period* after the fast frequency response, the power output decreases to a value that is lower than prefault values to recover the rotor speed. This results in a second frequency dip. Thus, the frequency response of wind turbines is non-linear. To avoid this recovery period and consequently the second frequency drop, a *de-loading* technique in low inertia periods can be used. As the turbine does not operate at maximum power output before the fault, there is a reserve for fast frequency response.

2.6 Power system stability considerations with increased NSG penetration

Specific stability phenomena are prevalent when a large share of the power demand is met through Non-Synchronous Generation (NSG). This chapter discusses two sources of complications caused by the addition of more NSG to the stability. These issues arise because of lower inertia of the system and lower short-circuit current contribution at the output of NSG.

Firstly, if synchronous generators are replaced by NSG, the amount of system inertia is reduced which affects the frequency and the rotor angle stability. As mentioned in section 2.2, less inertia leads to higher values of RoCoF and therefore higher values of MDF. An advantage of NSG to the frequency performance of a system is that fast frequency control of NSG can have smaller droop values and act quicker because it is not limited by physical turbine response time, but the electrical switching times [10]. Rotor angle stability is influenced by decreased inertia as well, as reduced inertia leads to large rotor swings. Furthermore, NSG reacts differently to rotor angle differences in a grid. Synchronous generators vary their output with regards to a voltage angle, whereas NSG does not. Because of this, they do not provide synchronizing torque [32]. Not just the amount of inertia is of importance, but also the distribution of inertia in the system. The network is heterogeneous if NSG is not uniformly distributed over the grid. After a disturbance, different RoCoF levels make it more difficult to keep the generators in synchronism.

Secondly, NSG contributes limited short-circuit current because the law of constant flux does not apply to NSG [33]. This reduces the system strength, i.e. the stiffness of the grid. System strength is used to describe the voltage sensitivity of the grid to changes in output currents of the converter, related to the equivalent impedance. A strong system means there is low sensitivity and vice versa. In a weak part of the system the voltage phase angle differs more easily which affects the capability of the Phase Lock Loop (PLL) to track it and keep the output of the converter in synchronism with the grid [30]. Furthermore, the voltage reaction to the PQ control can be larger than expected in sensitive grids. Thus, a weak system may result in stability issues for NSG.

Different indices are used to quantify the system strength. The most basic index is the Short Circuit Ratio SCR_{PCC} which can be calculated with equation 2.14 at the Point of Common Coupling (PCC) for NSG [30]:

$$SCR_{PCC} = \frac{SCMVA_{PCC}}{P_{nom,\,NSG}} \tag{2.14}$$

With $SCMVA_{PCC}$ as the short circuit apparent power from a three-phase line to ground fault at the PCC without short circuit contribution of NSG, and $P_{nom,\,NSG}$ as the nominal power of NSG connected at the PCC. Equation 2.14 is mainly used in the industry for LCC-HVDC links. A disadvantage of index SCR_{PCC} is that it does not take into account other NSG in close proximity. Nearby power plant with NSG share the system strength, so the actual SCR is even lower.

[33] observed an increased interaction between voltage and frequency in a heterogeneous system with a high penetration of NSG. During frequency events with reduced voltage, active power of wind power plants was reduced to be able to increase reactive power for voltage support. This caused the frequency to be even further reduced. To conclude, the stability of the power system is influenced by the increase of NSG. As a result, the influence of the control requirements for NSG by TSOs increases with respect to the physics of the synchronous generators [32].

3 Development of dynamic model

In this chapter, the dynamic model of the Nordic Power System in 2030 is developed. The Nordic Power System is modeled in the simulation software DIgSILENT PowerFactory. The chapter starts therefore with a brief explanation of this software program in section 3.1. Section 3.2 introduces the starting point of the model, the base model by Aas [1]. All generator models in the base model are Hydro. However, the dynamic response differs per power plant type. This is especially the case for Wind Turbines (WTs) and Synchronous Generators, but a distinction between hydro power plants and thermal steam units is also necessary. Therefore, Section 3.3 presents a possible distribution of the power plant types. This results in an operational scenario with 60% NSG. Section 3.4 continues with an overview of the specific modifications of the base model, which includes the dynamic models of the VSC-HVDC-links and all generators. The modeled grid is then subjected to a small frequency event in Section 3.4 to confirm if the model shows typical frequency behavior.

3.1 Explanation DIgSILENT PowerFactory models

The Nordic Power System is modeled in the simulation software DIgSILENT PowerFactory. PowerFactory has a graphical single-line interface where electrical components and their connections can be drawn as elements in a diagram. The electrical parameters can be edited for each element individually, but they can also be assigned to an Equipment Type. As multiple components can have the same Equipment Type, elements can be modified simultaneously.

For dynamic system modeling, time-domain models are used. This is done hierarchically. A control system is described in a Composite Frame, which encompasses at least one system element, controller types, and the signals between them. A single controller type is specified in a Common Model. An example of a Composite Frame is shown in figure 3.1. In this case, the Composite Frame presents the dynamic model of a synchronous generator. The controllers for the Power System Stabilizer (PSS), the Automatic Voltage Regulator (AVR), and the governor are defined in Common Models, depicted in pink.

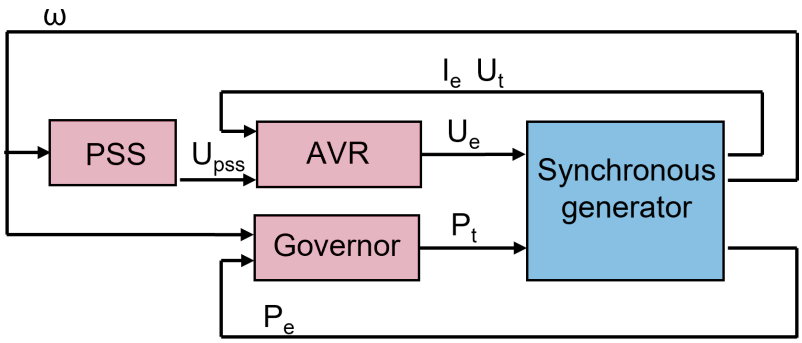

Figure 3.1: Example of Composite Frame. The Common Models are depicted in pink, and the system element in blue. The interaction between the models and the system elements are defined in the composite frame as signals.

3.2 Description Base model Nordic Power System 2030

The dynamic model builds on the PowerFactory simulation model produced by Even Strand Aas in 2016 [1]. The focus of this project is to model the expansion of HVDC links connecting the Nordic Grid and analyse the resulting load flow scenarios. For the model by [1], different scenarios were created for load flow such as high import and high export of power in 2021 and 2030.

The model developed by [1] is an aggregated model consisting of 31 nodes at transmission voltage. The grid has four different transmission voltage levels (400 kV, 300 kV, 220 kV and 22 kV), as depicted in figure 3.2. The nominal voltage of the transmission grid in Norway is 420 kV instead of 400 as defined in the model. The loads, generators and SVCs compensate for this difference by applying a voltage setpoint of 1.05 p.u..

The total capacity of the HVDC transport is 20500 MW for the 2030 scenario.

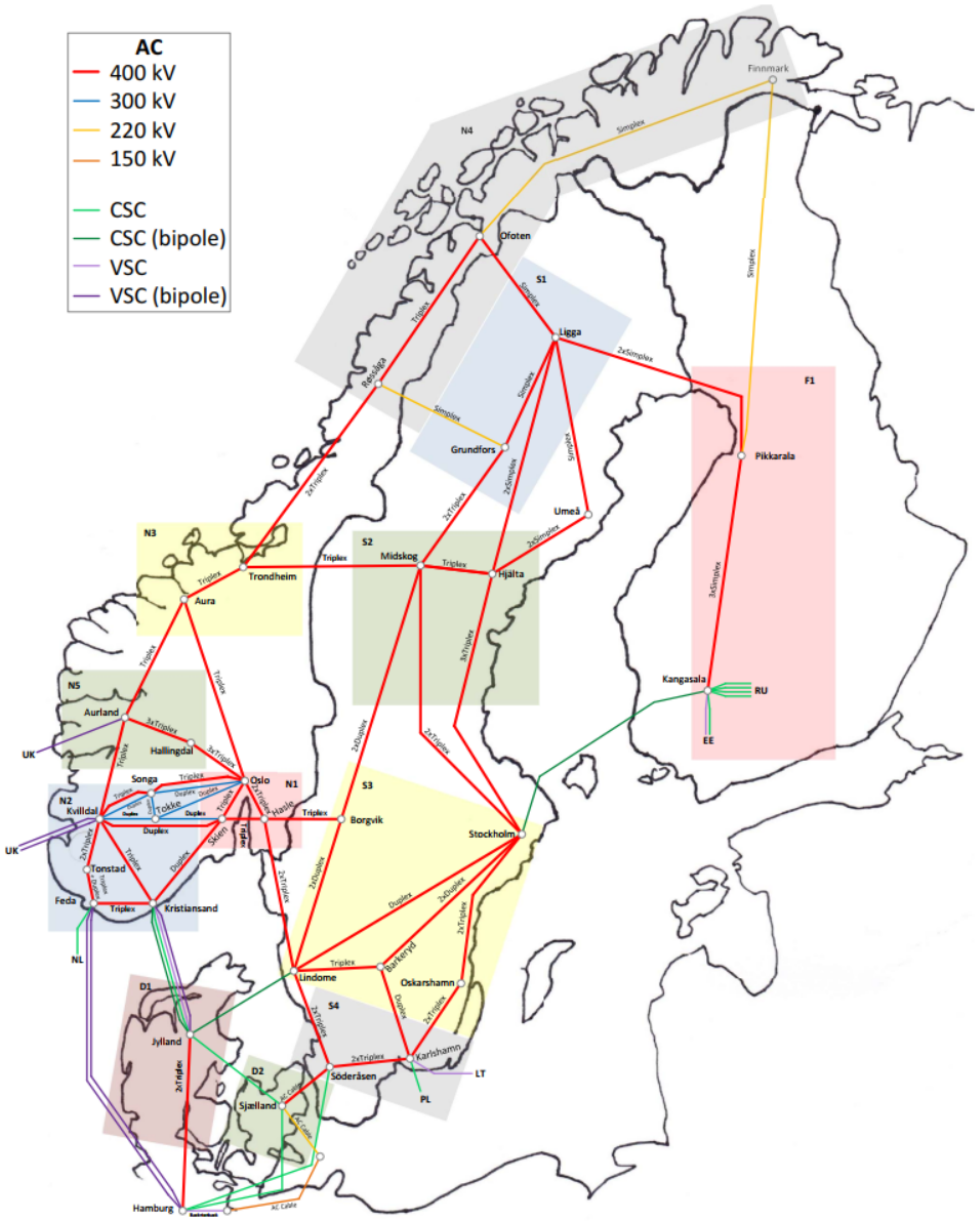

Figure 3.2: Overview of the Nordic Grid model by [1]. The system consists of different nominal transmission voltages depicted in different colors. The HCDC-links in 2030 are depicted in green and purple

Each node represents the total generation and demand of the region modeled by a load and a synchronous generator connected to the high voltage transmission grid with a transformer. The loads can have unlimited active and reactive power output. For the synchronous generators, a generic 250 MVA salient pole synchronous machine is used. The power outputs are scaled by multiplying the number of generators in the grid. All synchronous generators operate in the 'constant voltage' mode, which is set at 1.05 p.u..

The lines are presented by π equivalent models. there are four different Equipment Types. Information about the lines is presented in Appendix A.2. This includes information of the types and lengths between the nodes in table A.3 and the electrical parameters per line type in table A.2

The loads are of the 'General Load' equipment type, the technical reference can be found in [34]. The voltage dependency of the loads can be specified on the LoadFlow page. The loads can be represented by a combination of constant power, constant current, or constant impedance model. The loads are modeled as 30% power, 30% current and 40% impedance models, The voltage setpoints are all set at 1.05 p.u..

Seven nodes which have tatic Var Systems to maintain reactive power balance. Information about the reactive power limits per node can be found in table 3.1.

Table 3.1: Parameters Static Var Compensator

Node	Max nr. Capaciators	Qmax
HLD	4	100
HSL	16	400
KAN	20	500
KHM	25	1000
KRI	25	500
SKI	8	200
SDR	25	1000

Six two-winding transformer types are used in the model. The transformers of the synchronous generators which transform the LV output of 22 kV to 220, 300, and 400 kV respectively, the transformer of the wind turbine (WTG Trf 0.4 -20 kV), and the transformers connecting the 300 kV, 220kV, and the 400 kV grids. Electrical parameters for the transformers are found in Appendix A.3.

3.3 Development of operational scenario with 60% NSG

To evaluate the frequency response of the Nordic Power System for the potential occurrence of low system inertia, the model described in the previous section is adapted. Specifically, a scenario is defined where 60% of the power demand is met by Non-Synchronous Generation (NSG) which does not contribute to the initial inertial frequency response of the system. In this study, the term NSG includes the import (and export) of HVDC, which is also the case in [32];

$$\%\text{NSG} = 100\% \frac{P_{\text{NSG}} + P_{\text{HVDC}_{\text{import}}}}{P_{\text{demand}} + P_{\text{HVDC}_{\text{export}}}} \tag{3.1}$$

The type of power plant is differentiated to account for specific dynamic responses determined by the turbine dynamics of the power plant. The three power plant types are hydro, thermal and wind. For synchronous generation, hydro, gas and nuclear were differentiated because the dynamics of hydro differs significantly from steam units. For example the response time of hydro turbines to a change in power is larger than that of gas turbines. Gas and Nuclear are modeled in the same way except for the inertia constant, which is higher for nuclear.

The capacity per power plant type of the different biding zones and the predicted changes to the NPS are leading in the allocating process. The Mid-term Adequacy Forecast (MAF) by ENTSO-E estimates the capacity per area in MW [35]; The MAF gives the predicted capacity in distinct categories for all ENTSOE-E Areas. A summary for the of the relevant areas is shown in figure 3.3. The division of the areas correspond to the one in figure 3.2, except for Norway. Norway is divided into three areas, Centre (NC), North(NN) and South(NS). South corresponds to the areas N1, N2, and N5, Centre to N3 and North to N4 of figure 3.2.

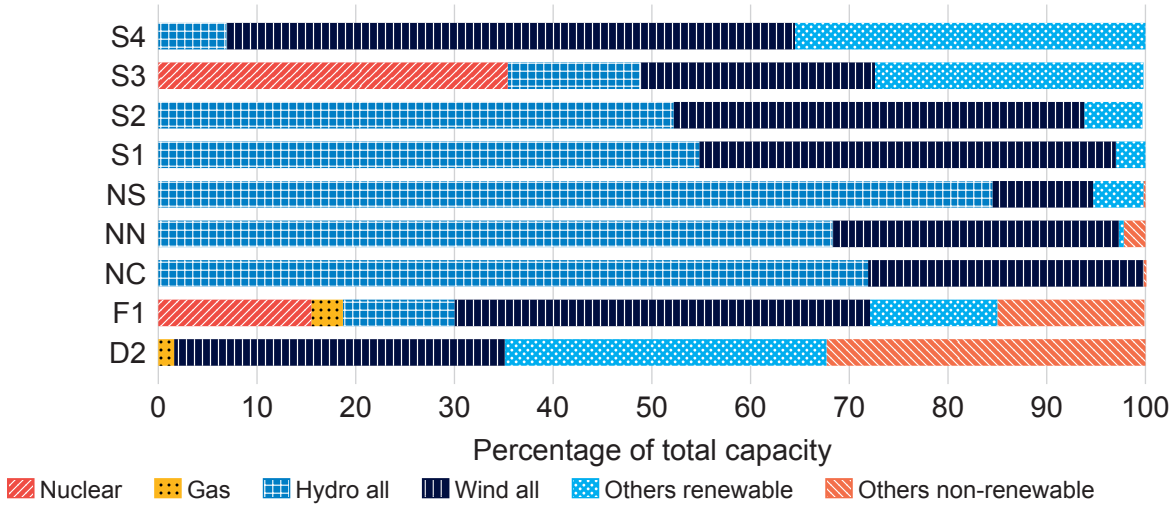

Figure 3.3: Capacity per generation type in percentage for the Nordic Power System, adapted from the MAF database [35]

The distribution of the different generation types of the proposed model are presented in figure 3.4. It is important to note that this operational scenario represents a specific moment, rather than an average load flow or a indication of capacity. The capacity per generation type is presented by the MAF, each region was checked whether the capacity is available. The choice for specific distribution is influenced by the following factors;

- Wind production is expected to increase in the northern part of Sweden and Norway. [4]. This corresponds to wind farms in Ligga (LIG), Finnmark (FIN), Umeå (UME) and Hjälta (HJT).
- The current considerable share of wind power in Sjælland (SJA), or East-Denmark will continue to grow [36].
- Tokke (TOK), Kristiansand (KRI) and Stockholm (STK) increase the percentage of NSG to 60 %. Their capacity corresponds to the MAF [4].
- Oskarhamn (OSK) is an existing nuclear plant. In Finland, Nuclear and Biomass will continue to have a significant share of installed capacity [36]. Consequently, Kangasala (KAN) is modelled as a nuclear plant and Pikkarala (PIK) is modelled as Biomass. As the phasing out of nuclear energy in Sweden is only expected to start after 2030, Lindome (LIN) is modelled as a Nuclear plant to better represent the amount of nuclear in the Swedish generation mix.

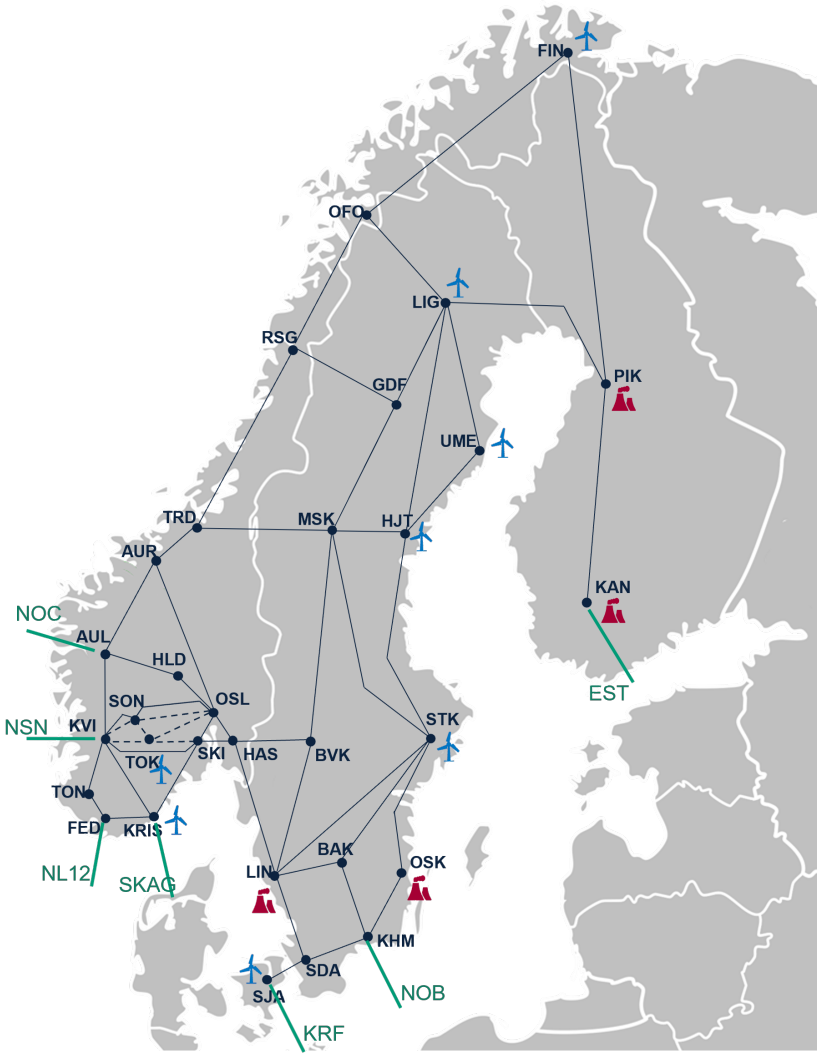

Figure 3.4: Distribution of generation types for the 60% NSG scenario. Wind farms and thermal generation are indicated by the blue and red symbols respectively. The green lines represent the VSC-HVDC import. Note that only the VSC-HVDC is indicated, LCC-HVDC links are modelled as negative loads. Nodes without a symbol have Hydro generation

3.4 Power System Model Modifications of the base model

To reach the 60% NSG scenario, multiple modifications of the base model are made. This section gives an overview of these modifications. The structure of this section is as follows; First, the procedure for the modifications is explained. This includes a description of the complications in the system that occurred. Next, an overview is given of the loadflow setpoints. Finally, a subsection is dedicated to each electrical component type which includes the dynamic model for RMS simulations. The Composite Frame and Common model of each dynamic type can also be found in Appendix B.

3.4.1 Modelling procedure

The process to modify the base power system to the 60% NSG scenario is depicted in figure 3.5.

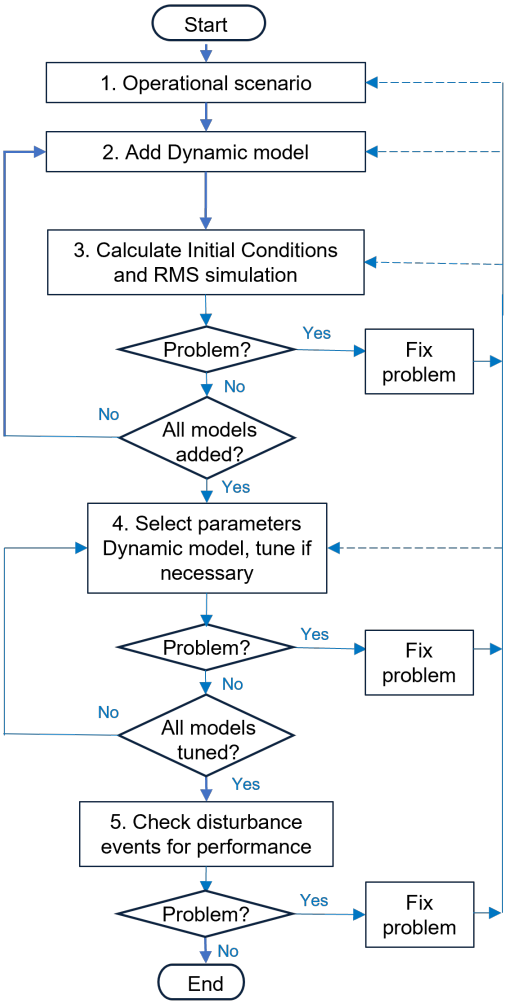

Figure 3.5: Flowchart of procedure to modify the base scenario to the 60% NSG scenario

1. The operational scenario is modified. Some of the synchronous generators are replaced with the wind turbines, the VSC-HVDC terminals are replaced by static generators and the LCC-HVDC links are modeled as negative loads. Furthermore, the total amount of generators is also adjusted. In the base system, the generators are loaded till 20%. The amount of kinetic energy a unit can deliver is directly proportional to the number of generators available. The number of generators is therefore decreased to a loading of 80%. The decrease of the generator systems including the transformers and the addition of wind turbines affect the loadflow significantly; The change in transformer losses and the operational setpoints of wind turbines closer to a power factor of 1 resulted in different bus results. Setpoints of loads were used to maintain voltages.
2. The dynamic models of the different generation types were added one a time, starting with the Hydro. Afterward, the dynamic models were checked for their dynamic performance for small increases of load and tuned if necessary.
3. To check if the dynamic models are correct, all state variables are initialized using the 'Initial Conditions' calculation. The values are taken from the results of the steady state Loadflow calculation that precede each RMS calculation. Additionally, the RMS simulation is run for 5 seconds without an event to see if the initialization results in constant powerflows.
4. The parameters of the dynamic models are tuned with a small frequency event.
5. Problems in the system became only apparent during the investigation into the critical disturbances. The model was modified iteratively.

As shown in figure 3.5, problems had to be solved in different domains and were discovered at different stages. Some examples of these problems were:

- After a first evaluation, rotor angle stability was found to be an issue. By increasing the amount of generator at low-generating busses and decreasing the amount at ac busses with large generation, the system became less heterogeneous. This resulted in less contrast of initial frequency response at each ac bus and prevented loss of synchronism.
- In the north of Norway, especially FIN and OFO, the voltages reacted volatile to changes in active power. This was further investigated by checking the load characteristic of these busses without dynamic composite models in service. A load event of sudden power increase of 20% at FIN was simulated for different setpoint values of the load at FIN and the setpoint with the least deviation was chosen.

The system is complex, and changes in one domain affected other domains. The voltage-load characteristic of loads are dependent on the loadflow, which affect the tuning of the dynamic models. Parameter selection of dynamic models and loadflow changes both affect the initialisation. A change in one location of the system had an effect on other geographical areas of the system and testing for one disturbance does not ensure performance for other disturbances. As a result, large part of the process was based on trial and error.

As explained in the previous section, the loadflow has changed from the base model. The set-points of the loads and generators can be found in table 3.2. As can be seen from the table, the amount of generators differ significantly per node. The nodes with wind generation (FIN, HJL, KRI, LIG, SJL, STK, TOK and UME) have a nominal setpoint of 6 MW, as explained in section 3.4.4. The synchronous generators are not all loaded to 80-100%, which would be a better representation. This was needed to maintain rotor angle stability.

Table 3.2: Active and reactive power set-points of the load and generation per node for the 60% NSG operational scenarop

Node		Load		Generation		
name	id	P_{set} [MW]	Q_{set} [MVar]	$P_{set,i}$ [MW]	n machines	$P_{set,\ total}$ [MW]
Aura	AUR	177	300	100	3	300
Aurland	AUL	1025	275.6	198	4	792
Barkeryd	BAK	450	150	38	3	113
Borgvik	BVK	155	-30	50	3	150
Feda	FED	2759	-387.9	120	2	240
Finnmark	FIN	250	61	6	40	240
Grundfors	GDF	889	267	200	18	3600
Hallingdal	HLD	180	10	170	5	848
Hasle	HAS	126	-940	38	4	150
Hjälta	HJT	200	611	6	135	810
Kangasala	KAN	4000	-135.8	200	18	3600
Karlshamn	KHM	898.1	-200	100	4	400
Kristiansand	KRI	895	-340	6	25	150
Kvilldal	KVI	1	1	200	6	1200
Ligga	LIG	285	672	6	122	732
Lindome	LIN	3947	229	200	13	2600
Midskog	MSK	2333	300	132	4	528
Ofoten	OFO	175	140	117	3	352
Oskarshamn	OSK	1506	159	180	8	1440
Oslo	OSL	3742	347	183	6	1099
Pikkarala	PIK	1805	400	200	7	1400
Røssåga	RSG	1707	395	190	9	1708
Sjælland	SJL	1700	280	6	100	600
Skien	SKI	1104	-500	80	2	160
Songa	SON	1	1	140	1	140
Stockholm	STO	1269	750	6	387	2322
Söderåsen	SDA	8636	25	167	18	3000
Tokke	TOK	1	1	6	33	198
Tonstad	TON	4	1	150	2	300
Trondheim	TRD	1515	213	172	3	517
Umeå	UME	200	50	6	90	540

3.4.2 Synchronous generators

The generation type and the size, or rated power, determines the amount of inertia a synchronous generator can offer. Each generator was assigned its own equipment type, which makes it possible to change the inertia constant individually in the RMS page of the equipment types. The inertia values used in the model are taken from [37] and are shown in 3.3.

Table 3.3: Inertia Constants H(s) related to nominal apparent power Sgn according to [37]

Production type	H [s]
Nuclear	6.3
Other thermal	4
Hydro	3

Using equation 2.11, the amount of kinetic energy in the 60% scenario is 161 GWs. For comparison, the total kinetic energy capacity in the Nordic Power System in 2015 was calculated to be 390 GWs [37].

In the base case, the synchronous generator was a salient pole 280 MVA synchronous machine. This is adjusted with values taken from the equipment type 255 MVA ST taken from the DiGSILENT library in the RMS simulation tap. Furthermore, the reactive power limits were set at the maximum value. The new parameters are displayed in table 3.4.

Table 3.4: Variables synchronous generator type: RMS simulation

	Variable	Unit	Value
	model		standard
	rotor type		round rotor
rstr	Stator resistance	p.u.	0
xl	Stator leakage reactance	p.u.	0.14
Td’	Transient time constant, d	s	1.08
Tq’	Transient time constant, q	s	1.08
Td”	Subtransient time constant, d	s	0.018
Tq”	Subtransient time constant, q	s	0.018
xd	Synchronous reactance, d	p.u.	2.01
xq	Synchronous reactance, q	p.u.	1.89
xrld	Rotor mutual reactance, d	p.u.	0
xrlq	Rotor mutual reactance, q	p.u.	0
xd’	Transient Reactance, d	p.u.	0.21
xq’	Transient Reactance, q	p.u.	0.34
xd”	Subransient Reactance, d	p.u.	0.16
xq”	Subransient Reactance, q	p.u.	0.17

3.4.3 Dynamic model for synchronous generators

The dynamic model for synchronous machines consists of three components; the Governor, the Automatic Voltage Regulator (AVR) and the Power System Stabilizer (PSS). The Composite Frame with the interactions between the AVR, PSS and Governor is shown in figure 3.6. As explained in section 2.2 the function of the governor is to maintain the frequency by adjusting the power output with a predefined droop value. It regulates the turbine part of the generator. The AVR is responsible for the voltage control. By adjusting the excitation voltage, the voltage at the output of the generator is controlled. It needs to

be fast-acting to have a sufficient response in the transient time. Because there is a lag between the excitation voltage and voltage at the output, a strong acting AVR can lead to oscillations and therefore instability. This is specifically the case with pre-existing power oscillations because of rotor angle swings. A PSS can be added to dampen the oscillations caused by the AVR. A PSS is equipped with a dead-band, thus it will exclusively act during an event.

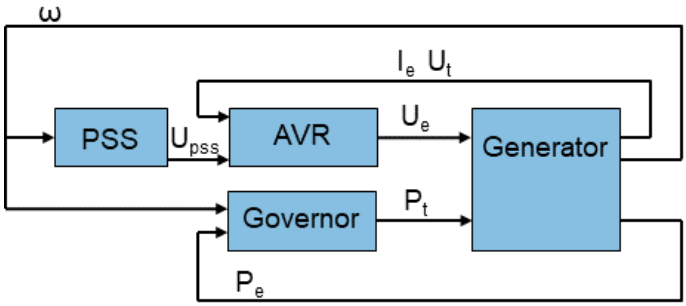

Figure 3.6: Composite model of Synchronous Generator with Common Models for PSS, AVR and Governor. The input signals are on the left side of the block, whereas the output signals are on the right side of the block. The generator signals the excitation current (I_e) and the terminal voltage (U_t) to the AVR, the electrical power (P_e) to the Governor and the speed (w) to the governor and the PSS. As an input signal it receives the excitation voltage (U_e from the AVR and the turbine power (P_t) from the Governor. The PSS sends a reference voltage signal (U_{PSS}) to the AVR.

The governor of the Hydro generators is modelled as the HYGOV model available for PSSE Software (Power System Simulator for Engineering). According to [38] it is the standard model for hydro governor, with non-linear turbine model. 3.5 presents the relevant parameters for the HYGOV system, typical values given by the Norwegian TSO Stattnet [18] and the selected values for the model.

Table 3.5: Variables Governor Hydro turbine

	Definition	Typical values [18]	Selected values
R	Permanent droop (pu)	0.02 - 0.08	0.02
r	Temporary droop (pu)	0.3 - 1	0.3
Tw	Water Starting time (s)	1 - 2	1
Tr	Governor Time Constant (s)	5 - 10	5
Tg	Servo Time Constant (s)	0.2 - 1	0.4
Tf	Filter Time Constant (s)	< 0.1	0.05
Dturb	Frictional losses factor (pu)	-	0
qnl	No Load flow (pu)	-	0.08
At	Turbine gain (pu)	-	1.15
PN	Turbine Rated Power	-	0
Gmin	Minimum Gate limit (pu)	-	0
Velm	Gate Celocity LImit (pu)	-	0.2
Gmax	Maximum Gate limit (pu)	-	1

Relevant parameters are the permanent droop (R), the temporary droop (r), the qater starting time (Tw), the governor time constant (Tr) and the Servo Time Constant (Tg). The permanent droop (R) is the primary control parameter that adjusts the opening of the gate proportionally to difference in speed of the generator. The temporary droop (r) has the function to stabilize the output of the governor system, to reduce the overshoot caused by R. The water flow doesn't react instantaneously to changes in the mechanical changes

of the gates. This lag is described by the water starting time. Producers specify this for the unit at rated power and rated water head. The governor time constant is recognized as a damping time and is typically around around 5Tw, The Servo Time constant relates to the time it takes the servo gates to close and open. Tuning for these parameters was done for all hydro generators at the same time using the limits from table 3.5. The effect of these parameters is shown in figure 3.7.

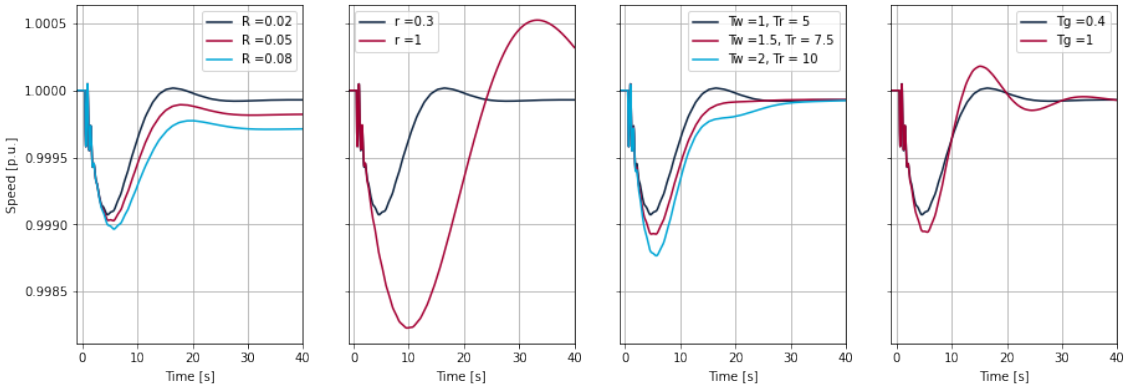

Figure 3.7: Speed time responses of Hasle for a sudden load increase of 10 % in Oslo for different HYGOV parameters. The load increase results in a power deficiency of 374 MW. Except for the corresponding parameter, the default values of table3.5 are used. The parameters are changed for each hydro unit in the system. The values for Tw and Tr are tested instantaneously according to the formula Tr = 5Tw

The AVR of the Hydro generators is modeled as a simplification of the DC1C excitation system of IEEE [39], omitting the non linear saturation effects and the lead lag block of the regulator. It includes an overexcitation limiter (OEL) to avoid windups and a PID of the AVR controller. Typical values for the excitation block and OEL values are not given by the IEEE. Instead, [40] provides performing criteria for small signal and large signal stability problems.

The PSS of the Hydro generators is shown in figure, it has one input, i.e. the rotor speed. The range of values defined by [40] and the selected values are shown in 3.6.

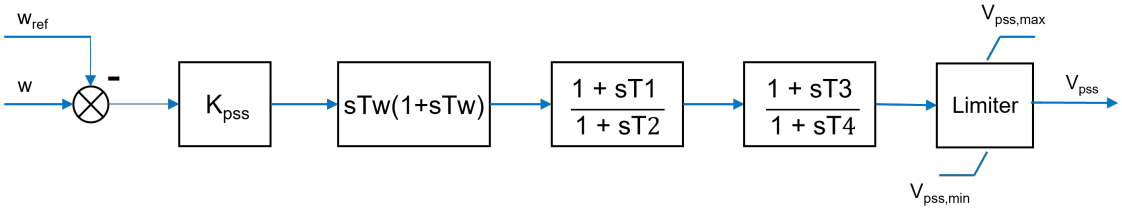

Figure 3.8: Common Model of PSS used for Hydro and Thermal, the input variables are the rotor speed (w) from the Synchronous Generator and the reference rotor speed (w_{ref}) initialised as the rotor speed at t = 0. The output signal Vpss is sent to the AVR, where it is summed with the voltage reference. The description of the parameters can be found in 3.6.

The governor of the thermal generators is represented as 'govSteam' provided by the library of DigSilent. Steam governors can be used for nuclear plants, as well as coal and biomass. It is the simplified model of IEEEG1 provided in [14]. Typical values are given in [41]. The relevant parameters of the governor are given in B.4

The AVR of the thermal generators is type AC4A as described in [40]. **The PSS of the thermal generators** is the same model as the one used for hydro generators. The values of the parameters are different as can be seen in table 3.6

Table 3.6: Parameters PSS Hydro and Thermal

Parameter	Description	Typical values [40]	Hydro	Thermal
T2	1st lead-lag denominator time constant	0.01 - 10	0.1	0.015
T1	1st lead-lag numerator time constant	0.03 - 2	0.3	0.08
T4	2nd lead-lag denominator time constant	0.01 - 10	0.1	0.015
T3	2nd lead-lag numerator time constant	0.03 - 2	0.3	0.08
Tw	Wash-out time constant (s)	0.5 - 50	0.5	5
Kpss	PSS gain [p.u.]	0.1 - 10	10	10
Vpssmin	Minimum PSS output	-0.1 - -0.02	-0.05	-0.05
Vpssmax	Maximum PSS output	0.02 - 0,1	0.05	0.05

3.4.4 Fully Rated Converter wind model

At 8 Nodes a wind turbine replaces the synchronous generator, as described in section 3.3. For this the General Template 'DIgSILENT FullyRatedConv WTG 6.0MW 50Hz' is used. Information for this template can be found in [42].

The WT is modeled as a static generator with an extra transformer. An example of the graphical interface of PowerFactory for a bus with a wind turbine is shown in figure. The transformer is a 6.7MVA 0.4KV-20kV DYN5 three phase transformer. the HV-side voltage is increased to 22 kV to match the voltage level of the low voltage bus of the synchronous generator where it is placed. The required power output is reached by increasing the number of parallel transformers and static generators. This model was chosen because it gave no problems with initialisation, the RMS simulation without events gave a steady input after 5 seconds. For other models, initialisation was problematic when the wind turbines did not operated at a reactive setpoint other than zero and thus the load flow was adjusted. The wind turbines therefore operate at nominal power and power factor. The controller is set on 'Const Q' as is the default case for Wind turbines.

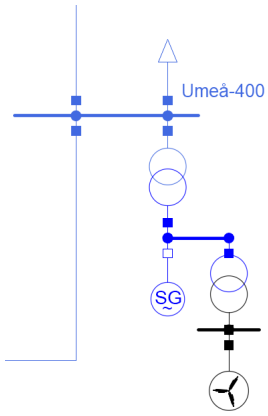

Figure 3.9: Graphical interface of PowerFactory model of the AC bus Umeå with a wind turbine and a load. The synchronous generator is not connected to the bus

The Composite Frame of the wind turbine is shown in figure 3.10. The measurement devices are shown in pink. Measurements for active and reactive power, ac voltage, and ac currents are taken at the low voltage side of the wind turbine transformer, the bus depicted in black in figure 3.9. During the initialisation of the model, the initial values of the reactive power, ac voltage, and ac current are taken from the loadflow, and during the dynamic control, the PQ controller and the current controller adjust their output with the goal to keep the power values close to initial values. Furthermore the Phase Lock Loop

(PLL) block measures and adjusts the signals for the frequency and the angle phi which is the rotor position of the direct axis respect to the reference bus voltage.

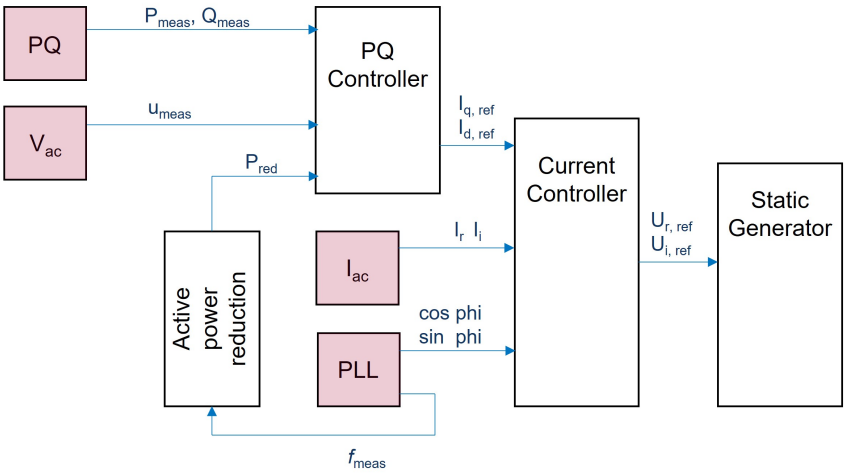

Figure 3.10: Composite frame Fully Rated Converter Wind model by [42]. Measurement devices are depicted in pink

The control blocks in the composite models function as follows:

- **The PQ control** in figure 3.10 uses these measurements and compares them with reference values taken from the initial load flow calculation and adjusts them with PI control. If the voltage deviation is higher than a predefined value, an extra gain is added to the Q signal, but normally the wind turbine does not contribute to voltage regulation. The reference value for P can be adjusted by the signals from the Active power reduction blocks. Lastly, the direct, quadratic and combined current, and internal voltage are limited if predefined values are reached. The common model of the PQ controller is found in appendix A.
- **The current controller** calculates the 1st sequence voltage references. First, the measured two phase currents I_r and I_r are transformed into two static currents in a rotating frames as explained in section 2.3. The PLL contributes the position of the direct axes compared to the voltage angle. Second, a PI controller adjusts these currents with the reference signals from the PQ controller before it is calculated back to two phase voltage values.
- **The Active Power Reduction block** decreases the power reference during over frequency events. Its operation is shown in figure 3.11. When frequency trigger f_{up} is reached, the active power reduction starts and the reference is decreased with gradient PHZ until the frequency reaches f_{low} which stops the control. The Emulated Inertia block completes the frequency control for the wind turbine as it works for underfrequency events. The Emulated inertia is described in section 4.2, and is out of service for the remainder of this chapter.

As mentioned above, the PQ current has a control loop for voltage support which has a deadband. The ΔI_q-ΔU characteristic of the voltage support is shown in figure 3.12. The voltage dead band (deltaU) determines when this control starts. Two control possibilities are possible; following the transmission code 2007 (a) ,or SDLWIndV in 2007 (b) . Both can be implemented in the model, the default value is the one according to SDL Wind.

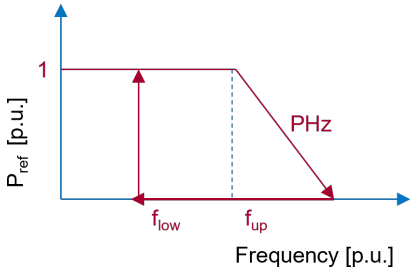

Figure 3.11: Frequency-Active Power characteristic of the Active Power Reduction block. If the frequency reaches or exceeds f_{up} the power reference is reduced with gradient PHz until f_{low} is reached. It is explained in [42]

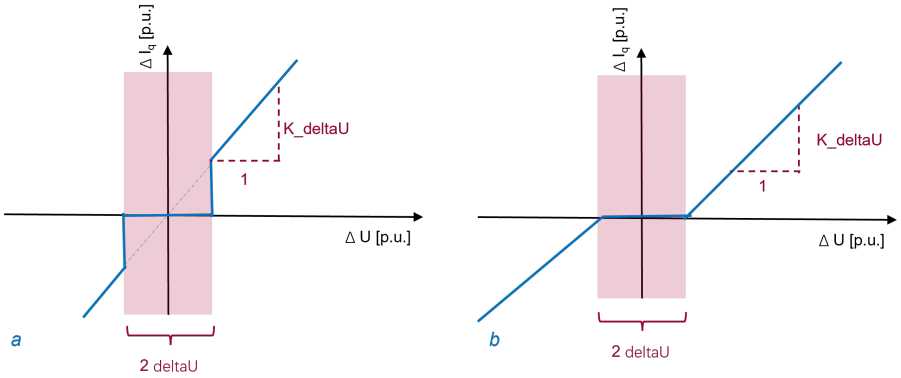

Figure 3.12: Voltage support of the Fully Rated Converter WT model as explained by [42]. The voltage support is found in the PQ controller of the composite model of the WT. The reactive current reference will be adjusted if the voltage deviation is bigger than deltaU. In a) the voltage is adjusting according to the transmission code 2007 [43], in b) the control mode according to SLDWindV [44] is presented

According to [18] wind parks with a production of 10 MW or higher should partake in voltage stability. However, changing the deadband parameter deltaU to 0 resulted in initialisation problems of the wind turbine. Figure 3.13a shows the effect of decreasing the deadband deltaU on the voltage magnitude measured at the LV Output of HJT WT. For deltaU = 0.1, the voltage deviation is not bigger than the deadband and the reactive current is not changed. Only in this case, the voltage does not decrease, furthermore, in the other cases, large spikes can be seen in the voltage. The effect of changing the deadband parameter deltaU on the frequency can be seen in figure 3.13b. Changing the voltage deadband results in volatile frequency characteristics. Changing the values for the reactive current gains and the delays in the PQ controller and the current controller did not result in stable operation. Note that without the voltage support, the reactive power of all WTs are set at zero. The deadband parameter deltaU is set to the default parameter 0.1.

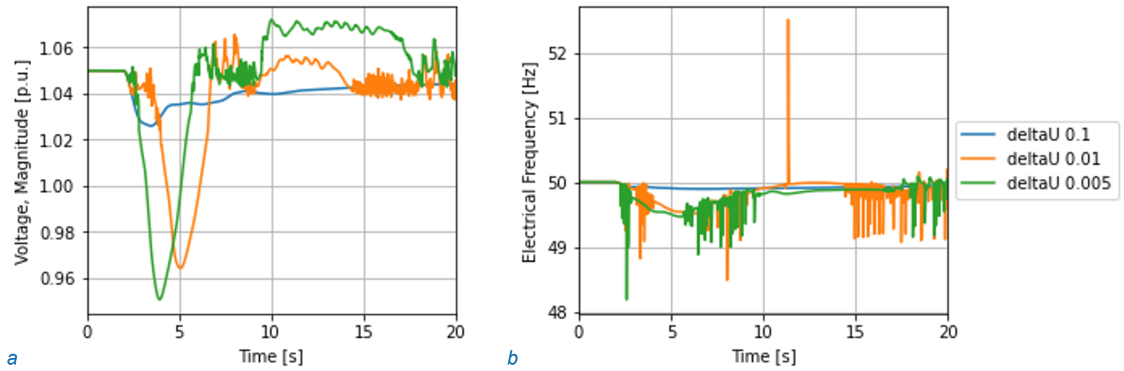

Figure 3.13: Effect of different values of deadband deltaU on the voltage magnitude (a), and frequency (b) measured at the output of the HJT WT after a 20 % load increase in Oslo

3.4.5 HVDC links

The HVDC links in the base model loadflow were not suitable for dynamic simulations as they did not initialise. New representation was necessary. The LCC-HVDC links were therefore modelled as negative loads. Table 3.7 gives an overview of the location of the LCC-HVDC links, the names and the active and reactive setpoints of the loads. The active and reactive powers were taken from the output of the LCC-HVDC links from the base model. The loads were modelled as 100 % constant power load, which acts as a fully static during RMS simulations.

Table 3.7: Location and setpoints LCC-HVDC links

Name	Location	P (MW)	Q (MVar)
NorNed	FED	-191	638
Vyborglink 1-4, Fenno Skan, Estlink2	KAN	-950	31
SwePol	KHM	-498	100
Skag 1-3	KRI	-600	200
Konti-Skan	LIN	-600	0
Kontek, Storebaelt	SJL	-1200	250
Baltic cable	SDR	-700	0
Fenno Skan	STK	-802	0

All VSC-HVDC links, regardless of topology, are represented by the model 'HVDC MMC 2-Terminal LInk (RMS Balanced) of the DIgSILENT library of PowerFactory 2021. Unfortunately, no technical reference of the model exists. DC voltage levels and rated powers are specified per link. Table 3.8 gives an overview of the rated voltages and powers per HVDC link, taken from the base model by [1].

Table 3.8: Overview HVDC links in system

	Full name	S_{rated} [MVA]	$V_{DC\ rated}$ [kV]	P setpoint [MW]
EST	Estlink	670	400	300
KrF	Kriegers Flak	670	400	500
NL1	NL1	785	500	600
NL2	NL2	2220	525	1200
NSN1	NSN1	1570	525	1250
NSN2	NSN2	2220	525	1750
NOB	NordBalt	1570	300	600
NOC	NorthConnect	785	525	1300
SK4	Skag 4	1110	500	600
SK51	Skag 5-1	1110	525	900
SK52	Skag 5-2	785	525	900

For loadflow calculations, VSC-HVDC is modeled by means of two static generators as the HVDC link terminals. Figure 3.14 shows the frame for HVDC link. The value for the active power flow is determined in a separate Quasi-Dynamic Simulation model. HVDC converter 1/A controls the active power and sets the P setpoint. HVDC converter 2/B is modelled as the converter controlling the DC voltage, its power output is calculated in the Quasi-Dynamic Simulation model. After that, these signals are taken by the HVDC-link control block and the DC voltages and currents at both sides are calculated using the user defined values including capacitance, resistance, reactance, link length and rated load flow properties. The HVDC terminals then control these values to specific needs.

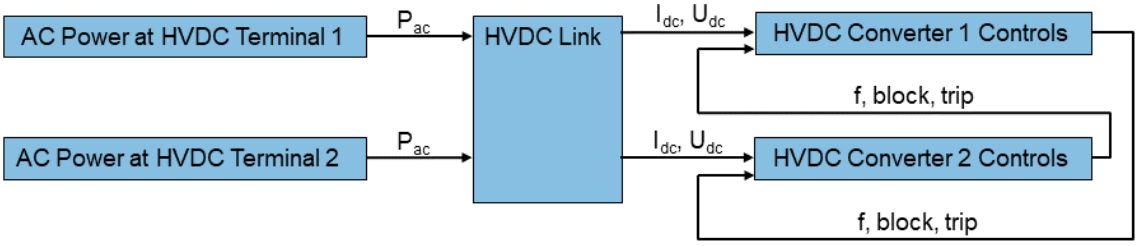

Figure 3.14: Composite Frame for VSC-HVDC link. Power setpoints are sent from the HVDC terminals to the HVDC link. The results from the quasi-steady state calculation in the HVDC link are sent to the Composite Frames of the Converters.

The Composite Frame and the Common Models of the terminal converters can be found in Appendix B.3. A rough summary can be seen in figure 3.15. Its controls can be categorized in 5 sections: Measurement and Signal Processing, Protection, Outer Loop Dynamics dynamics, Inner Loop Control Islanded Control and Operating Mode Selector. A brief explanation of a general VSC-HVDC Converter is given is section 2.2.

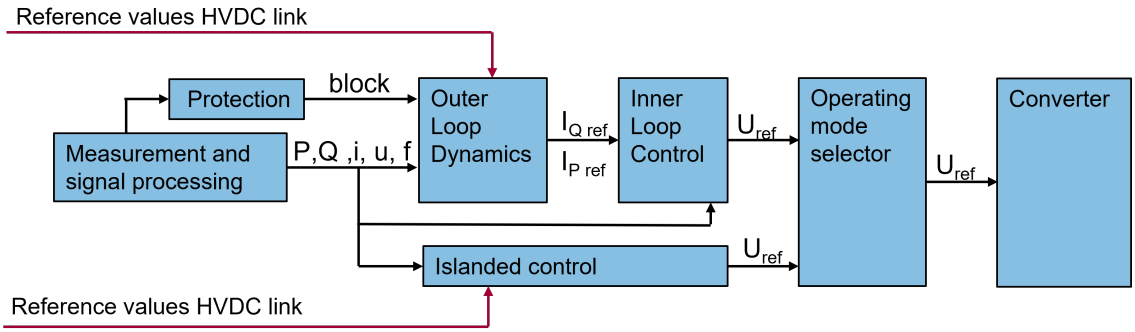

Figure 3.15: Summary VSC-HVDC converter control. The reference values of the VSC-HVDC link are calculated in the Composite Model of the HVDC link. These are the DC voltages and currents, trip and block protection and frequency signals from the other converter.

The measurement and signal processing collects and calculates the signals for voltage and current as well as the phase angle and frequency from the PLL. The **protection** block then checks whether the voltages, currents and frequencies are in between the operational limits and opens circuit breakers if necessary.

In the **Outer Loop Dynamics** the setpoints for active power and reactive power are created. The outer loop consists of the following models:

- *Emergency Power Control* can adjust the active power reference when triggered. This is done by a signal that is set by a parameter event. It can therefore represent external control by the TSO. It is set out of service for this study.
- *The Synthetic inertia* control block adjusts the power reference proportional to the RoCoF to mimic inertial response from synchronous generators. This is out of service for the remainder of the chapter, but is further discussed in section 4.2.
- *Frequency Sensitive Mode* adjusts the active power reference upwards or downwards with a specified power frequency characteristic defined by the TSO.
- *Power Oscillation Damping* is the equivalent of the PSS for synchronous generator; its function is to damp power system oscillations with a lead-lag control block. The input signal is specified by the user; the options are P, Q, AC voltage or frequency. It can adjust either the active or reactive power references.
- The active power references are combined with the power measurement in the *P/Vdc control* block. It can either regulate the DC voltage or the active power. PI controllers adjust the measured P/Vdc to the reference values. These adjusted signals are checked with (ramp) limits. Additionally, it is possible to have droop control in both Vdc and P control.

  It is custom that the sending terminal controls the active power while the receiving end controls the DC voltage. For the high import scenario, the converters connected to the Nordic Power System were first controlling the active power. However, this led to initialisation problems; Without external grids, the power flow in the Nordic Power System does not start with a perfect steady power flow. These discrepancies were aggravated by the dynamic models if the initialisation values were not the same as from the Loadflow calculation. The output of the converter controlling the P is more robust and led to a more stable initialization. It is uncommon to have the receiving end controlling the active power, but preferred in weaker grids. Furthermore, as explained in section 2.4, some authors found that the synthetic inertia has

a better performance with the P control than the Vdc control. The converters connected to the Nordic Power System have the power control mode and the converters connected to external grids have the responsibility of maintaining the DC voltage.

- The *Q/Vac Control* regulates either the reactive power or the AC voltage in the same manner as the P/Vdc block, i.e. with PI control. Unlike the P/Vdc control block, it is not necessary to have both controls active in a VSC-HVDC link. In this case, both the converters connected to the Nordic Power System as the converters connected to the external grids regulate the reactive power. Furthermore, it is operating in droop control mode, so the reactive power is influenced by the AC voltage. This helps stabilizing the voltages in the Nordic Power System and gave a quicker steady state in the RMS simulation.
- The last control block in the outer controller is the *Fault Ride Through Controller*. It receives the active and reactive power signals from the P/Vdc and Q/Vac control blocks and sends them to the the inner loop control if there is no system fault. During a system fault, the q control is adjusted proportional to the voltage drop to help with voltage regulation. For models in unbalanced simulation with unbalanced controls, asymmetric faults can also be regulated.

The **Inner Loop Control** consists of three parts. First, the *Current Limiter* checks the reference values and decreases it if it is above predefined limits. The *Current Controller* regulates the measured direct and quadratic currents with the reference signals from the inner control using PI control and translate them into reference voltage signals. Again the signal is checked if it's not to high in the *Output Limiter* block.

The HVDC converter has the option to operate in an islanded mode i.e. for handling of an offshore grid. Instead of following the frequency and voltage it forms it. The **Islanded Control** circumvent the inner and outer controls, but uses the signals to regulate the active and reactive powers and send it to the **Operational Mode Selector** which selects which of the signals to send to the converter according to which mode is in service.

3.5 Evaluation 60% NSG scenario to a small frequency event

To show the dynamic performance of the system, a sudden load increase of 10% at Oslo (OSL) is simulated at t = 5 s. This results in a power deficiency of 374 MW. The total load in the system is 36.2 GW. The electrical frequency at FED, OSL, PIK, RSG and SDR is shown in figure 3.16. A map of the locations is presented in 3.17. As can be seen in figure 3.16, rotor swings occur close to the fault, in PIK the rotor swings are not visible. The figure indicates different inertia levels of the areas by various RoCoF at the start. The frequency dip is reached at 7 seconds, whereas the quasi steady state is reached after 25 seconds after the fault. This is in the range described by [14].

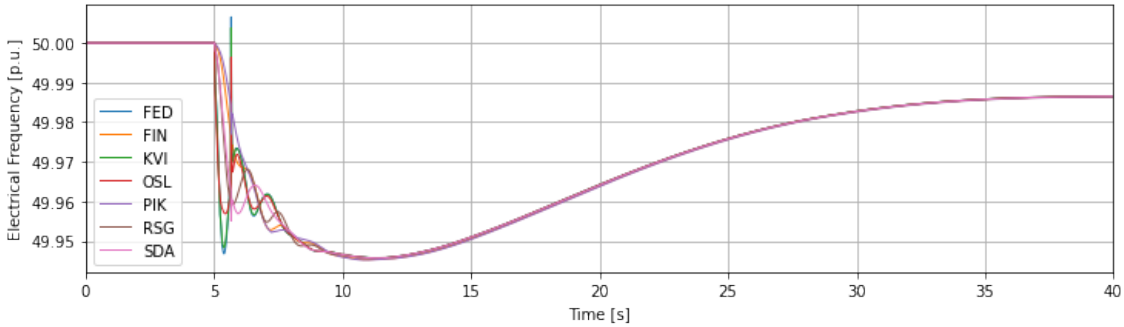

Figure 3.16: Frequency response at geographical dispersed locations after a sudden load event of 10% at OSL resulting in a power deficit of 374 MW.

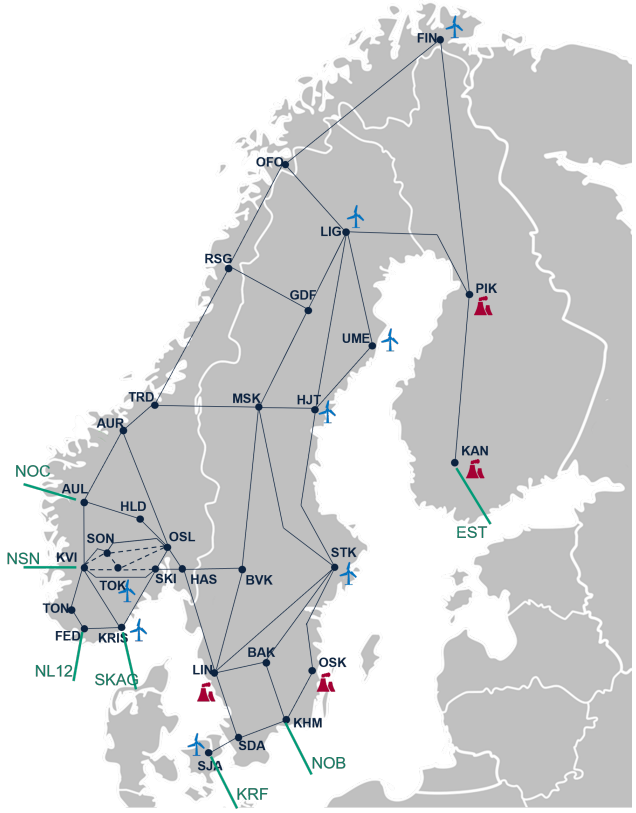

Figure 3.17: Distribution of generation types for the 60% NSG scenario. Wind farms and thermal generation are indicated by the blue and red symbols respectively. Nodes without a symbol have Hydro generation. The green lines represent the VSC-HVDC import.

To compare the dynamic models of the different production types, the frequency and voltage response at the output of the thermal, hydro and wind is described in the following section. For each case the generators are subject to the same load event, i.e. the sudden load increase of 10 % at Oslo.

3.5.1 Dynamic response of hydro synchronous generators

Figure 3.18a shows the frequency response of the hydro generators at OSL, HSL, HLD and SKI. Because of the close proximity to each other, the frequency response is similar. There is a small overshoot in the first swing. Figure 3.18b shows the voltage characteristic of the hydro generators at OSL, HSL, HLD and SKI. As can be seen in figure 3.4 the locations are all in close proximity of the fault location OSL. Voltage oscillations in the first few seconds are quickly restored. The initial voltage is not restored, but a constant voltage level is reached after 40 seconds.

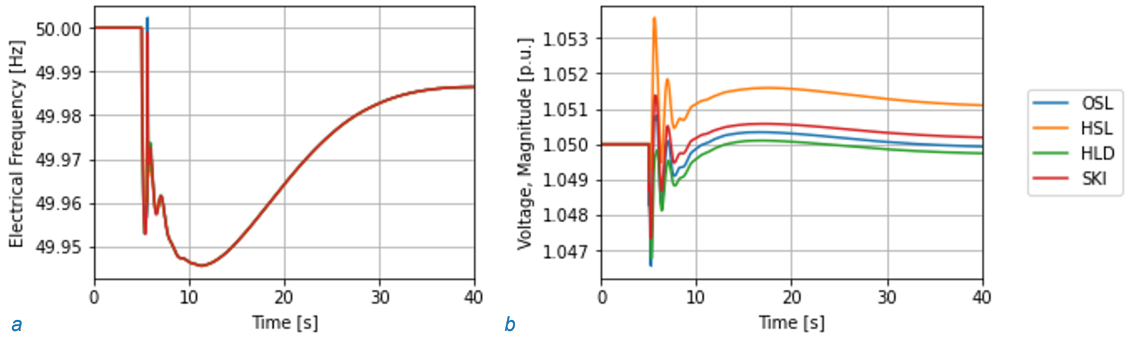

Figure 3.18: a) Frequency response of OSL, HSL, HLD and SKI after a 10% load increase in OSL. OSL, HSL, HLD and SKI have a dynamic model representing a Hydro generator. Measurements are taken from the synchronous generator. b) Voltage response of OSL, HSL, HLD and SKI after a 10% load increase in OSL. OSL, HSL, HLD and SKI have a dynamic model representing a Hydro generator. Measurements are taken from the generator.

3.5.2 Dynamic response of thermal synchronous generators

Figure 3.19a shows the frequency response of the generators with a dynamic model representing a thermal power plant. As the generators are further apart, the frequency response differs in the first couple of seconds. The voltage response of the busses with thermal generation is depicted in figure 3.19b. Compared with the hydro generation models, voltages take longer to get to the quasi steady state. Furthermore there is an overshoot.

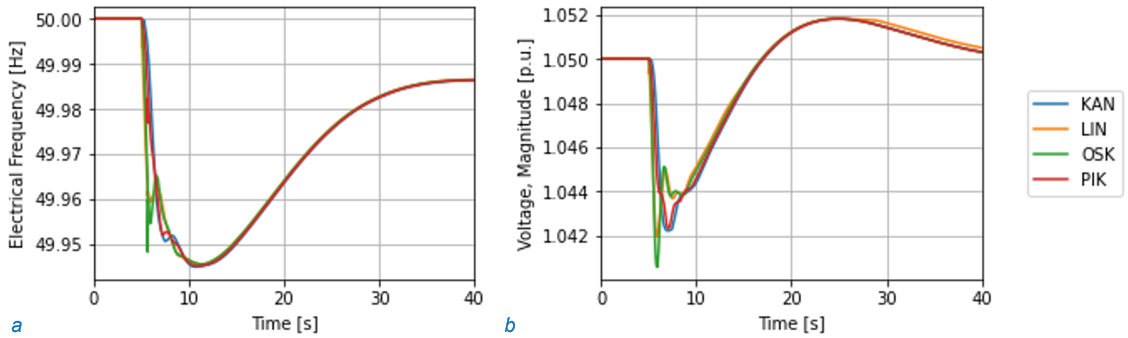

Figure 3.19: a) Frequency response of KAN, LIN, OSK and PIK after a 10% load increase in OSL. KAN, LIN, OSK and PIK have a dynamic model representing an Thermal generator. Measurements are taken from the synchronous generator. b) Voltage response of KAN, LIN, OSK and PIK after a 10% load increase in OSL. KAN, LIN, OSK and PIK have a dynamic model representing a Thermal generator. Measurements are taken from the synchronous generator.

3.5.3 Dynamic response of static generators with a dynamic wind control model

Figure 3.20a depicts the frequency of the busses with WT. Compared to the figure 3.18 and 3.19, the frequency in the first few seconds after the event show many oscillations and high values of RoCoF. This can be explained by the fact that there is no natural inertia at busses with wind. Figure 3.20b shows the voltage response of all wind turbines. KRI and TOK are smaller wind turbines that are surrounded with synchronous generators and the voltage at those points are quickly restored. The voltage characteristics of STK, UME, HLT, FIN and LIG have similar developments. UME experiences the biggest voltage dip. As can be seen in figure 3.17, UME is solely connected with nodes that have wind generation. As explained in section 3.4.4, the wind turbines do not partake in voltage regulation. The control system is only regulating the reactive power output to remain at initial value.

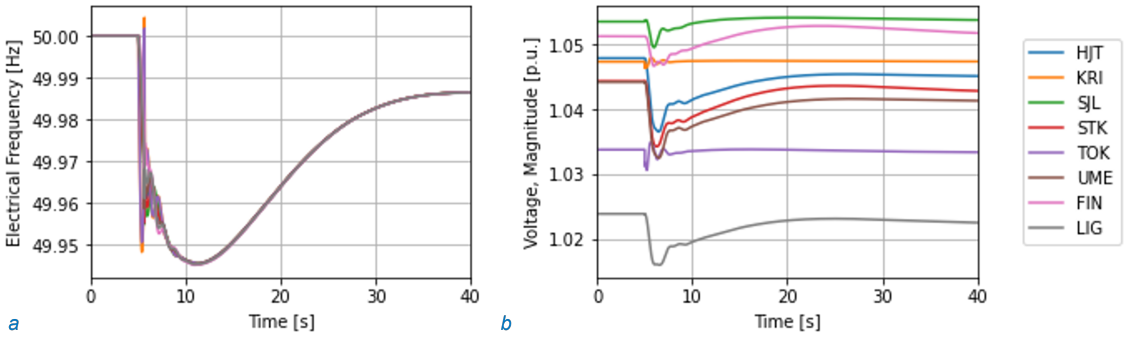

Figure 3.20: a) Frequency response of static generators with wind models after a 10% load increase in OSL. Measurements are taken from the LV bus of the static generator. b) Frequency response of static generators with wind models after a 10% load increase in OSL. Measurements are taken from the LV bus of the static generator.

4 Effect of Fast Frequency Response on frequency performance

In this chapter the effectiveness of the Fast Frequency Response (FFR) of the VSC-HVDC and the WT are analyzed. First, the critical disturbance is found in chapter 4.1. The disturbance is then used to analyze the frequency responses of the VSC-HVDC links and the WTs. Section 4.2 explains the two control models. Section 4.3 continues with the optimization of the values of the control parameters. Finally, section 4.4 concludes with an analysis of the combinations of elements participating in FFR.

4.1 Investigation into critical disturbances

The purpose of this section is to find the disturbance in the 60% NSG operational scenario that leads to the highest MDF values.

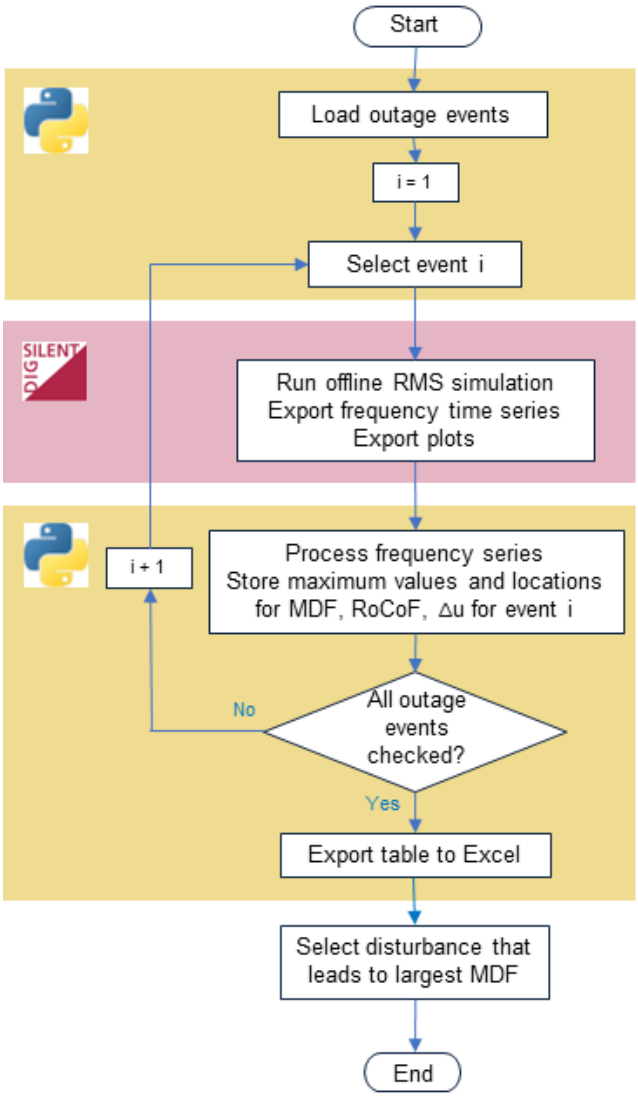

Figure 4.1: Procedure of selection of critical disturbance. The action points in the yellow areas are conducted with Python, the action point in the red area is done with PowerFactory

The procedure to select the critical disturbance is shown in figure 4.1. It is an iterative process using an external Python script whereby one element at a time is the subject of an outage event during an RMS simulation. The elements that are simulated to be out of service include the WTs, the synchronous generators, and the VSC-HVDC. After each simulation of 40 s, figures with the frequency, voltage magnitude, and voltage angle at each generator output were exported.

Additionally, from the time series data of the electrical frequency, the derivative of the electrical frequency and voltage magnitude of each generator output worst cases were selected and stored together with the name of the corresponding bus. When all the events are simulated, an excel sheet containing the value and location of the largest voltage and frequency deviation and highest absolute RoCoF is exported. The selection of the critical disturbance is done using this excel sheet and with a visual inspection.

Visual inspection was necessary because electrical frequency signals have spikes that do not represent the overall frequency. The biggest frequency deviation repeatedly occurred during the first, local, rotor swing, which did not give information on the MDF of the system. Moreover, oscillations after the first swing can indicate a lack of damping, and pole slips are shown in the rotor angle series, which would represent problems other than frequency.

The outage events resulting in the largest MFD are shown in table 4.1. The locations of the AC nodes can be found in figure 4.2.

Table 4.1: Outage events that resulted in the largest MDF

Case	Outage of generation	P [GW]	Min Freq [Hz]	Node min Freq	RoCoF [Hz/s]	Node RoCoF
1	KAN	3.15	35.7	FIN	-26.0	FIN
2	GRU	3.15	47.0	FIN	-4.0	FIN
3	PIK	1.23	47.3	FIN	-3.9	FIN
4	LIN	2.27	48.7	STK	-2.6	STK
5	STK	2.32	49.1	UME	-1.6	UME
6	NSN2	1.5	49.6	FED	-0.4	KRIS

Of these cases, the following were rejected:

1. Cases 1, 2, 4, and 5 are rejected because the size of the fault is unlikely. The power output at these locations is above 2000 MW. This is aggregated generation in an area and does not present a single unit. As the current dimensioning event is at 1450 MW, they are rejected for the case.
2. Case 3 is rejected as a critical disturbance because the frequency is only extreme at local busses, and is not felt in the rest of the system. This can be seen in figure 4.3a which shows the frequency response at different locations for the outage event of PIK. Figure 4.3a shows that FIN and PIK have spikes, but the frequency in the rest of the grid has less frequency deviation than the case where NSN2 is taken out of service, shown in figure 4.3b.

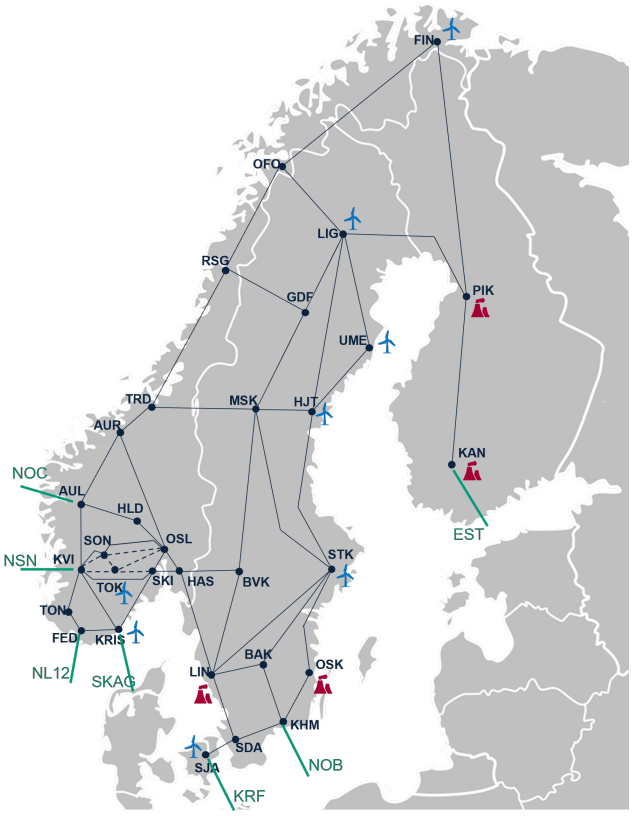

Figure 4.2: Distribution of generation types for the 60% NSG scenario. Wind farms and thermal generation are indicated by the blue and red symbols respectively. Nodes without a symbol have Hydro generation. The green lines represent the VSC-HVDC import.

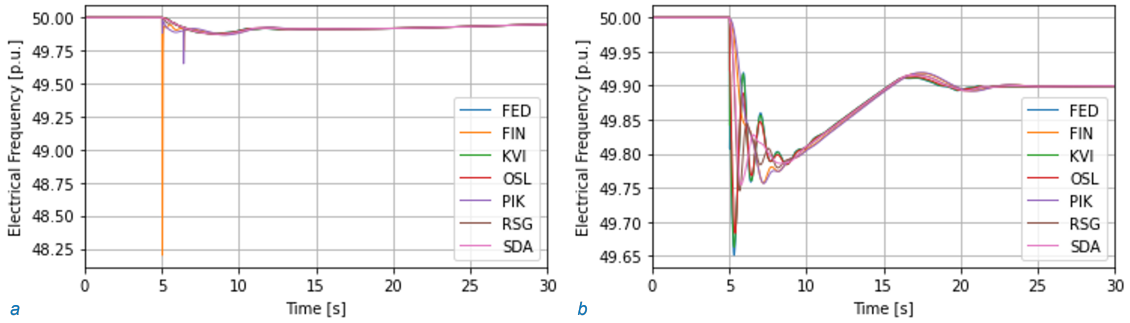

Figure 4.3: a) Frequency response in FED, FIN, KVI, OSL, PIK, RSG and SDA for an outage event of the generation in PIK. b) Frequency response in FED, FIN, KVI, OSL, PIK, RSG and SDA for an outage event of the NSN2 HVDC link,

The frequency spikes in figure 4.3a, shows instability in the north of the Nordic Power System. FIN also is the location with the biggest frequency deviations and RoCoF for the first five cases. FIN has no inherent kinetic energy and is surrounded by other WT areas. The system strength, calculated as the ratio of the short circuit power and the nominal active dc power for the different wind turbines is shown in table 4.2. As explained in section 2.6, the Short Circuit Ratio (SCR) demonstrates how sensitive the voltage is at that location for a difference in load. The SCR does not take into account the proximity of other NSG. The sensitivity of FIN may be explained because of high impedance caused

by long transmission lines, transmission voltage differences and the fact that the grid is not meshed in the north.

Table 4.2: Short Circuit Ratio value of Wind Turbines

	FIN	HJT	KRI	LIG	SJL	STK	TOK	UME
SCR	2.6	13.3	32.9	8.7	28.0	5.9	28.7	9.2

An outage of NSN2 is chosen as the critical disturbance. Figure 4.4 shows the frequency after the NSN2 event measured at the output of the synchronous generators in four areas. The largest deviation measured in the system is in FED (Feda). After 20 seconds, the frequency reaches a SSFD of 49 Hz, which is only just in the FCR-N band. The different RoCoFs show the heterogeneity of the system.

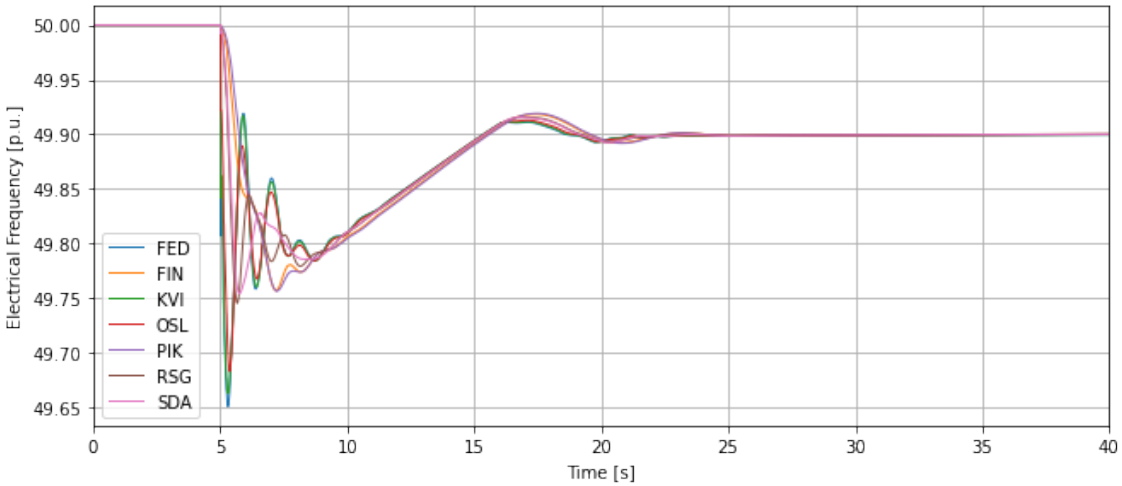

Figure 4.4: Frequency at in different locations for an outage event of the HVDC link NSN2, measured at the output of the synchronous generators

4.2 Fast Frequency Response control models

4.2.1 Fast Frequency Response control for WT: Emulated Inertia

In order to add Fast Frequency Response control to the WT, a supplementary Common Model is added to the Composite Frame of the WT. The control in the Common Model calculates a supplementary power output to react to the frequency event. The reference value $P_{\text{ref, emu}}$ is then summed with the reference values of the PQ controller. The adjusted Composite Frame is shown in figure 4.5. An explanation of the original Composite Frame is given in section 3.4.4.

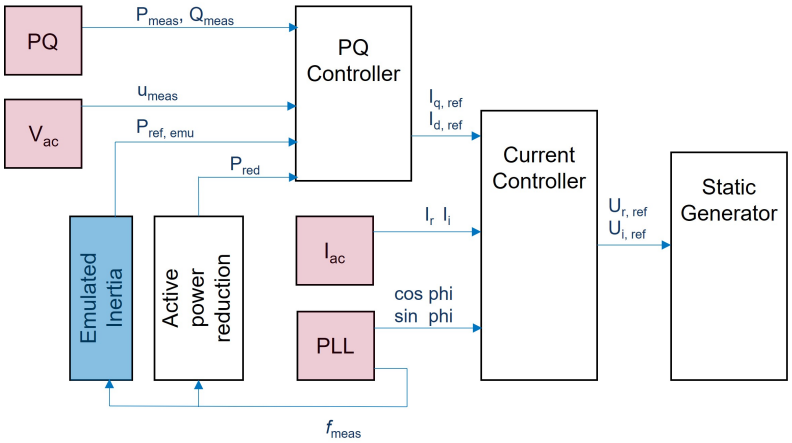

Figure 4.5: Composite Frame of the Fully Rated Converter Wind model by [42]. Measurement devices are depicted in pink, the added emulated inertia block is depicted in blue.

The Fast Frequency Response takes the form of the Emulated Inertia (EI) model developed by ENERCON and is currently used in Quebec[3]. It has shown to work for multiple operating points. As mentioned in section 2.4, the energy of fast power response for WT comes from changing the pitch angle to allow for operation above rated wind speed. Below rated wind speed, energy is extracted from the rotational energy of the wind turbines. This causes the wind turbines to slow down and a recovery period of acceleration is needed before rated power can be achieved. During this recovery period, the grid experiences a second frequency drop as the power output of the WT is not optimal and therefore lower than prefault values [3]. Because the Fully Rated Converter model of DIgSILENT neither has a pitch controller nor models fluctuating wind, the recovery period is not taken into account in this model.

Figure 4.6 shows the EI control. The input signal is the frequency ($f(t)$) measured by the Phase Lock Loop. The output signal is the reference value $P_{\text{ref, emu}}$. The control block can be summarized with the following equation:

$$P_{\text{ref, emu}} = \frac{f_{\text{trigger}} - f(t)}{f_{\text{trigger}} - f_{\text{pinmax}}} P_{\text{emu}} \tag{4.1}$$

P_{ref} [p.u.] is the reference value created by the control block, f_{trigger} [Hz] is the frequency at which the emulated inertia is turned on, f_{pinmax} [Hz] is the frequency extent for which the maximum power is released and P_{emu} [p.u.] is the maximum value of the reference signal in p.u.. The EI block is supplying extra power over a predefined time period, i.e. the $T_{\text{inertia max}}$ [s].

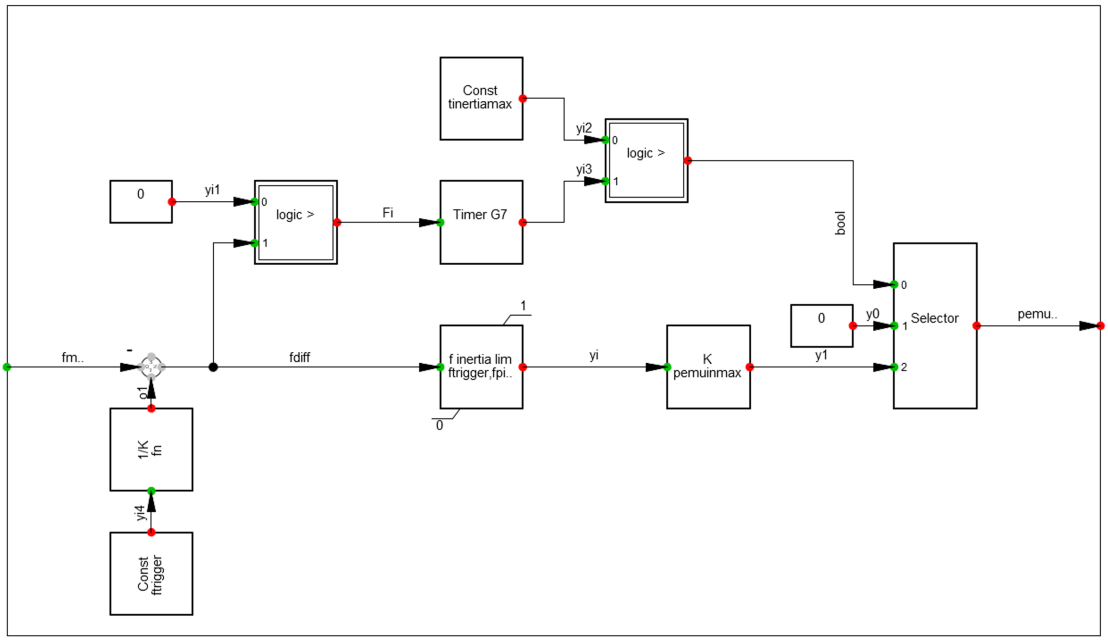

Figure 4.6: Emulated Inertia controller of the Enercon WT [3]

4.2.2 Fast Frequency Response Control for VSC-HVDC: Synthetic inertia

Fast Frequency Control for the VSC-HVDC links is modelled by the Synthetic Inertia (SI) control block. This is an optional setting of the VSC-HVDC model provided by DIgSILENT library.

Similar to the Fast Frequency control in the WT, the input is the frequency $f(t)$ measured by the PLL and the output is the reference value $P_{\text{ref, syn}}$. The reference value for the active power calculated is added to the reference value of the PQ controller in the outer controller of the Composite Frame of the converter. The SI control is based on the swing equation as and can be described with:

$$P_{\text{ref, syn}} = -\frac{2\text{H}}{\text{f}_{\text{nom}}}\frac{df(t)}{dt}$$

In order to covert the input signal $f(t)$ [Hz] to the RoCoF, the time constant Tf [s] is used. Because the IE block adjusts the power output proportional to RoCoF rather than frequency, it is subject to the 'derivative' classification. The inertia constant H and the time constant Tf can be chosen by the user. The default values are 5s voor H and 0.1 s for Tf.

4.3 Selection control parameter Fast Frequency Response

The procedure to select the optimal values of the Fast Frequency Response control blocks of the wind turbines and the VSC-HVDC converters is shown in figure 4.7. This is done for each VSC-HVDC and WT individually. As described in the chapter 4.1, the outage of NSN2 is chosen as the critical disturbance. As can be seen in the figure, the goal of this procedure is to select the parameters that lead to the smallest MDF at the output of the WT or the VSC-HVDC converter. This approach is us used as opposed to taking the worst MDF of the system because the FFR control blocks are modelled as local, primary control. All combinations of the parameters have been checked.

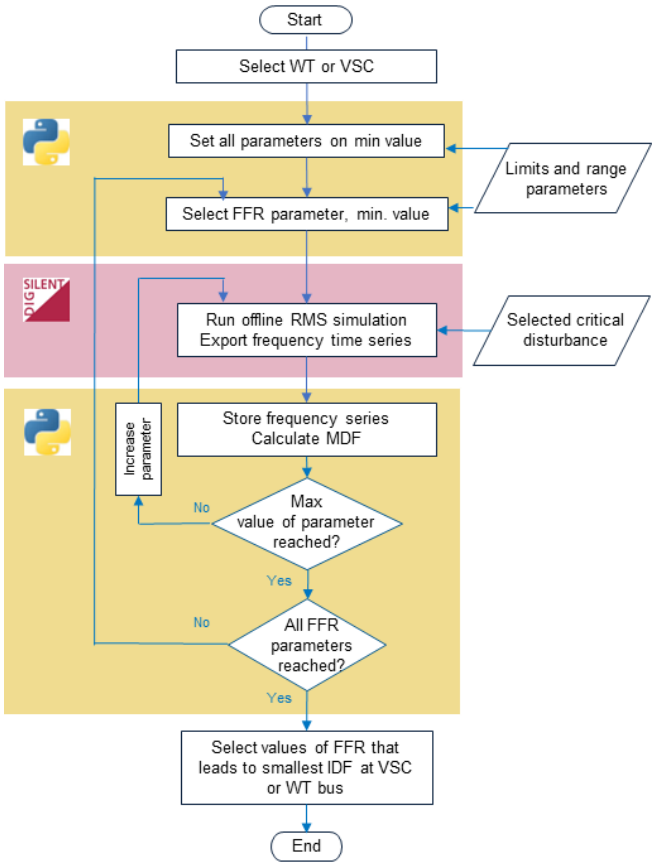

Figure 4.7: Selection Procedure of FFR variables. The action points in the yellow areas are conducted with Python, the action point in the red area is done with DIgSILENT PowerFactory

4.3.1 Optimization parameters FFR block wind turbines (WTs)

The control parameters for the FFR control of Wts were introduced in section 4.2. The range of the parameters are shown in table 4.3. The range for the frequency triggers ($f_{trigger}$, f_{pinmax}) are dependent on the freqyency containment policy of the TSO.

$f_{trigger}$ is the frequency at which the block start supplying power for frequency support. If the wind turbine partakes in FCR-N, the WT should continuously supply frequency support. This is not the design of this block; the wind turbine only supports during faults because it needs to recover afterwards. 49.95 was chosen as the maximum value. The minimum value is the frequency at which the FCR-D starts; 49.9.
f_{pinmax} is analysed in the range 49.9 - 49.5. f_{pinmax} cannot be higher or close to $f_{trigger}$ to prevent stability issues. The lower limit is required by the TSO. the Nordic TSOs state that the total extra active power should be released in 30 seconds after the frequency 49.5 Hz is reached [17], so f_{pinmax} is set at 49.5.

P_{emu} is the maximum gain which is constricted by the physical model. The maximum surplus power that a ENERCON wind turbine can deliver over nominal active power is 10%. This is represented in the maximum values in the Static Generator in PowerFactory. P_{emu}. Higher values will also lead to steeper active power slopes. Therefore, the maximum value is set on 0.2 in stead of 0.1. The minimum value is set on 0.05.

Table 4.3: Range of FRR parameters for sensitivity analysis

Parameter	minimum value	maximum value	reference value	unit
$f_{trigger}$	49.9	49.95	49.925	[Hz]
f_{pinmax}	49.5	49.9	49.7	[Hz]
P_{emu}	0.05	0.2	0.1	[p.u.]

Figure 4.8 illustrates the effect of $f_{trigger}$ on the frequency response of SJL WT for the outage event NSN2. The parameters that don't vary are set on a reference value for the figure, but all parameters were tested in the optimization procedure. The reference value can be found in table 4.3. Figure 4.8a shows the effect of different values of $f_{trigger}$ on the active power output of the WT. $f_{trigger}$ determines when the control is activated and how much power is supplied to the grid. As can be seen in figure 4.8b, the effect of an individual EI on the frequency is small. Higher values for $f_{trigger}$ lead to lower MFD values, and lower frequency during the entire time that the WT supplies FFR.

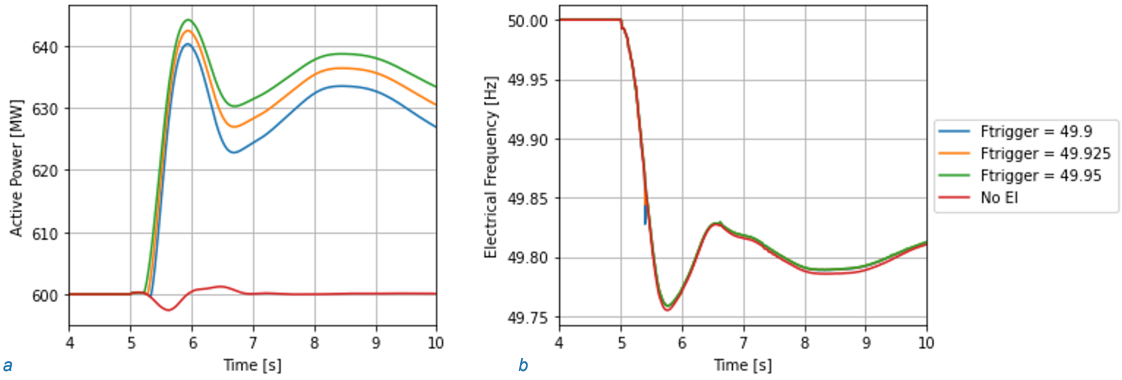

Figure 4.8: a) Effect of different values of $\mathbf{f_{trigger}}$ on the power output of SJL WT after an outage disturbance of NSN2. b) Effect of different values of $\mathbf{f_{trigger}}$ on the frequency at SJL WT after an outage disturbance of NSN2.

Figure 4.9a shows the effect of f_{pinmax} on the power output of SJL WT for the outage event NSN2. The value of f_{pinmax} determines the shape and the amount of power output, and the slope in the beginning, which can be explained with equation 4.1. If f_{pinmax} is 49.9, the power output will not get higher than 660 MW, which is the maximum output of the wind turbine. Figure 4.9b shows the effect of f_{pinmax} on the frequency at SJL WT. Higher values of f_{pinmax} lead to less frequency deviation. There is a small spike at 5.3 s, which is worse for lower values of f_{pinmax}.

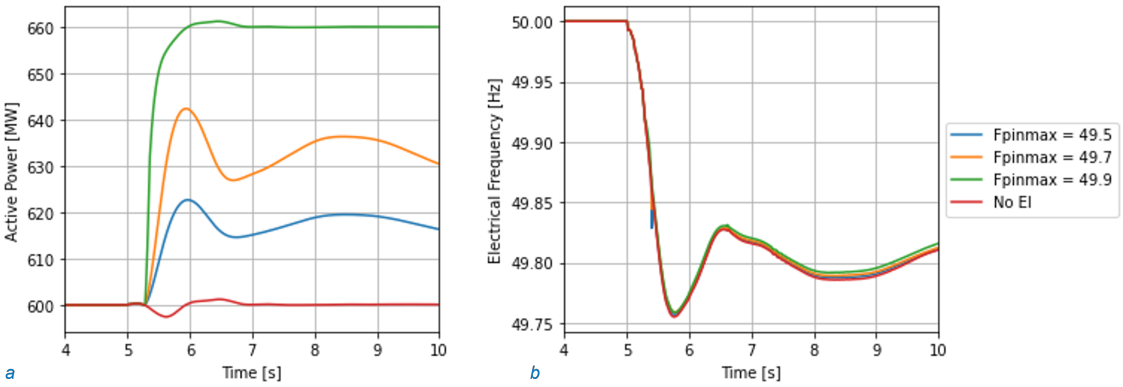

Figure 4.9: a) Effect of different values of $\mathbf{f_{pinmax}}$ on the power output of SJL WT after an outage disturbance of NSN2. b) Effect of different values of $\mathbf{f_{pinmax}}$ on the frequency at SJL WT after an outage disturbance of NSN2.

Figure 4.10a shows the effect of P_{emu}. on the power output of SJL WT for the outage event NSN2. Only the gain of the emulated power is influenced by P_{emu}. Again, the power output is capped by the maximum active power of the wind turbine. Figure 4.10b shows the effect of P_{emu} on the frequency. As expected, is the power output higher for higher values of P_{emu} which results in better frequency values.

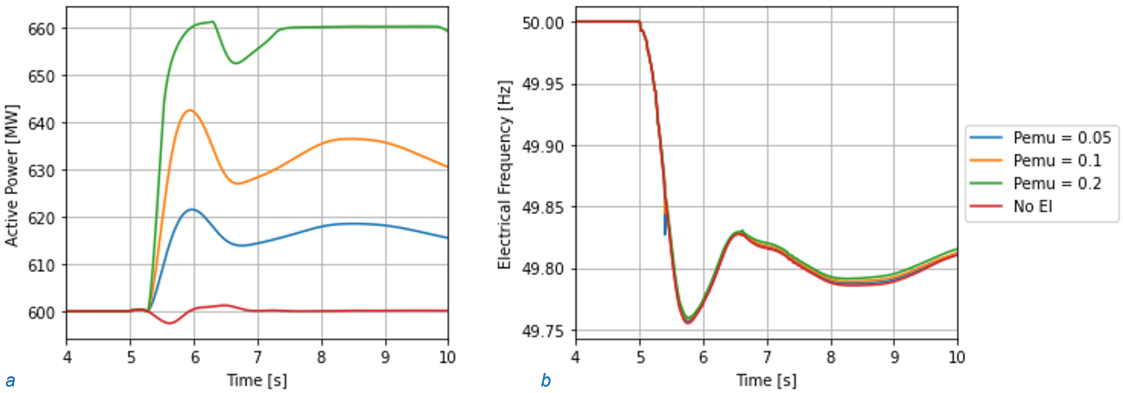

Figure 4.10: a) Effect of different values of $\mathbf{P_{emu}}$ on the power output of SJL WT after an outage disturbance of NSN2. b) Effect of different values of $\mathbf{P_{emu}}$ on the frequency at SJL WT after an outage disturbance of NSN2.

The optimal values per WT is presented in table 4.4.

Table 4.4: Result of parameter optimization of the lowest MDF at the output of the WT supplying FFR

WT	$f_{trigger}$ [Hz]	f_{pinmax} [Hz]	P_{emu} [p.u.]
FIN	49.95	49.7	0.05
HJT	49.95	49.5	0.2
KRI	49.9	49.7	0.1
LIG	49.95	49.5	0.1
SJL	49.9	49.7	0.2
STK	49.95	49.5	0.2
TOK	49.9	49.7	0.1
UME	49.95	49.7	0.05

As can be seen in table 4.4, the parameters that lead to the higher power output, such as high gain values of P_{emu}, did not always result in the best frequency performance. In some cases, too high gains resulted in power and frequency spikes. An example of the spikes in power output and in the measured frequency is seen in figure 4.11a and 4.11b respectively. As can be seen in figure 4.11a, only the value of 0.5 P_{emu} lead to stable operation.

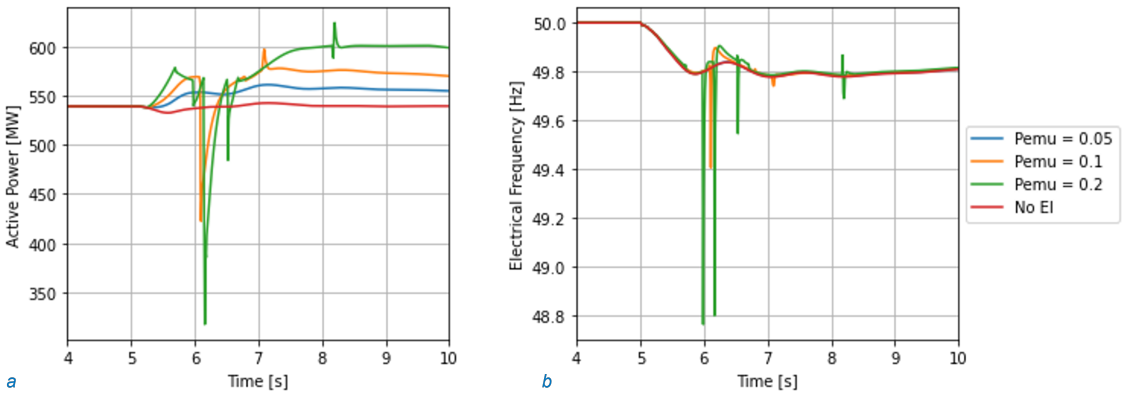

Figure 4.11: a) Power output of WT UME for different values of P_{emu}. b) Frequency response of WT UME for different values of P_{emu}

The spikes were especially seen at UME, FIN and HJT. A possible explanation is that the short circuit ratio is small in the north of the Nordic Power System, indicating voltage sensitivities. This could result in bad capability of the PLL to track the voltage angle, and therefore control the powers adequately. The effect of system strength is explained in section 2.6. The optimization weeded out the control settings that lead to power frequency spikes as illustrated in figure 4.11. The difference between the best value of P_{emu} and no Emulated inertia is less than 0.05 % for all cases.

Longer emulated inertia power will improve the frequency of the system. Therefore, the parameter $T_{inertia\ max}$ is set on its upper limitation (20s). The caused by the physical limitations of the wind turbine. Note that longer time has a detrimental effect on the second frequency dip caused by the recovery period of the wind turbine, which is not considered in this model.

4.3.2 Optimization parameters FFR block VSC-HVDC

The same procedure was used to find the best parameters for the FFR block for VSC-HVDC. The FFR of the VSC-HVDC is the Synthetic Inertia (SI) control, with the parameters H and Tf, as explained in chapter 4.2.2. The inertia constant H determines the gain of the frequency, whereas Tf determines how fast it reacts. For H(s) were checked 4, 5 and 6. The values for Tf were 0.05, 0.1 and 0.5. The output of the VSC-HVDC is mainly limited by ramp limits set by the TSO. In the VSC-HVDC model, this is controlled in the Output Limiter block as explained in Chapter 3.4.5. The SI control block of each VSC was optimized with the objective to minimize the frequency at the HV bus of the HVDC link.

Figure 4.12a show the power output for different values of H at NSN1. Tf was set on the default value for the figure. All parameters were tested during optimization. Figure 4.12a clearly indicates that H is a gain. Figure 4.12b shows the corresponding frequency at the NSN1 bus. Higher values for H result in lower frequency deviations. The frequency response starts directly after the fault, and its decreases not only the MFD, but the frequency swings as well.

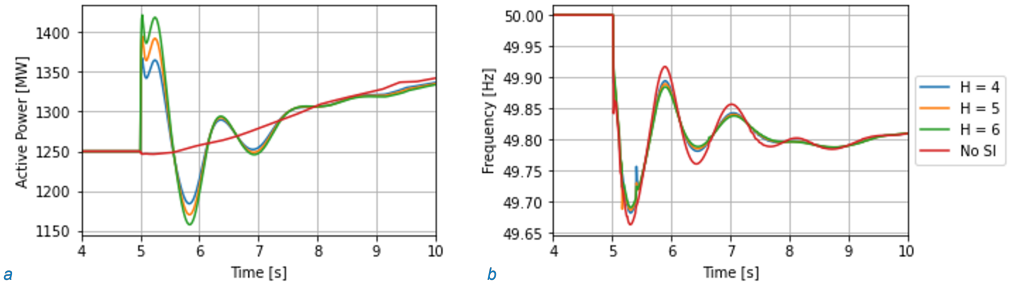

Figure 4.12: a) Power output of NSN1 after NSN2 outage for different values of H. Tf was set on 0.1.
b) Frequency measured at NSN1 after NSN2 outage for different values of H. Tf was set on 0.1

Figure 4.13a show the power output for different values of Tf at NSN1. Figure 4.12a shows that Tf influences the delay of the output. This results that the power output is also lower in lower power outputs. Figure 4.13b shows the corresponding frequency at the NSN1 bus. The smallest deviations are with low values for Tf.

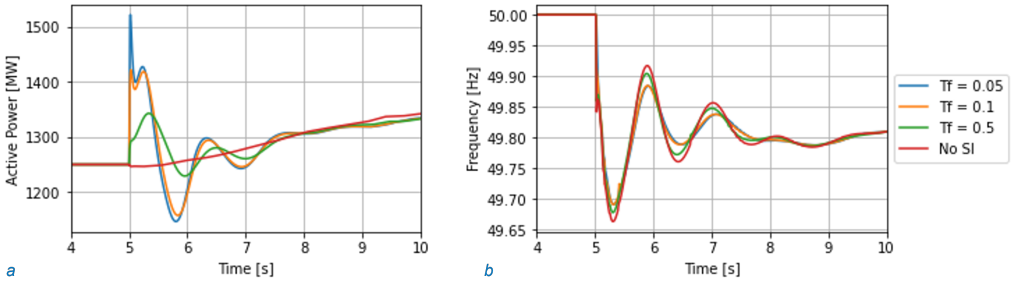

Figure 4.13: a) Power output of NSN1 after NSN2 outage for different values of Tf. H was set on 6.
b) Frequency measured at NSN1 after NSN2 outage for different values of Tf. H was set on 6

The optimization was done for each VSC-HVDC link. As expected, the highest value of H resulted in the smallest frequency deviation.The optimization of Tf resulted in different optimal values for each HVDC link. The best values for Tf and the distance to the fault is shown in table **??**. As can be seen in the table, higher values of Tf gave better results if the VSC was located further from the event. The RoCoF is always highest at the start of a frequency event. The time at which the MDF happens, is generally later for locations further away. Thus, the VSC-HVDC links benefit from higher TF values.

Table 4.5: Result of parameter optimization of the lowest MDF at the output of the VSC-HVDC supplying FFR

VSC	H [s]	Tf [s]	Distance [km]
EST	6	0.5	2400
KRF	6	0.5	870
NL1	6	0.1	160
NL2	6	0.1	160
NSN1	6	0.05	0
NOB	6	0.5	920
NOC	6	0.1	180
SK4	6	0.1	180
SK51	6	0.1	180
SK52	6	0.1	180

4.4 Effect FFR control WT and VSC-HVDC on frequency after critical disturbance

In the section the effectiveness of the different fast power control blocks, i.e. Emulated Inertia (IE) of the WT and Synthetic Inertia (SI) of the VSC-HVDC is described. This is tested on the largest frequency deviation after the disturbance of the NSN2 which is found at FED. First, the FFR of WTs is evaluated in section 4.4.1. The FFR of the VSC-HVDC links follows in section 4.4.2. Lastly, 4.4.3 compares the effect of the WT FFR with the VSC-HVDC FFR, and evaluates different combinations of NSG supplying FFR. In 4.4.3 the performance indices, introduced in chapter 2.2, are used.

4.4.1 Effect FFR of WT on frequency in FED

Table 4.6 shows the performance of the FFR control of the individual wind turbines on the MFD in FED. In each case, only the specific WT is participating in FFR. The prefault active power output of the WTs and the distance to FED are presented in table 4.6. TOK and KRI are the closest WTs to FED and are the best performing WTs followed by the largest WT farm in the system, that of STO. FIN, LIG, and SJL do not contribute to the frequency improvement at FED.

Table 4.6: Performance indices of the FFR control of the individual WT on the frequency of FED. The distance is to FED

	WT	Distance [km]	P [MW]	Frequency improvement [mHz]
1	KRI	75	150	2.62
2	TOK	260	198	2.51
3	STO	955	2330	0.45
4	HJT	1085	810	0.44
5	UME	1235	550	0.22
6	FIN	2315	240	0
7	LIG	1435	732	0
8	SJL	785	600	0

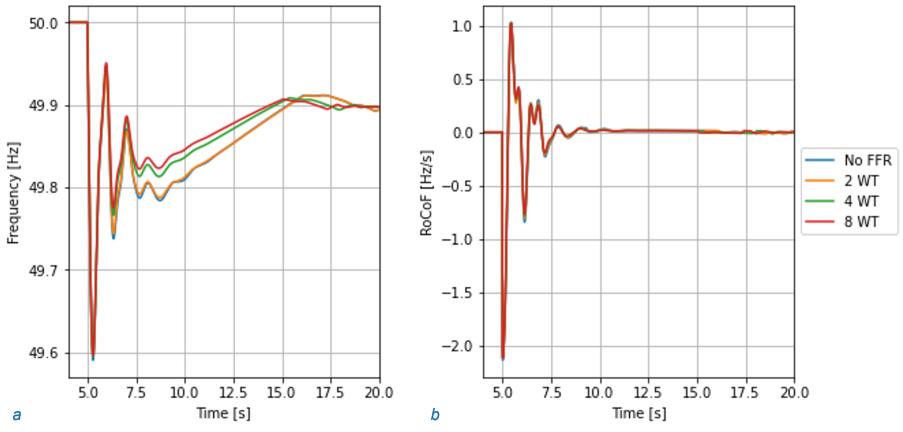

Figure 4.14: a) Frequency at FED with no, 2, 4, and all WTs applying FFR. b) RoCoF at FED with no, 2, 4, and all WTs applying FFR

Figure 4.14a shows the frequency at FED for cases with an increasing amount of WTs applying FFR. In each case, the WTs that supply FFR are the ones that lead to the biggest frequency improvement. For example, the WTs with indices 1, 2, 3, and 4 in table 4.6 are

in service in case 4WT. The figure illustrates that the FFR control of the WTs has little influence on the frequency in the first rotor swing. The control blocks do not contribute to the inherent inertia of the system and the activation is delayed till the frequencies of the WTs are smaller than the $f_{trigger}$. Figure 4.14a shows that FFR of WTs has greater impact after 2 seconds on the frequency and the recovery time is smaller with more WT's implementing inertia. Figure 4.14b shows the RoCof at FED with WTs supplying FFR. The FFR of the WT does not influence RoCoF. The RoCoF is higher than admissible by the TSOs and in this case, the loads will start to shed.

4.4.2 Effect FFR of VSC-HVDC on frequency in FED

Table 4.7 shows the frequency improvement by the individual VSC-HVDC partaking in FFR control. The utilization of Synthetic Inertia FFR control of the individual VSC-HVDC links results in greater frequency improvements than the Emulated Inertia FFR control of the WTs. NL2 is connected to the FED HV bus and has the greatest impact. NSN1 is next to the disturbance and is one of the bigger size links. EST barely contributes to frequency improvement in FED.

Table 4.7: Effect of FFR control blocks of individual VSC-HVDC on MFD in FED ranked on performance. The distance is relative to FED

	HVDC	Distance [km]	P [MW]	Frequency improvement [mHz]
1	NL2	0	1200	55.12
2	NSN1	160	1250	40.09
3	SK51	75	900	26.34
4	SK52	75	900	26.34
5	NL1	0	600	21.05
6	NOC	340	1300	18.97
7	SK4	75	600	19.96
8	NOB	835	600	0.11
9	KRF	785	500	0.09
10	EST	2315	300	0.02

Figure 4.15a shows the impact of multiple simultaneous used FFR blocks of VSC-HVDC links on the frequency at FED after the outage of NSN2. In each case, the chosen VSC-HVDCs that supply FFR are the ones that lead to the biggest frequency improvement. Figure 4.15a shows that already the utilization of FFR of three VSC-HVDCs decreases the frequency significantly. The synthetic inertia blocks also dampen the oscillations in the first 5 seconds after the fault. The recovery time of the frequency is slightly larger if the FFR of the HVDC links is employed. Figure 4.15b shows the impact of multiple simultaneous used FFR blocks of VSC-HVDC links on the RoCoF at FED after the outage of NSN2. The worst RoCoF, at the beginning of the fault, is decreased to a value that is smaller than the absolute value of 2 Hz/s. FFR of VDC-HVDC also positively influences the RoCoF swings.

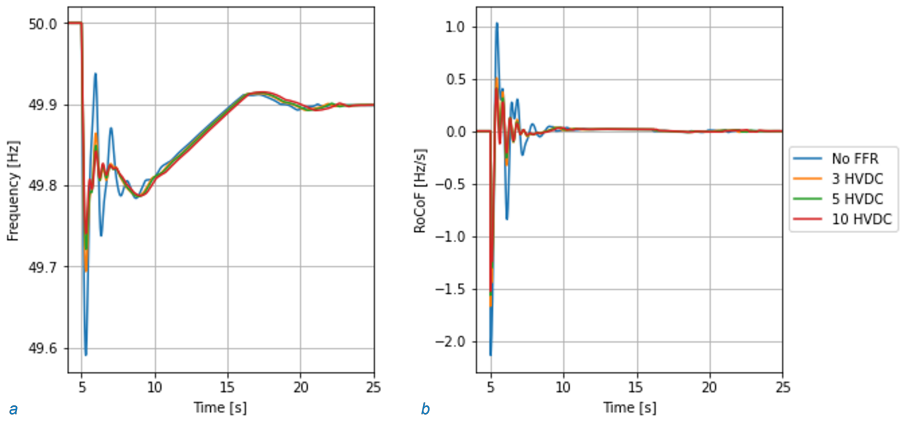

Figure 4.15: a) Effect of the amount of VSC-HVDC links applying SI on the frequency measured in FED. b) Effect of the amount of VSC-HVDC links applying SI on the RoCoF measured in FED.

4.4.3 Combination of WT and HVDC supplying FFR

As mentioned in the previous sections, not every FFR supplying unit has an equally significant impact on the frequency in FED. In this section, different combinations of FFR supplying units are evaluated. A distinction is made in location, size, and kind of FFR, i.e. the IE of the wind turbines or the SI of the VSC-HVDC links. The size and the locations of the WTs and VSC-HVDC links are given in table 4.6 and 4.7 respectively. An description of the combinations is given in table 4.8.

Table 4.8: Combination of FFR supplying generation units

Name	Description	FFR supplying units
All WT	All WTs	-
Loc WT	The 2 closest WTs	TOK, KRI
Size WT	The 2 biggest WTs	STK, HJT
All HVDC	All VSC-HVDC links	-
Loc HVDC	The 2 closest HVDC	NOC, NSN1
Size HVDC	The 2 biggest HVDC	NL1, NL2

The performance indices Maximum Frequency Deviation Index (MFDI), Total Frequency Deviation Index (TFDI), and Frequency Recovery Time Index (FRTI) are used to evaluate the FFR control blocks. The equations for the performance indices can be found in section 2.2. The recovery time is calculated as the first time that the frequency doesn't deviate from the quasi steady state 49.9 ± 0.005 Hz. The simulation time in the FRTI is set on 20 seconds. The deviation indexes show how close the frequency is to its limits, with zero being the lowest number, and one having crossed the limit. The performance indices for the case without any FFR are used as a benchmark, the measurement of the frequency is in FED.

First, the combinations with the best location and size for the WTs are compared. The results are shown in table 4.9. As can be seen in table 4.9, all performance indices are improved with each combination of FFR by WTs. The location improves the worst frequency, seen in a lower value of MFD, whereas the size of the WTs improves the recovery time (FRTI) and the total frequency deviation (TFDI). The different frequency responses at FED for the different combinations are also shown in figure 4.16. Figure 4.16 endorse the results in table 4.9.

Table 4.9: Performance indices of combinations of WT supplying FFR supplying. The combinations are explained in table 4.8

Combination FFR	T_{rec}	FRTI	TFDI	MFDI
All WT	17.360	0.579	0.149	0.404
Loc WT	20.119	0.671	0.160	0.404
Size WT	18.137	0.605	0.153	0.409
No FFR	20.142	0.671	0.161	0.409

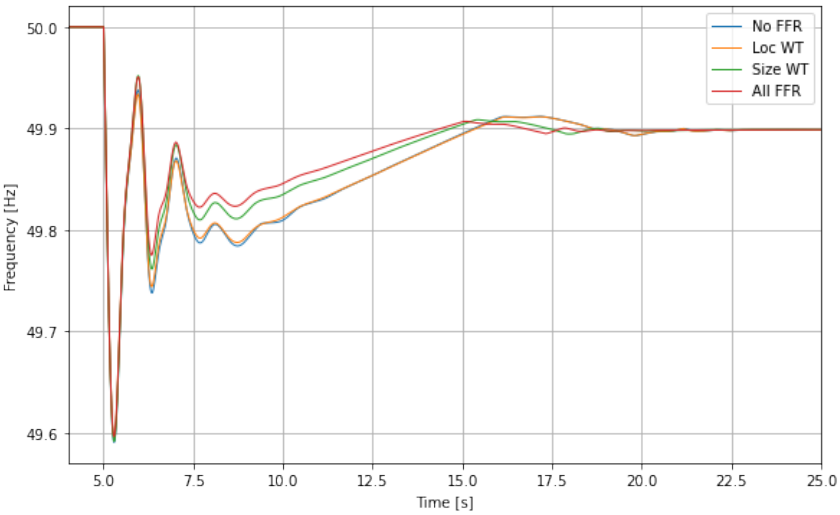

Figure 4.16: Effect of location and size of WT links applying FFR on frequency in FED

Second, the combinations with the best location and the combination with the biggest size of the VSC-HVDC links supplying FFR are presented in table 4.10. The recovery time is larger for each combination of HVDC links, and consequently, the FRTI is higher for all cases. Furthermore, the TFDI is not improved with the Synthetic Inertia blocks of the VSC-HVDC links. TFDI is calculated with the area of the frequency deviation. The area stays the same because the frequency swings are also diminished, as shown in figure 4.18. The MFDI index is better for the combination with the closest HVDC links.

Table 4.10: Performance indices of combinations of HVDC supplying FFR supplying. The combinations are explained in table 4.8

Combination FFR	T_{rec}	FRTI	TFDI	MFDI
All HVDC	21.923	0.731	0.161	0.259
Loc HVDC	20.675	0.689	0.161	0.338
Size HVDC	20.668	0.689	0.161	0.354
No FFR	20.142	0.671	0.161	0.409

The performance indicators of the frequency at FED for the combination of all FFR, FFR of all HVDC links, FFR of all WTs, and no FRR are presented in table 4.11. The frequency performance indicators show that the WT and the HVDC complement each other when supplying frequency support; the EI blocks of the Wind improve the recovery time and consequently the FRTI. Additionally, they improve the total frequency response shown in the indicator TFDI. The Synthetic Inertia control blocks of the HVDC links significantly improve the maximum frequency deviation, the MFDI.

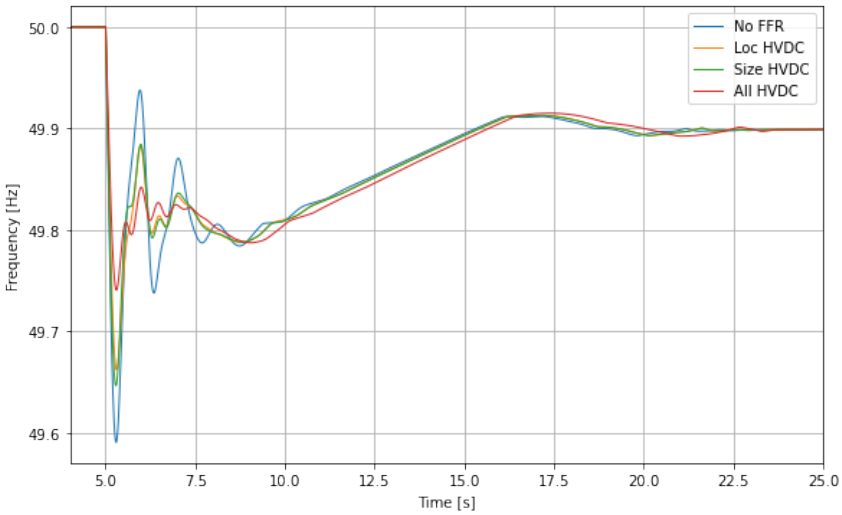

Figure 4.17: Effect of location vs size of VSC-HVDC links applying SI on frequency in FED

Table 4.11: Performance indices of combinations of HVDC and WTs supplying FFR supplying. The combinations are explained in table 4.8

Combination FFR	T_{rec}	FRTI	TFDI	MFDI
All	17.008	0.567	0.150	0.257
All HVDC	21.923	0.731	0.161	0.259
All WT	17.360	0.579	0.149	0.404
No FFR	20.142	0.671	0.161	0.409

The effect of the different control strategies of the WT (EI) and HVDC (SI) can also be seen in figure 4.18. Ye FFR control blocks of VSC and HVDC show better performance at different time frames; The HVDC-VSC improves the first $\pm$ 5 seconds after the fault and dampens the oscillations, whereas the effect of the WT is seen after the first rotor swings. By supplying extra power, the frequency is quickly restored to a steady state value.

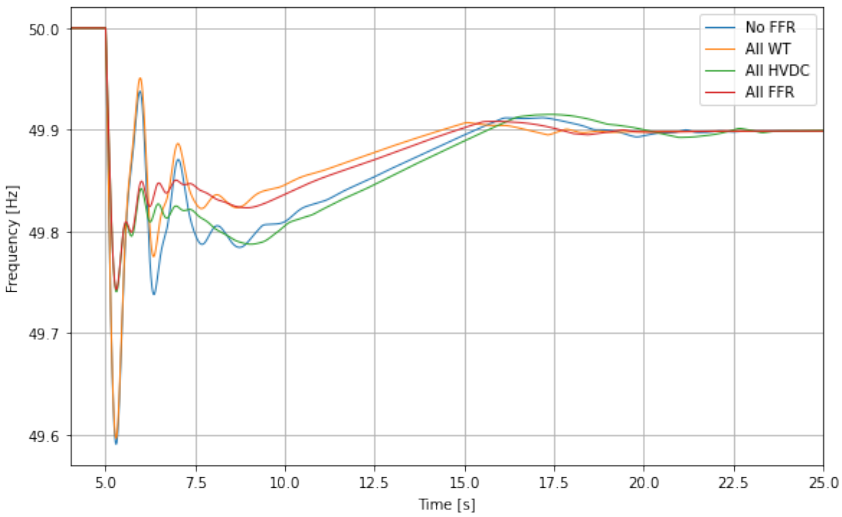

Figure 4.18: Effect of HVDC links and WTs applying FFR on frequency in FED

5 Conclusions and recommendations

5.1 Conclusions

The purpose of this project was to develop a dynamic model of the 2030 Nordic Power System as a tool to develop and research for stability studies with emphasis on frequency stability. This dynamic model in PowerFactory DIgSILENT was then used to answer the main research question:

To what extent will the frequency performance of the Nordic Power System of 2030 be affected by Non-Synchronous Generation?

To do so, the existing base model of Even Strand Aas was modified to represent a low inertia system of 60% NSG by adding Voltage Source Converter HVDC and type 4 Fully Rated Converter wind turbines. Specific for the Nordic Power System in 2030 is the substantial increase of HVDC links to the system. The resulting model is shown in figure 5.1:

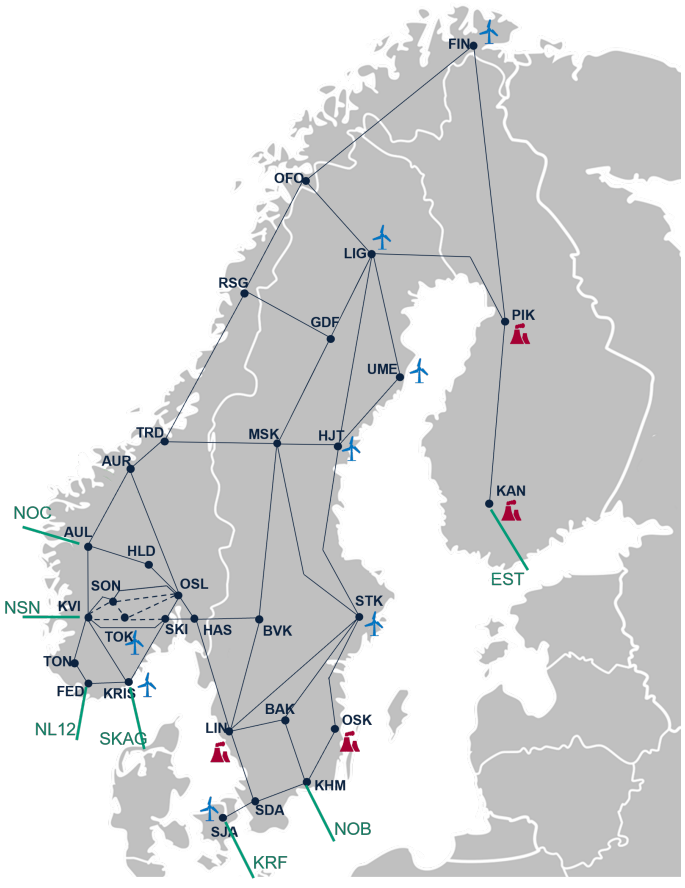

Figure 5.1: Distribution of generation types for the 60% NSG scenario. Wind farms and thermal generation are indicated by the blue and red symbols respectively. The green lines represent the VSC-HVDC import. Note that only the VSC-HVDC is indicated, LCC-HVDC links are modelled as negative loads. Nodes without a symbol have Hydro generation

The model shown in figure 5.1 is reflected the following developments of the Nordic Grid up until 2030;

- Expansion of HVDC links connecting the Nordic Power System to other synchronous areas
- Increase of Wind Power, particularly in the North of Sweden and Norway and in the east of Denmark.
- Decrease of system inertia during periods of high import and low load.

The main question is answered by focusing on the following sub questions:

What generic dynamic models can be used to represent the generators of the Nordic Power System in 2030?
Because generators of different power plants have particular dynamic models describing their response to unbalances and particular inertia, each node was assigned a production type. For Synchronous Generators encompassing Nuclear, Gas and Hydro plants parameters for the turbine determine their frequency response. Hydro governors were modelled as the non-linear HYGOV model available for PSSE software. Nuclear and Gas plants were modelled as Steam Generators, the governors are a simplified model of IEEE G1 provided by the IEEE [14]. Governor parameters are in typical ranges given by the Norwegian TSO Stattnett [18].

Both modern HVDC links as type 4 Fully Rated Converter use Voltage Source Converter to adjust the active and reactive currents independently. This is done by tracking the phase angle of the grid and using this to translate the three-phase currents to constant direct and quadratic currents in a rotating frame. This is done with the Clarke and Park Transform. Figure 5.2 shows the control structure of a converter terminal of an HVDC link, but the same concepts apply to a Fully Rated Converter wind turbine. In the Outer Controller, reference values for P and Q are created. This is done with PI control. In the inner control the measured, and calculated signals of reactive and active powers are controlled with these reference values and typically PI controllers. The resulted signals are translated into three-phase voltage reference values. The voltage of the converter with respect to the grid voltage determines the power flows. The VSC-HVDC link is represented by the model 'HVDC MMC 2-Terminal LInk (RMS Balanced) of the DIgSILENT library of PowerFactory 2021'. The WTG is represented by the model 'DIgSILENT FullyRatedConv WTG 6.0MW 50Hz'.

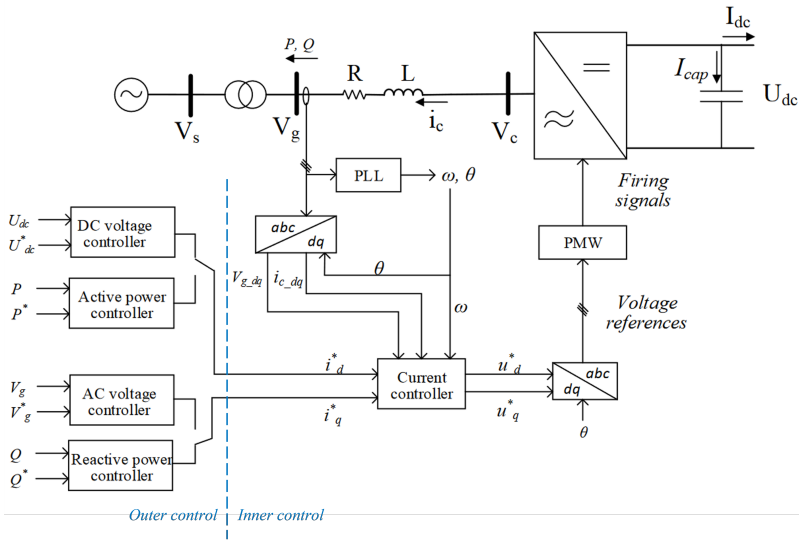

Figure 5.2: Control structure VSC adapted from [23]

To test the frequency performance of the Nordic Power System model including the dynamic models for the synchronous generators, wind turbines and VSC-HVDC links, an sudden load increase of 10% at OSL is simulated. This results in a power deficiency of 374 MW at a total power load of 36.2 GW. The system frequency dip of 0.055 Hz is reached at 7 seconds, whereas the quasi steady state is reached after 25 seconds after the fault. The time frames are in the range of a typical frequency event as described by the IEEE [14]. The values for RoCoF (-0.20 Hz/s) and MDF (0.055Hz) are much lower than the admissible values for RoCoF and MDF.

What are the critical disturbances in the Nordic Power System in 2030?
To find the critical disturbance of the NPS, outage events of each generation plant and VSC-HVDC link were simulated and compared. Outages of generation units with a power output of more than 2000 MW were rejected from the analysis as they represent aggregated generation of that area instead of a single unit that could trip, and the power outage was higher than the current dimensioning incident.

The disturbances that led to the highest local values of MDF and RoCoF included faults in the North of the Nordic Power System. The system strength, defined as the ratio of Short Circuit Power to the DC nominal active power of inverter-coupled generation is a measurement of the converter stability. Low values of Short Circuit Ratio (SCR) represent busses where the load of the bus cannot accept the power of the converter. FIN has the lowest SCR. This can be explained by the remoteness, resulting in high impedance and proximity to other win turbines. FIN is the weak point of the system with local spikes in powers, frequencies, and voltages. The local spikes in frequency are not seen at different busses.

The critical disturbance that is chosen for further evaluation is the HVDC-link NSN2. The power discrepancy caused by an outage of the NSN2 is larger than that of the current dimensioning event in the Nordic Power Grid, because the specific HVDC-link has a higher power output than the largest power plant unit. Thus, an increase in HVDC links in the next decade will result in higher outage risks. The outage of NSN2 leads to a Maximum Frequency deviation (MDF) of 0.4 HZ at the output of the generator at FED and a RoCoF of 3 Hz/s. The RoCoF is larger than the admissible value of 2 Hz/s.

The inertia of the grid is not uniform because the increase in NSG is location specific and reinforced by the aggregated representation of generation and load at transmission voltage. Furthermore, the number of generators, and therefore the amount of inertia differs significantly per node.This causes the model to have different frequency responses throughout the system; values for the Rate of Change of Frequency vary per location. Furthermore, rotor swings dominate before the frequencies converge to a uniform system frequency.

How can Fast Frequency Response of Non-Synchronous Generation be used to improve the frequency performance?
Fast Frequency Response Control for invert-connected generation comes in many forms. ENERCON wind turbines are currently employed with an Emulated Inertia control block, that supplies extra power to the system when the frequency passes certain triggers. HVDC has multiple options to supply active power in frequency events. One such control model is the Synthetic Inertia control block. This mimics the inertial response of synchronous generators by supplying active power proportionally to the RoCoF of the system.

The parameters of the FFR control blocks are optimized to minimize the MDF at the output to model it as a primary control system. The individual effect to minimize the MDF caused

by the NSN2 differs as well as the combination of the control systems. The frequency response for these systems is shown in figure 5.3. As can be seen in the figure, the two control systems lead to different frequency responses;

- The SI control of the VSC-HVDC acts instantaneously after an event and the additional FFR active power output is inversely proportional to the RoCoF measured at the output of the converter. Because the highest RoCoF are in the beginning of the event, the effect can be mostly seen in the first few seconds after the event, as shown in figure 5.3. The employment of all EI dampens the frequency oscillations. It decreases the MDF from 49.6 till 49.7 Hz. The frequency after t=10s is close to the original frequency response at FED without FFR support.
- The EI control of the WTs only starts after the trigger frequency is reached, and reaches its maximum output not in that instant. Because of this, it does not have a large effect on the MDF. As can be seen in figure 5.3, the effect is stronger at the second frequency dip and it mostly improves the frequency after 3 seconds. The frequency at FED also reaches the quasi steady state quicker.
- Employment of both EI of the WT and SI of the VSC-HVDC leads to the best results; both the MDF and RoCoF are improved, and the frequency is recovery time is smaller.

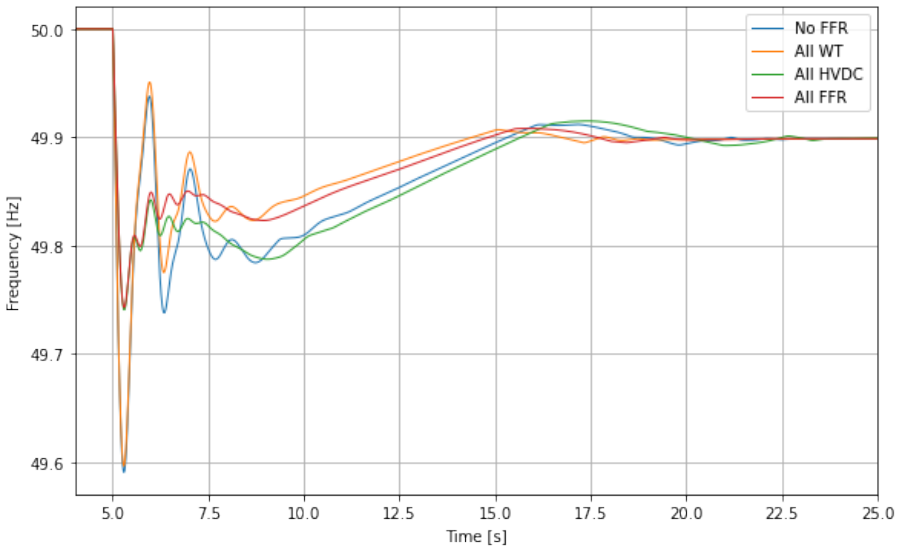

Figure 5.3: Effect of WT vs VSC-HVDC applying SI/EI on frequency in FED after an outage event of NSN2

Simulations also demonstrated that for this disturbance, there is a positive correlation between the location of the NSG producing FFR control and the MFD improvement. This applies to both the HVDC-VSC and for the WTs participating in frequency control. VSC-HVDC links mimic the inertia of the generators. The frequency in FED decreases substantially because there is little inertia in the area, so improving the inertia, and supplying power close to the highest MDF and the fault, leads to an decrease in MDF. The Wind Turbines providing EI also gave better results when they were closer to the fault. This may be explained by the fact that the trigger frequency is sooner reached at these locations, and the response time is important for this MDF. As expected, rated power is also an important factor. For the EI of the wind turbines this can be mostly observed in the frequency after 2.5 seconds.

To conclude, frequency performance in the Nordic Power System is affected by the in-

crease of Non-Synchronous Generation. It leads to less system inertia, and more heterogeneity in the system, which leads to rotor swings and high RoCoF values in certain areas after an event. NSG also offers solutions by fast frequency response controls. Derivative models that use RoCoF to change the output can complement models that regulate their output according to frequency deviation as they offer a different kind of frequency support.

With the development of the dynamic model specific for frequency response, the effect of (heterogeneous) inertia and fast frequency response of VSC-HVDC and WTS should be be further investigated.

5.2 Recommendations for future study

These conclusions about frequency performance are for the specific fast power control blocks and this specific model of the Nordic Power System. In future studies, other load-flows scenarios should be developed and studied. The FFR control blocks that were studied in this work were the Emulated Inertia block of ENERCON, and the Synthetic Inertia block of the HVDC link. Other FFR controls should be studied, such as Emergency Power Control of the HVDC links, FFR proportional to frequency deviation, and synthetic inertia for wind turbines.

The model should be be improved with the following points;

- The system strength in the North of the System can be studied and improved. At the moment, only the SCR is calculated, but this does not take into account the effect of other NSG in the system. System strength can be improved by changes in the network topology, which would not model the Nordic Power System, or by adding a synchronous condenser, adding synchronous generation to nodes with only wind, or omitting wind turbines altogether at weak points in the grid.
- The wind turbine control block does not take into account the recovery period after the discharge of extra power by the EI block. This is because the Wind Turbine model does not include wind dynamics or pitch control. Complex models with pitch control and wind dynamics exist. If the system strength at certain points in the grid is enlarged, this complex model should be added.
- The inertia of the system is too rigid. The system has only one type of power plant per node. This result in nodes with no inherent inertia. The model can be improved by adding extra power plants per node. The inertia constant of the synchronous generators can also be specified with open data from SCADA measurements of the Nordic TSOs.
- The Wind Turbines (WTs) do not partake in continuous voltage support, this should be added.
- Frequency response of LCC-HVDC and loads can be further modeled.

Furthermore, the effect on the location of the NSG participating in frequency control can be further investigated.

Bibliography

[1] E. S. Aas, "Simulation Model of the Future Nordic Power Grid Considering the Impact of HVDC Links," no. July, 2016.

[2] The Nordic prime ministers, *Declaration on Nordic Carbon Neutrality*, 2019. [Online]. Available: https://www.norden.org/en/declaration/declaration-nordic-carbon-neutrality.

[3] S. Engelken, A. Mendonca, and M. Fischer, "Inertial response with improved variable recovery behaviour provided by type 4 WTs," *IET Renewable Power Generation*, vol. 11, no. 3, pp. 195–201, 2017, ISSN: 17521424. DOI: 10.1049/iet-rpg.2016.0333.

[4] FINGRID, Landsnet, Svenska Kraftnät, Stattnett, and Energinet.dk, "Nordic Grid Development Plan 2019," no. June, p. 83, 2019. [Online]. Available: http://www.statnett.no/Global/Dokumenter/Media/Nyheter%202014/Nordic%20Grid%20Development%20Plan.pdf.

[5] A. Ulbig, T. S. Borsche, and G. Andersson, *Impact of low rotational inertia on power system stability and operation*, 3. IFAC, 2014, vol. 19, pp. 7290–7297, ISBN: 9783902823625. DOI: 10.3182/20140824-6-za-1003.02615. [Online]. Available: http://dx.doi.org/10.3182/20140824-6-ZA-1003.02615.

[6] A. Tosatto, M. Dijokas, T. Weckesser, S. Chatzivasileiadis, and R. Eriksson, "Sharing Reserves through HVDC: Potential Cost Savings in the Nordic Countries," pp. 1–11, 2020. [Online]. Available: http://arxiv.org/abs/2001.00664.

[7] Nordic TSOs, "Report: Challenges and Opportunities for the Nordic Power System," p. 66, 2016. [Online]. Available: http://www.statnett.no/Global/Dokumenter/Challenges%20and%20opportunities_Report.pdf.

[8] DIgSILENT, "PowerFactory 2020 User Manual," pp. 0–1253, 2020.

[9] P. Kundur, J. Paserba, V. Ajjarapu, *et al.*, "Definition and classification of power system stability," *IEEE Transactions on Power Systems*, vol. 19, no. 3, pp. 1387–1401, 2004, ISSN: 08858950. DOI: 10.1109/TPWRS.2004.825981.

[10] N. Hatziargyriou, J. Milanovic, C. Rahmann, *et al.*, "Definition and Classification of Power System Stability - Revisited & Extended," *IEEE Transactions on Power Systems*, vol. 36, no. 4, pp. 3271–3281, 2021, ISSN: 15580679. DOI: 10.1109/TPWRS.2020.3041774.

[11] IEEE, "Stability definitions and charecterization of dynamic behavior in systems with high penetration of power electronic interfaced technologies," *Power and Energy Society, Tech Rep.*, vol. PES-TR77, 2020.

[12] P. S. Kundur, *Power System Stability and Control Volume I*, New York, 1994.

[13] J. Machowski, Z. Lubosny, J. W. Bialek, and J. R. Rumby, *Power System Dynamics Stability and Control*, 3rd ed. John Wiley & Sons, 2020, ISBN: ISBN 9781119526384.

[14] IEEE Task Force on Turbine-Governor Modeling, "Dynamic Models for Turbine-Governors in Power System Studies," *Technical Report PES-TR1*, pp. 1–117, 2013, ISSN: 1098-2272. [Online]. Available: http://sites.ieee.org/fw-pes/files/2013/01/PES_TR1.pdf%0Ahttp://resourcecenter.ieee-pes.org/year/2013/dynamic-models-turbine-governors-power-system-studies-pdf/.

[15] F. Gonzalez-Longatt, *Frequency Control and Inertial Response Schemes for the Future Power Networks*, 9783319032238. 2014, vol. 0, pp. vii–ix, ISBN: 9789814585293. DOI: 10.1007/978-981-4585-30-9.

[16] ENTSO-E, "FCR - D design of requirements," *Report*, p. 36, 2017. [Online]. Available: https://www.google.nl/url?sa=t&rct=j&q=&esrc=s&source=web&cd=1&ved=0ahUKEwjj5O7xnrTZAhWBKMAKHYE4DIYQFggoMAA&url=https%3A%2F%2Fenerginet.dk%2F-%2Fmedia%2FEnerginet%2FEl-RGD%2FEl-PBU%2FDokumenter%2FFCR-Dokumenter%2FFCR-D-design-of-requirements.pdf%3Fla%3Dda.

[17] European Commission, "Commission Regulation (EU) 2017/1485: Establishing a guideline on Electricity Transmission System Operation (SO GL)," *Official Journal of the European Union*, vol. L 220, no. 25 August 2017, p. 120, 2017. [Online]. Available: http://eur-lex.europa.eu/legal-content/EN/TXT/PDF/?uri=CELEX:32017R1485&from=EN.

[18] Statnett, "Funksjonskrav i kraftsystemet (FIKS)," 2012.

[19] E. Orum, L. Haarla, M. Kuivaniemi, *et al.*, "Future system inertia 2," p. 153, 2018. [Online]. Available: https://onlinelibrary.wiley.com/doi/full/10.1002/2050-7038.12128%20%0Ahttps://www.statnett.no/globalassets/for-aktorer-i-kraftsystemet/utvikling-av-kraftsystemet/nordisk-frekvensstabilitet/future-system-inertia-phase-2.pdf%0A.

[20] N. Flourentzou, V. G. Agelidis, and G. D. Demetriades, "VSC-based HVDC power transmission systems: An overview," *IEEE Transactions on Power Electronics*, vol. 24, no. 3, pp. 592–602, 2009, ISSN: 08858993. DOI: 10.1109/TPEL.2008.2008441.

[21] M. Yu, A. Dysko, C. D. Booth, A. J. Roscoe, and J. Zhu, "A review of control methods for providing frequency response in VSC-HVDC transmission systems," *Proceedings of the Universities Power Engineering Conference*, vol. 1, 2014. DOI: 10.1109/UPEC.2014.6934693.

[22] A. S. Elansari, S. J. Finney, J. Burr, and M. F. Edrah, "Frequency control capability of VSC-HVDC transmission system," *IET Seminar Digest*, vol. 2015, no. CP654, pp. 1–6, 2015. DOI: 10.1049/cp.2015.0030.

[23] A. G. Endegnanew and K. Uhlen, "Global analysis of frequency stability and inertia in AC systems interconnected through an HVDC," *2016 IEEE International Energy Conference, ENERGYCON 2016*, 2016. DOI: 10.1109/ENERGYCON.2016.7514110.

[24] J. Zhu, C. D. Booth, G. P. Adam, A. J. Roscoe, and C. G. Bright, "Inertia emulation control strategy for VSC-HVDC transmission systems," *IEEE Transactions on Power Systems*, vol. 28, no. 2, pp. 1277–1287, 2013, ISSN: 08858950. DOI: 10.1109/TPWRS.2012.2213101.

[25] J. Wu, Z. Wang, H. Rao, Y. Chen, and W. Huang, "A Review of Control Strategies for Inertia Support in VSC-HVDC System," *2019 4th IEEE Workshop on the Electronic Grid, eGRID 2019*, 2019. DOI: 10.1109/eGRID48402.2019.9092740.

[26] J. Fang, H. Li, Y. Tang, and F. Blaabjerg, "On the Inertia of Future More-Electronics Power Systems," *IEEE Journal of Emerging and Selected Topics in Power Electronics*, vol. 7, no. 4, pp. 2130–2146, 2019, ISSN: 21686785. DOI: 10.1109/JESTPE.2018.2877766.

[27] J. Fradley, R. Preece, and M. Barnes, "VSC-HVDC for frequency support (a review)," *IET Conference Publications*, vol. 2017, no. CP709, 2017. DOI: 10.1049/cp.2017.0062.

[28] J. Huang and R. Preece, "HVDC-based fast frequency support for low inertia power systems," *IET Conference Publications*, vol. 2017, no. CP709, pp. 1–6, 2017. DOI: 10.1049/cp.2017.0040.

[29] A. Ellis, Y. Kazachkov, E. Muljadi, P. Pourbeik, and J. J. Sanchez-Gasca, "Description and technical specifications for generic WTG models - A status report," *2011*

IEEE/PES Power Systems Conference and Exposition, PSCE 2011, pp. 1–8, 2011. DOI: 10.1109/PSCE.2011.5772473.

[30] North Americal Electric Reliability Coroporation (NERC), "Integrating Inverter-Based Resources into Low Short Circuit Strength Systems," *Reliability Guideline*, no. December, p. 47, 2017. [Online]. Available: https://www.nerc.com/comm/PC_Reliability_Guidelines_DL/Item_4a._Integrating%20_Inverter-Based_Resources_into_Low_Short_Circuit_Strength_Systems_-_2017-11-08-FINAL.pdf.

[31] R. Eriksson, N. Modig, and K. Elkington, "Synthetic inertia versus fast frequency response: A definition," *IET Renewable Power Generation*, vol. 12, no. 5, pp. 507–514, 2018, ISSN: 17521424. DOI: 10.1049/iet-rpg.2017.0370.

[32] H. Urdal, R. Ierna, J. Zhu, C. Ivanov, A. Dahresobh, and D. Rostom, "System strength considerations in a converter dominated power system," *IET Renewable Power Generation*, vol. 9, no. 1, pp. 10–17, 2015, ISSN: 17521424. DOI: 10.1049/iet-rpg.2014.0199.

[33] A. Adrees, J. V. Milanović, and P. Mancarella, "Effect of inertia heterogeneity on frequency dynamics of low-inertia power systems," *IET Generation, Transmission and Distribution*, vol. 13, no. 14, pp. 2951–2958, 2019, ISSN: 17518687. DOI: 10.1049/iet-gtd.2018.6814.

[34] DIgSILENT GmbH, "Technical Reference General Load," *PowerFactory 2021 Brochure*, pp. 1–28, 2021. [Online]. Available: file:///C:/Users/45035571/AppData/Local/Temp/MicrosoftEdgeDownloads/775edfc7-63f7-4ddf-bf12-371e5b0c6156/PF2021_Brochure%20(EN).pdf.

[35] ENTSO-E, *Mid-term Adequacy Forecas 2020 Dataset*, 2020. [Online]. Available: https://www.entsoe.eu/outlooks/midterm/.

[36] Nordic Council of Ministers, "Capacity adequacy in the Nordic electricity market," *Capacity adequacy in the Nordic electricity market*, 2015. DOI: 10.6027/tn2015-560.

[37] E. Ørum and M. Kuivaniemi, "Nordic Report: Future System Inertia," *Entso-E*, pp. 1–58, 2015. [Online]. Available: https://www.entsoe.eu/Documents/Publications/SOC/Nordic/Nordic_report_Future_System_Inertia.pdf.

[38] V. Koritarov, L. Guzowski, J. Feltes, *et al.*, "Review of Existing Hydroelectric Turbine-Governor Simulation Models," pp. 1–102, 2013.

[39] PES, *IEEE Recommended Practice for Excitation System Models for Power System Stability Studies*, April. 2006, vol. 2005, pp. 1–85, ISBN: VO -. DOI: 10.1109/IEEESTD.2006.99499. [Online]. Available: http://ieeexplore.ieee.org/lpdocs/epic03/wrapper.htm?arnumber=1489146.

[40] "EEE Guide for Identification, Testing, and Evaluation of the Dynamic Performance of Excitation Control Systems," *IEEE Std 421.2-2014 (Revision of IEEE Std 421.2-1990)*, pp. 1–63, 2014. DOI: 1109/IEEESTD.2014.6845300.

[41] I. C. Report, "Dynamic Models for Steam and Hydro Turbines," *IEEE Transactions on Power Apparatus and Systems*, vol. PAS-92, pp. 1904–1915, 1973. DOI: 10.1109/TPAS.1973.293570.

[42] "Technical Reference DIgSILENT Fully Rated Converter WInd Turbine Templates," DIgSILENT GmbH PowerFactory 2021, Gomaren, Germany, Tech. Rep., 2020.

[43] H. Berndt, M. Hermann, H. Kreye, R. Reinisch, U. Scherer, and J. Vanzetta, "TransmissionCode 2007 Network and System Rules of the German Transmission Operators," *Vervand der Netzbetreiber VDN*, no. August, 2007. [Online]. Available: www.vdn-berlin.de.

[44] SDLWindV, "Ordinance on System Services by WInd Energt Okabts," Tech. Rep. 1, 2019, pp. 1–9. [Online]. Available: http://www.ichgmbh.com/wp-content/uploads/2016/06/doc_Deutsch_ordinance-on-system-services-by-wind-energy-plants.pdf.

A Parameters

In this appendix, the electrical parameters of the Equipment Types used in the model is given.

A.1 Electrical parameters synchronous generators

Table A.1: Variables synchronous generator type: basic data and loadflow

	Variable	unit	value
Sn	Rated Apparent Power	MVA	281.25
Vn	Rated Voltage	p.u.	22
	Rated power factor	-	0.8
	Min Q Limit	p.u.	-1
	Max Q Limit	p.u.	1
xo	Reactance, zero seq.	p.u.	0.1
r0	Resistance, zero seq.	p.u.	0
x2	Reactance, negative seq.	p.u.	0.2
r2	Resistance, negative seq.	p.u.	0.001

A.2 Information Lines

Table A.2: Electrical parameter of line types. The model also includes a type fror a Simple 220 kV line, this has the same properties as the Simple400 except for the voltage

parameter	Triplex400	Double400	Simple400	Duplex300	Cable400	unit
Nominal voltage	400	400	400	300	400	kV
Rated Current	3.555	2.422	1.211	2.422	1	[kA]
AC-Resistance 1,2 seq.	0.02	0.028	0.055	0.028	0.05	[Ω/km]
AC-Resistance 0 seq.	0.16	0.224	0.44	0.224	0.05	[Ω/km]
Reactance 1,2 seq.	0.268	0.328	0.438	0.315	0.079	[Ω/km]
Reactance 0 seq	0.697	0.853	1.139	0.819	0.079	[Ω/km]
Capacitance 1,2 seq.	0.013	0.011	0.008	0.011	0.15	[µF/km]
Susceptance 0 seq	2.45	2.059	1.508	2.145	47.124	[µS/km]
Conductance 1,2 seq.	0.004	0.004	0.004	0.004	0.04	[µS/km]
Conductance 0 seq	0.004	0.004	0.004	0.004	0.04	[µS/km]

Table A.3: Information of type of line and km between nodes 1/2

Node1	Node2	type	Voltage [KV]	n	Length [km]
AUL	AUR	Triplex	400	1	400
AUR	TRD	Triplex	400	2	150
AUR	OSL	Triplex	400	1	400
TRD	RSG	Triplex	400	2	400
RSG	OFO	Simplex	400	1	600
FIN	OFO	Simplex	220	1	600
KAN	PIK	Simplex	400	3	480
LIG	PIK	Simplex	400	2	400
OFO	LIG	Simplex	400	1	300
RSG	GDF	Simplex	220	1	150
LIG	GDF	Simplex	400	1	330
LIG	HJT	Simplex	400	2	450
LIG	UME	Simplex	400	1	200
HJT	UME	Simplex	400	1	150
GRF	MID	Triplex	400	2	240
TRD	MID	Triplex	400	1	270
MSK	HJT	Triplex	400	1	110
MSK	BGV	Duplex	400	2	470
MSK	STK	Triplex	400	2	520
HJT	STK	Triplex	400	3	460
STO	LIN	Duplex	400	1	440
STO	BAK	Duplex	400	2	280
STI	OSK	Triplex	400	2	250
OSK	KHM	Triplex	400	2	160
HAS	LIN	Triplex	400	1	200
HAS	BVK	Triplex	400	1	110
LIN	BVK	Duplex	400	2	200
LIN	BAK	Triplex	400	1	160
BAK	KHM	Duplex	400	1	190
LIN	SDR	Triplex	400	2	210
SDR	KHM	Triplex	400	2	110
SDR	SJL	Cable	400	2	60

Table A.4: Information of type of line and km between nodes 2/2

Node1	Node2	type	Voltage [KV]	n	Length [km]
KRI	SKI	Triplex	400	1	140
KRI	KVI	Triplex	400	1	180
KRI	FED	Triplex	400	1	75
FED	TON	Triplex	400	1	50
FED	TON	Duplex	400	1	50
TON	AUL	Triplex	400	1	300
AUL	HAL	Triplex	400	3	110
AUL	KVI	Triplex	400	1	180
TON	KVI	Triplex	400	1	110
TON	KVI	Triplex	400	1	110
KVI	SKI	Duplex	300	1	200
KVI	SKI	Duplex	400	1	200
SKI	HAS	Triplex	400	1	100
HAL	OSL	Triplex	400	3	160
OSL	HAS	Triplex	400	1	80
KVI	SON	Triplex	400	1	70
SON	OSL	Triplex	400	1	200

A.3 Transformer types

Table A.5: Electrical parameters of the transformer types. In the model, there are also transformators transforming the 22kV to 300kV and from 22 to 220 kV. These transformators have the same electrical parameters as the 'Trx 400/22' and are therefore omitted in the table.

	Trx 400/22	Trx 400/300	Trx 400/220	WTG Trf	unit
Nominal Frequency	50	50	50	50	[Hz]
Power Rating	250	1000	1000	6.7	[MVA]
Rated Voltage, HV	400	400	400	22	[kV]
Rated Voltage, LV	22	300	220	0.4	[kV]
Vector Group, HV	YN	YN	YN	YN	-
Vector Group, LV	YN	YN	YN	D	-
Phase Shift	0	0	0	5	[°]
SHC-Voltage 1,2 seq.	6	4	6	6	[%]
Copper losses	0	3000	5000	6.67	[kW]
SHC Voltage 0 seq HV	3	3	3	3	[%]
SHC-Voltage Uk0r	0	0	0	0	[%]
No Load Current	0	0	0	0	[%]
No Load Losses	0	0	0	0	[kW]
x, 1,2 seq, HV	0.5	0.5	0.5	0.5	[p.u.]
x, 1,2 seq, LV	0.5	0.5	0.5	0.5	[p.u.]
r, 1,2 seq, HV	0.5	0.5	0.5	0.5	[p.u.]
r, 1,2 seq, LV	0.5	0.5	0.5	0.5	[p.u.]
z, 0 seq HV	0.9	0.9	0.9	-	[p.u.]
z, 0 seq HV LV	0.1	0.1	0.1	-	[p.u.]
Mag. Impedance/uk0	100	100	100	-	-
Mag. R/X	0	0	0	-	-

B PowerFactory Models

In this appendix, the PowerFactory Composite Frames and Common Models of the synchronous generator, wind model and VSC-HVDC links are given. These include the common models.

B.1 Synchronous generator

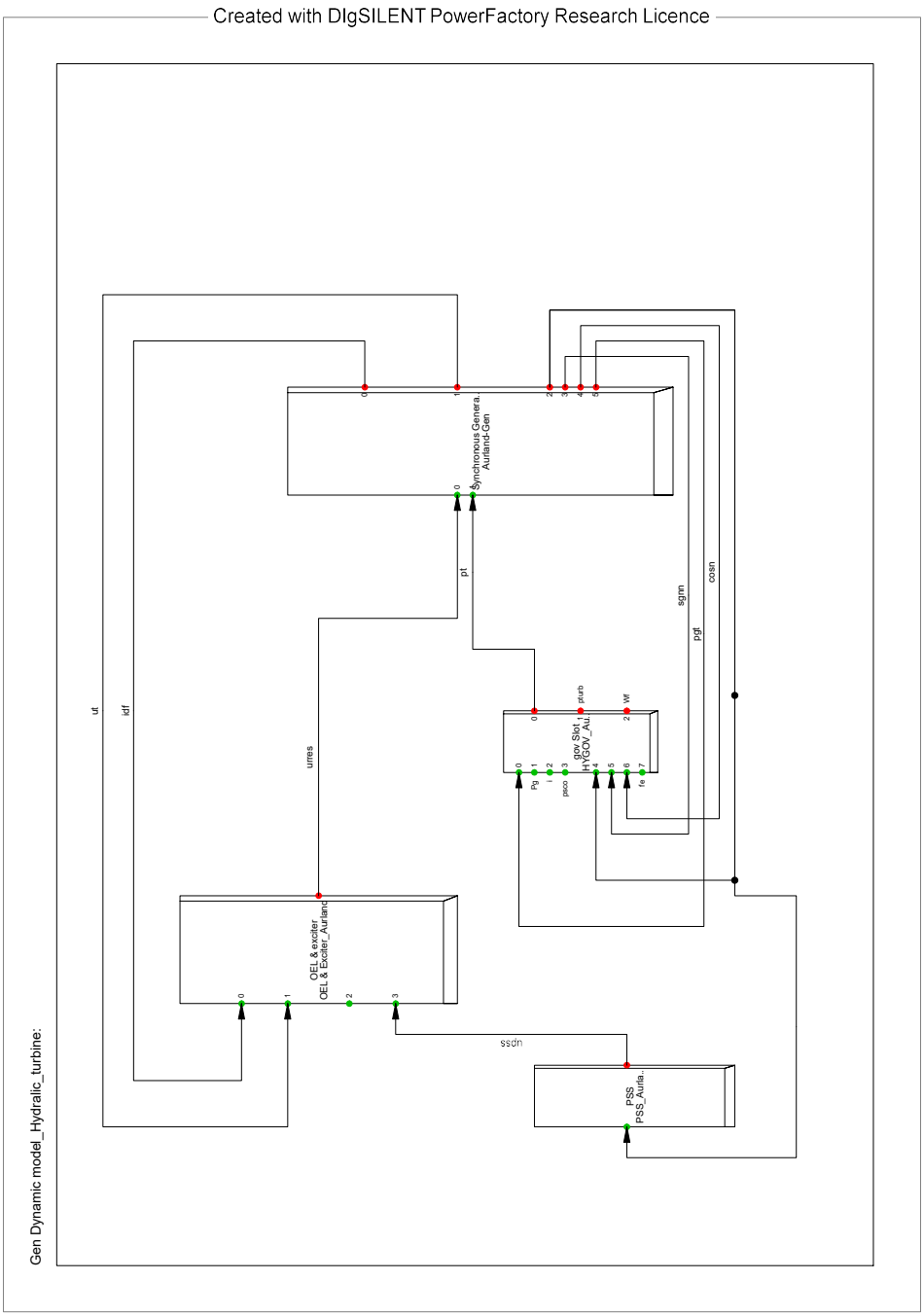

Figure B.1: Composite frame Hydro synchronous generator

Table B.1: Variables Hydro Governor

	Definition	Typical values [18]	Selected values
R	Permanent droop (pu)	0.02 - 0.08	0.02
r	Temporary droop (pu)	0.3 - 1	0.3
Tw	Water Starting time (s)	1 - 2	1
Tr	Governor Time Constant (s)	5 - 10	5
Tg	Servo Time Constant (s)	0.2 - 1	0.4
Tf	Filter Time Constant (s)	< 0.1	0.05
Dturb	Frictional losses factor (pu)	-	0
qnl	No Load flow (pu)	-	0.08
At	Turbine gain (pu)	-	1.15
PN	Turbine Rated Power	-	0
Gmin	Minimum Gate limit (pu)	-	0
Velm	Gate Celocity LImit (pu)	-	0.2
Gmax	Maximum Gate limit (pu)	-	1

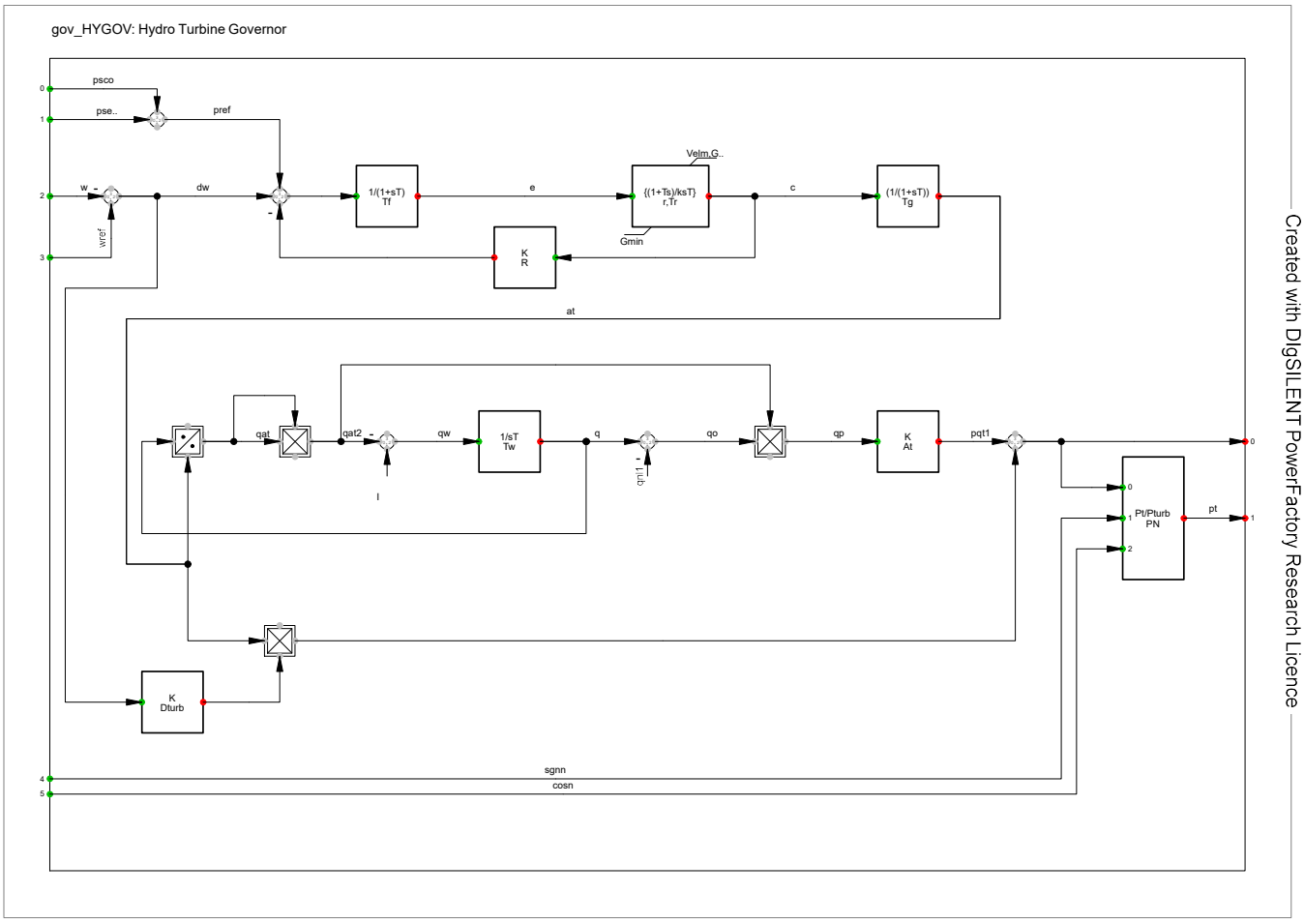

Figure B.2: Hydro governor model

Table B.2: Parameters Hydro AVR and OEL

Parameter	Description	Value
idf_lim	maximum excitation current	3
Ke	Exciter gain [s]	1
Te	Exciter delay [s]	0.1
Ka	Controller Gain [pu]	50
Ta	Controller delay [s]	0.01
Kg	OEL Gain [pu]	0.048
Ki	OEL Integral Gain [pu]	5
Tu	input filter time constant	0.02
Kf	Rate feedback gain	0.05
Tf	Rate feedback time constant	1.5
L2	maximum exciter voltage [pu]	4
vt_ref		1

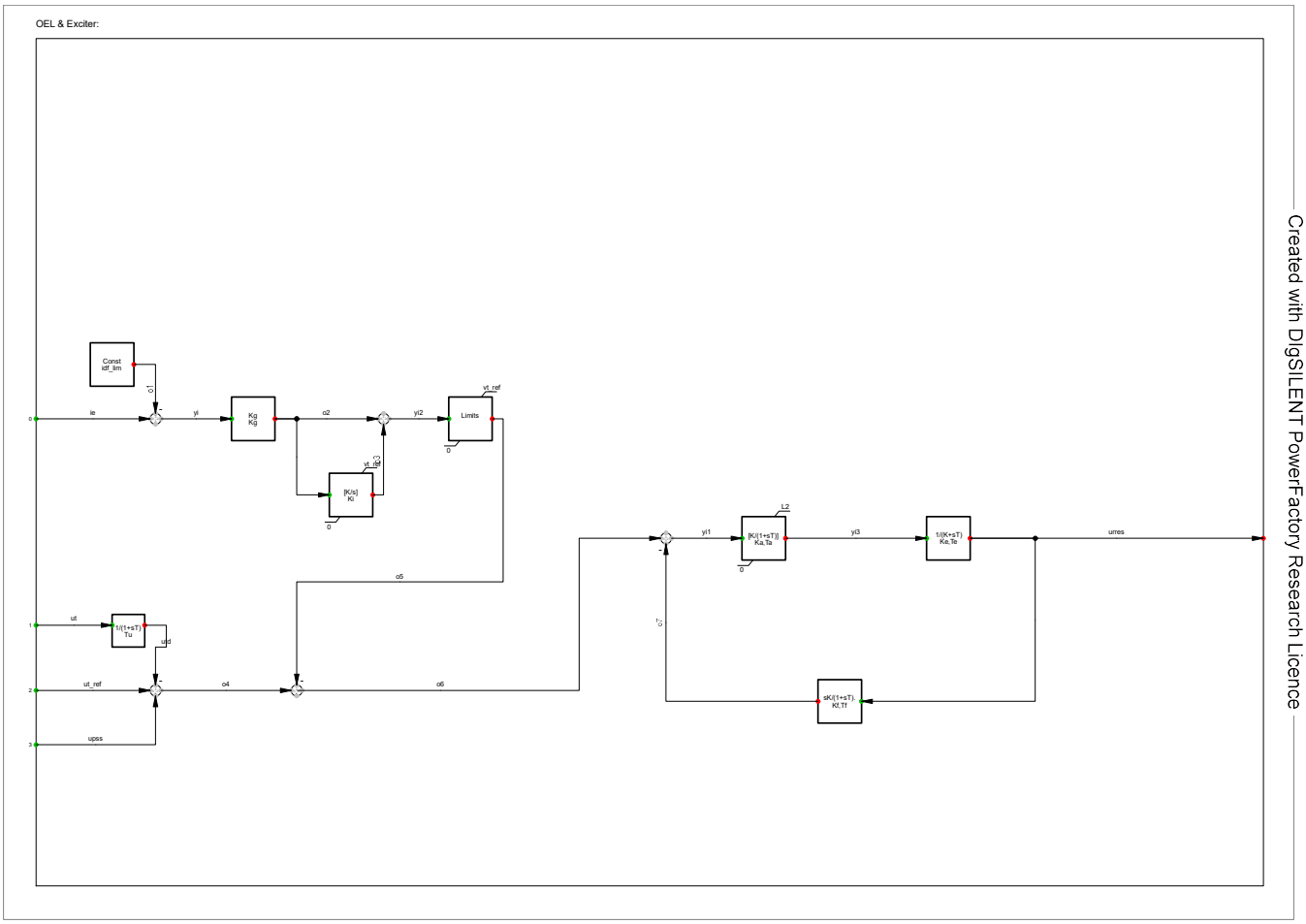

Figure B.3: Model hydro gene AVR

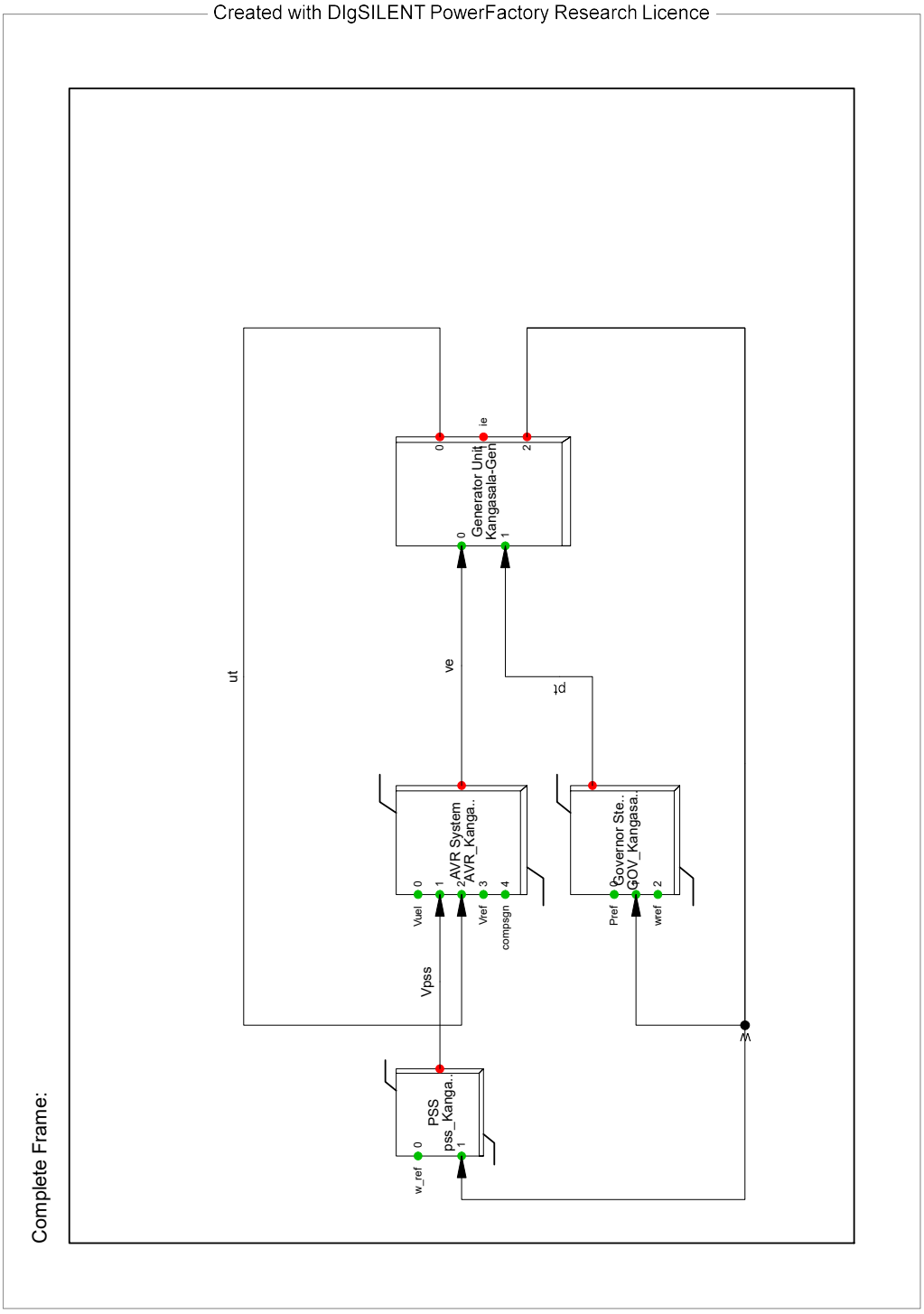

Figure B.4: Composite frame AVR thermal generator

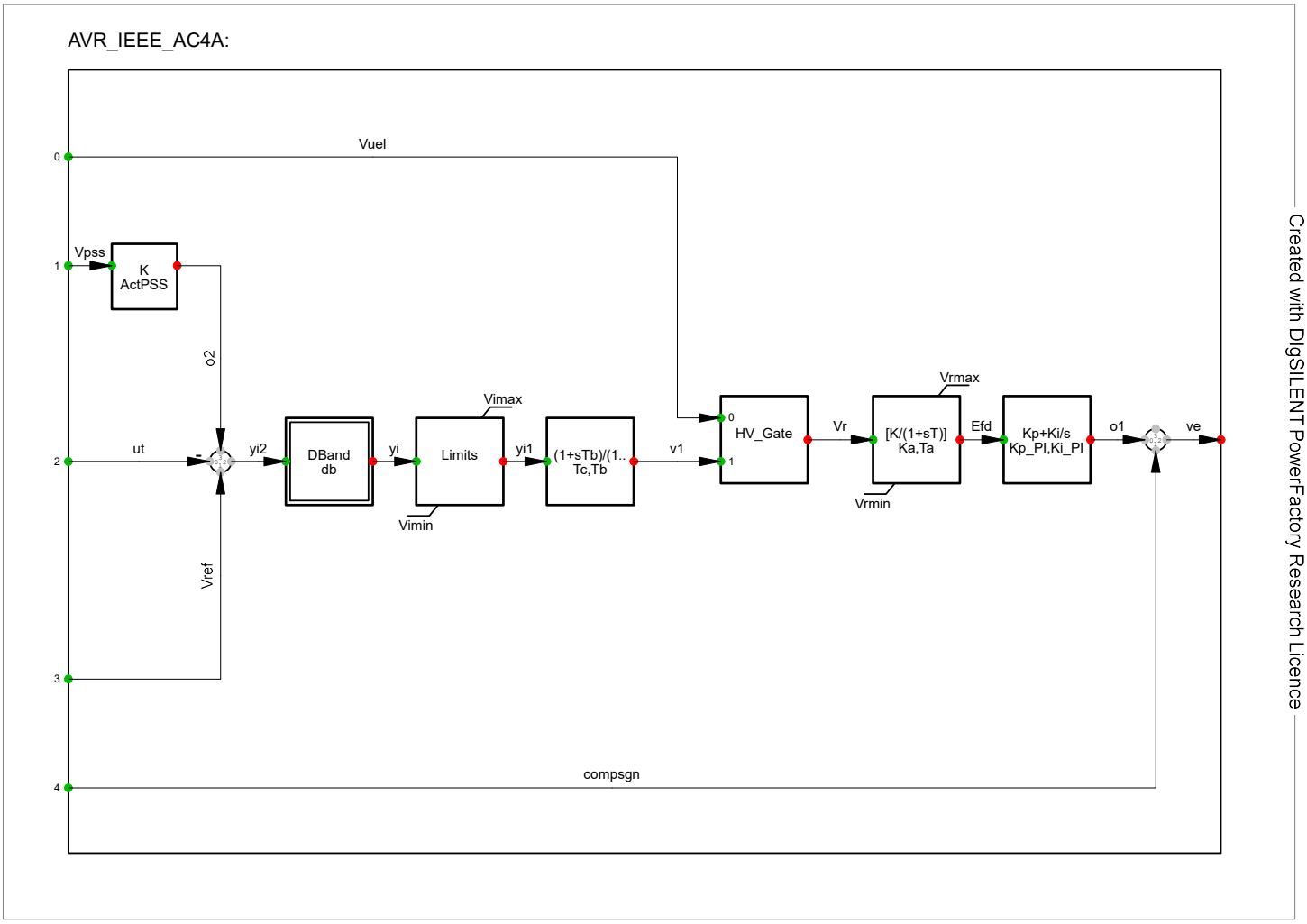

Figure B.5: Model AVR thermal generator

Table B.3: Parameters Thermal AVR

Parameter	Description	Value
Tc	Inherent AVR Zero constant [s]	0.1
Tb	Inherent AVR Pole constant [s]	0.001
kpPI	Proportional AVR constant [pu]	20
kiPI	Integral AVR constant [pu]	0.5
db	Deadband [pu]	0.0001
Ka	Exciter gain [pu]	200
Ta	Firing thyristors time constant [s]	0.04
ActPSS	PSS Activation [pu]	1
Vr min	Excitation voltage min limit [pu]	-4.53
Vi min	Voltage error lower limit [pu]	-1
Vr max	Proportional AVR constant [pu]	5.64
Vi min	Excitation voltage max limit [pu]	1

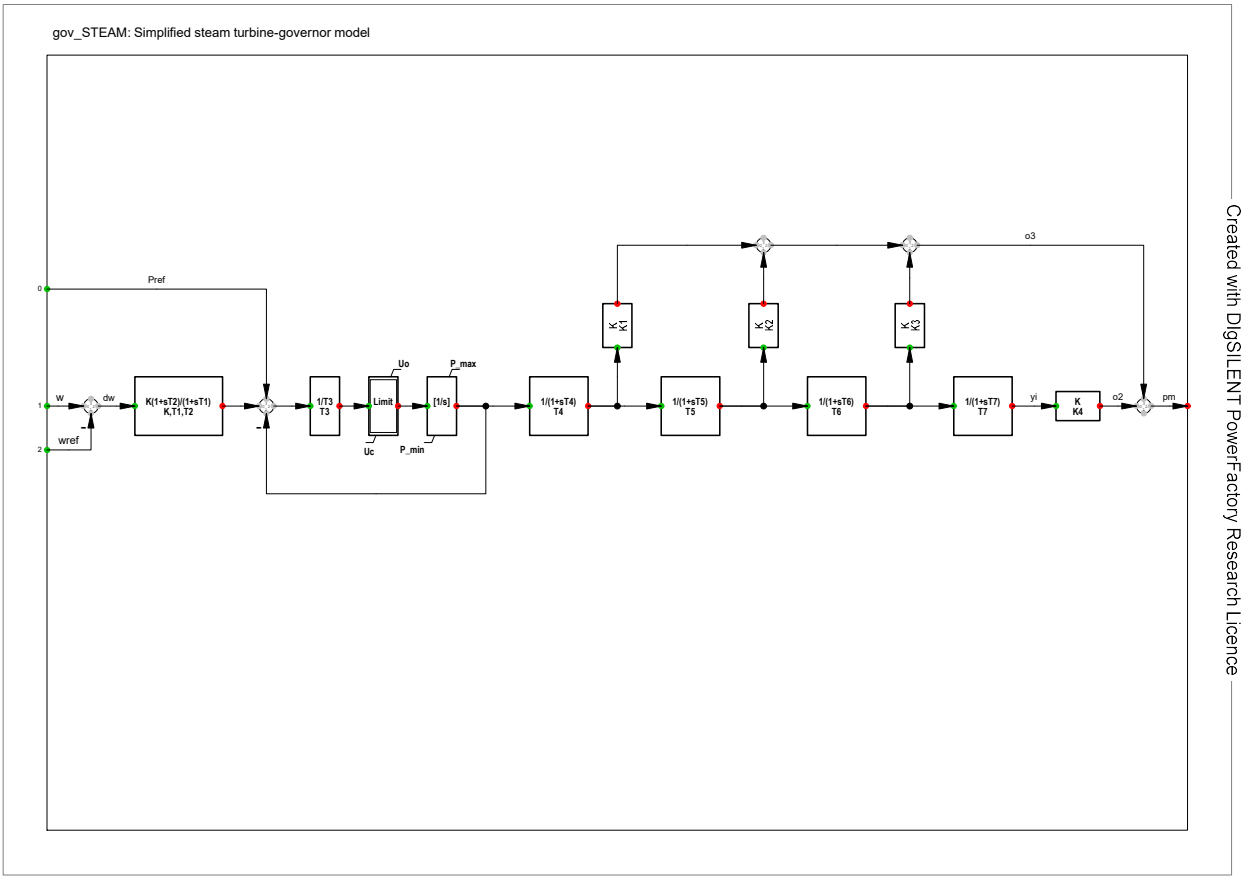

Figure B.6: Model governor thermal generator

Table B.4: parameters thermal governor

Parameter	Description	Typical values [40]	Selected Value
K	Governor Gain [p.u.]	20	25
T1	Governor lag time constant [s]	0 - 0.3	0.2
T2	Governor lead time constant [s]	0 - 1	0.15
T3	Valve positioner time constant [s]	0.025 - 0.1	0.1
T4	Inlet piping/steam bowl time constant [s]	-	0.1
T5	Second boiler pass time constant [s]	-	7
T6	Third boiler pass time constant [s]	-	5
T7	Fourth boiler pass time constant [s]	-	5
K1	Fraction of first boiler pass [p.u]	-	0.3
K2	Fraction of second boiler pass [p.u]	-	0.25
K3	Fraction of third boiler pass [p.u]	-	0.3
K4	Fraction of fourth boiler pass [p.u]	-	0.15
Uc	Maximum valve closing velocity [p.u]	-	-0.3
P_min	Minimum valve opening [p.u]	-	0
Uo	Maximum valve opening velocity [p.u.]	-	0.3
P_max	Maximum valve opening velocity [p.u.]	-	1

B.2 Powerfactory model WTG

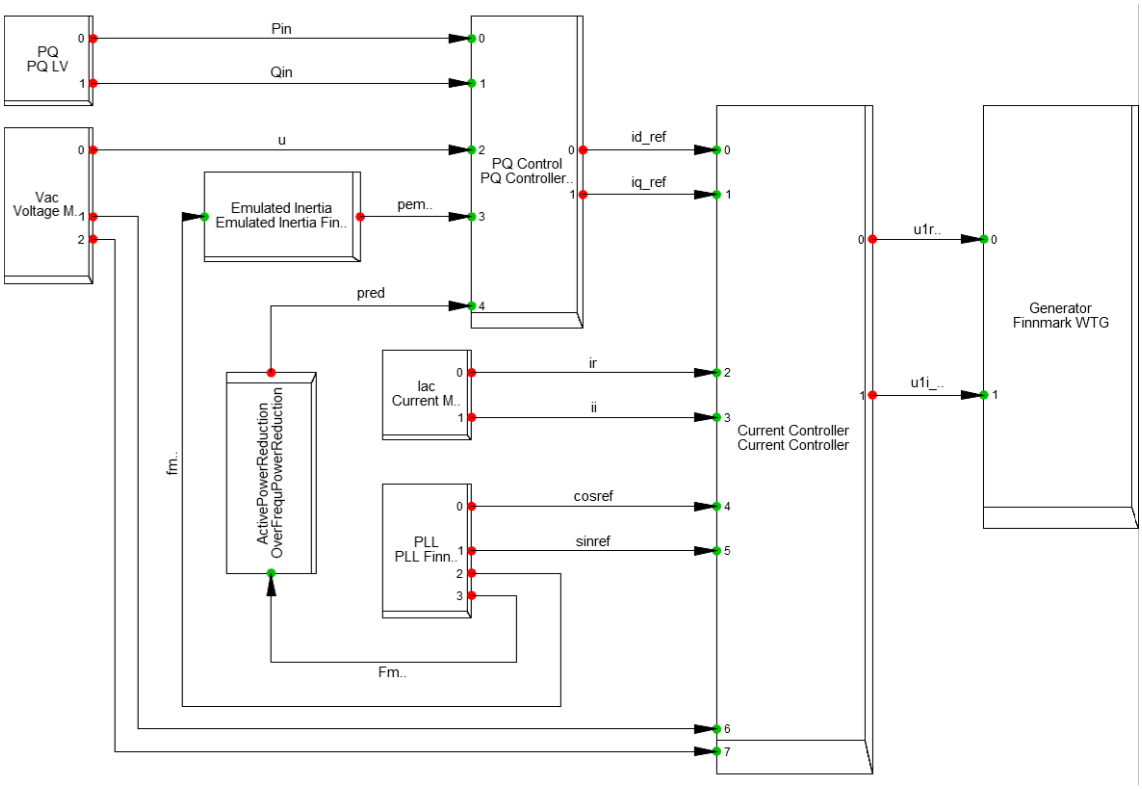

Figure B.7: Composite frame Fully Rated Converter Wind Turbine with EI block

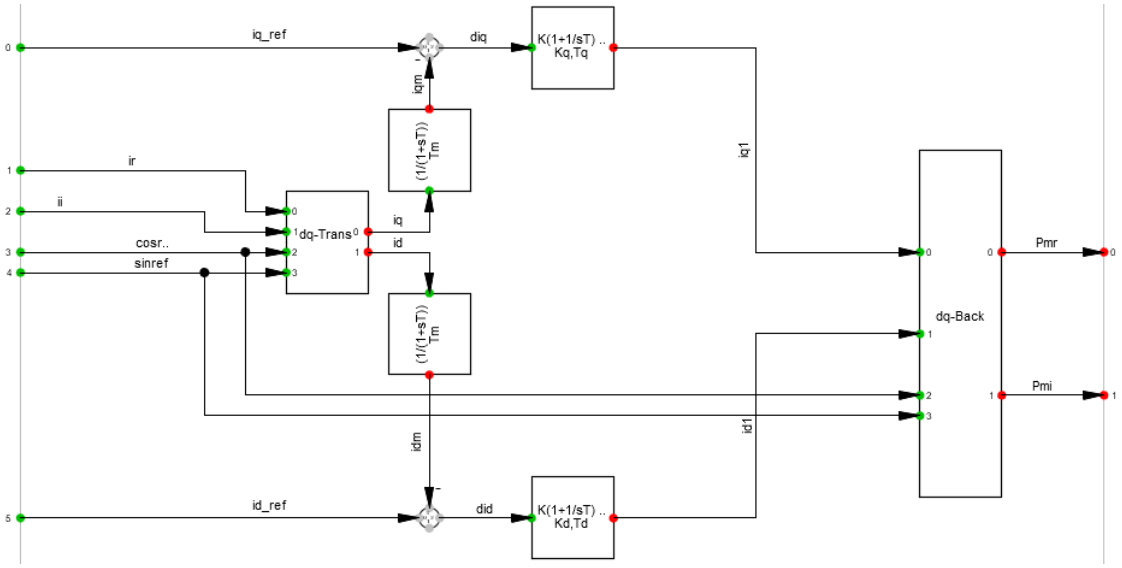

Figure B.8: Model Current controller in wind turbine

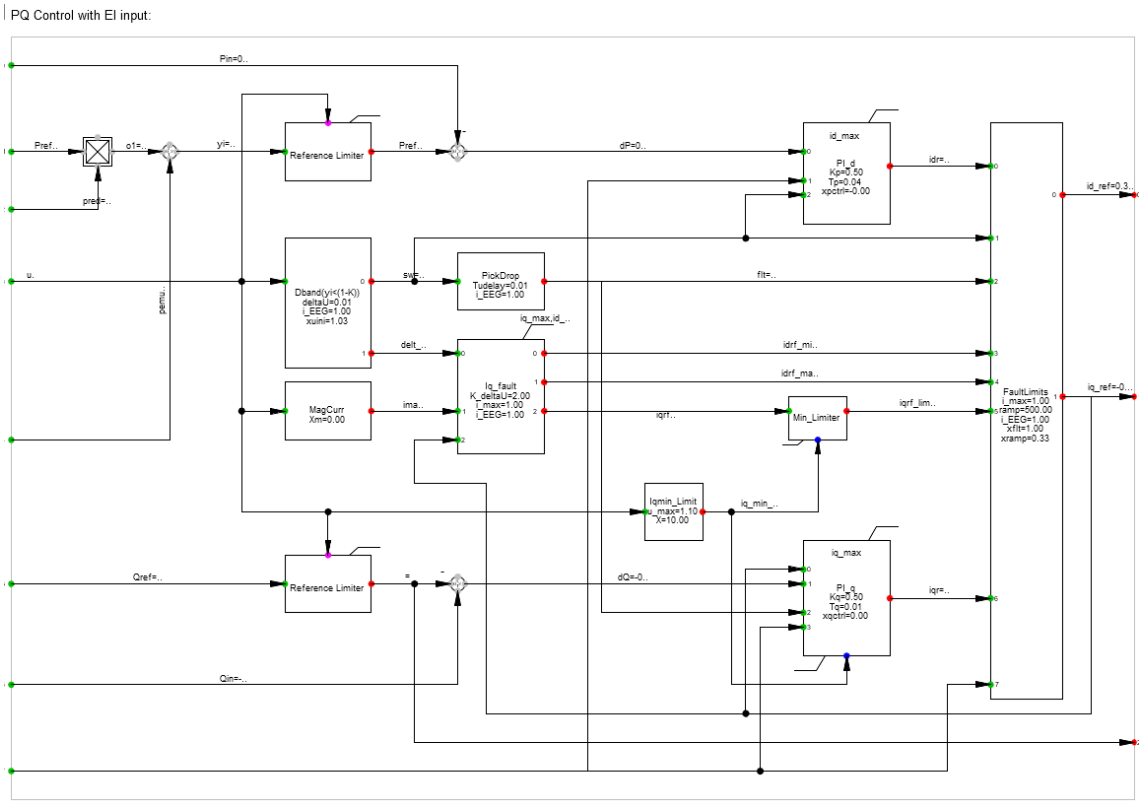

Figure B.9: Model PQ controller in wind turbine

Table B.5: Parameters PQ controller

Parameter	Description	Value
Kp	Active Power Control Gain [p.u.]	0.5
Tp	Active Power Control Time Constant [s]	0.04
Kq	Reactive Power Control Gain [p.u.]	0.5
Tq	Reactive Power Control Time Constant [s]	0.01
Xm	Magnetizing reactance at Pbase [p.u.]	0
deltaU	Voltage Dead Band [p.u.]	0.005
i_EEG	FRT mode (0=acc. TC2007, 1=acc. SDLWindV') -	1
Tudelay	Voltage Support Delay [s]	0.01
K_deltaU	Reactive support gain (dyn. voltage support) [p.u.]	2
i_max	Combined current limit [p.u.]	1
ramp	Active Power Ramp after FRT [[%/s]	500
u_max	max. allowed internal voltage [p.u.]	1.1
X	Coupling Reactance [%]	10
id_max	id current limit [p.u.]	1
iq_max	iq current limit [p.u.]	1

B.3 PowerFactory model HVDC converter A

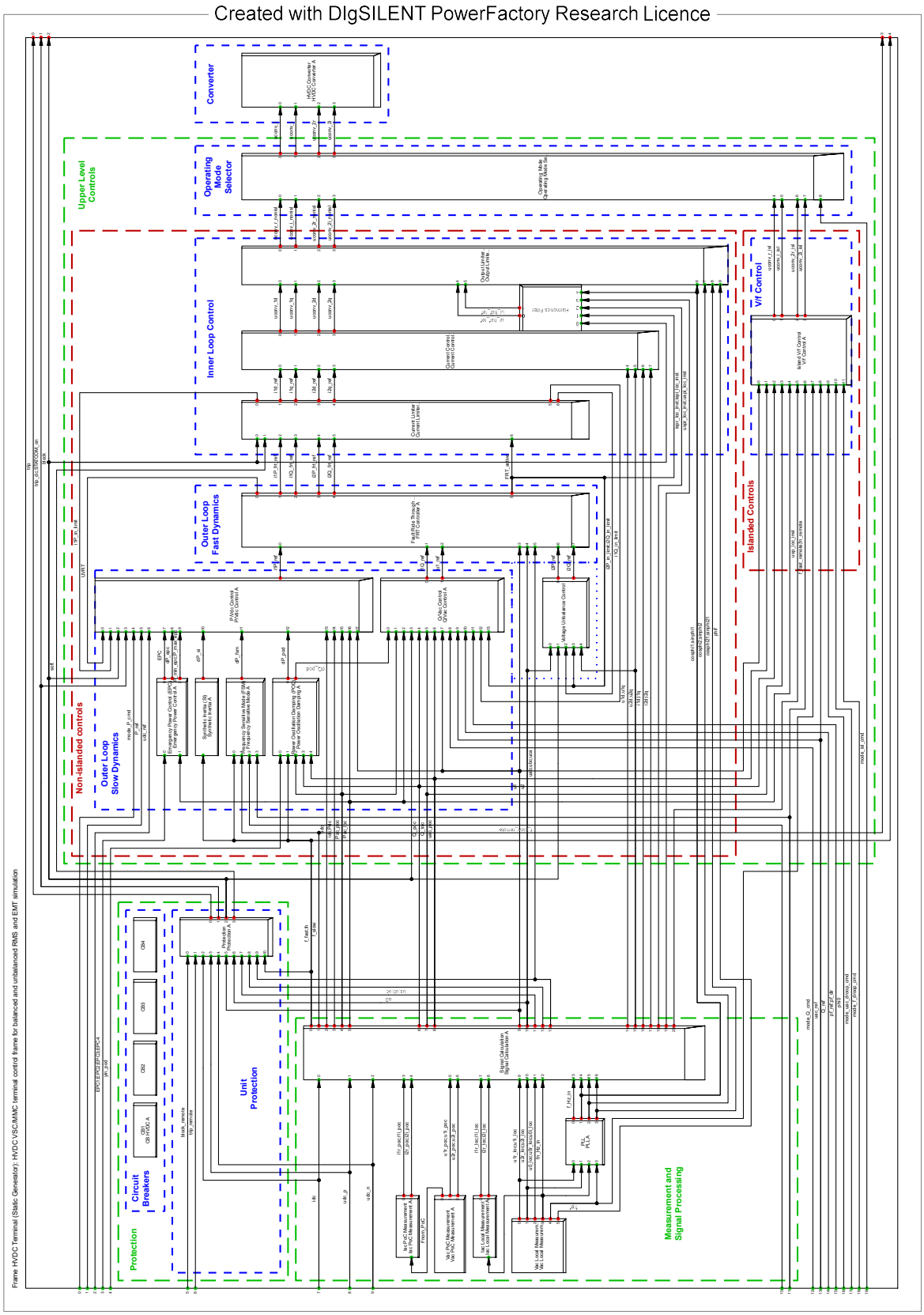

Figure B.10: Composite frame HVDC converter terminal

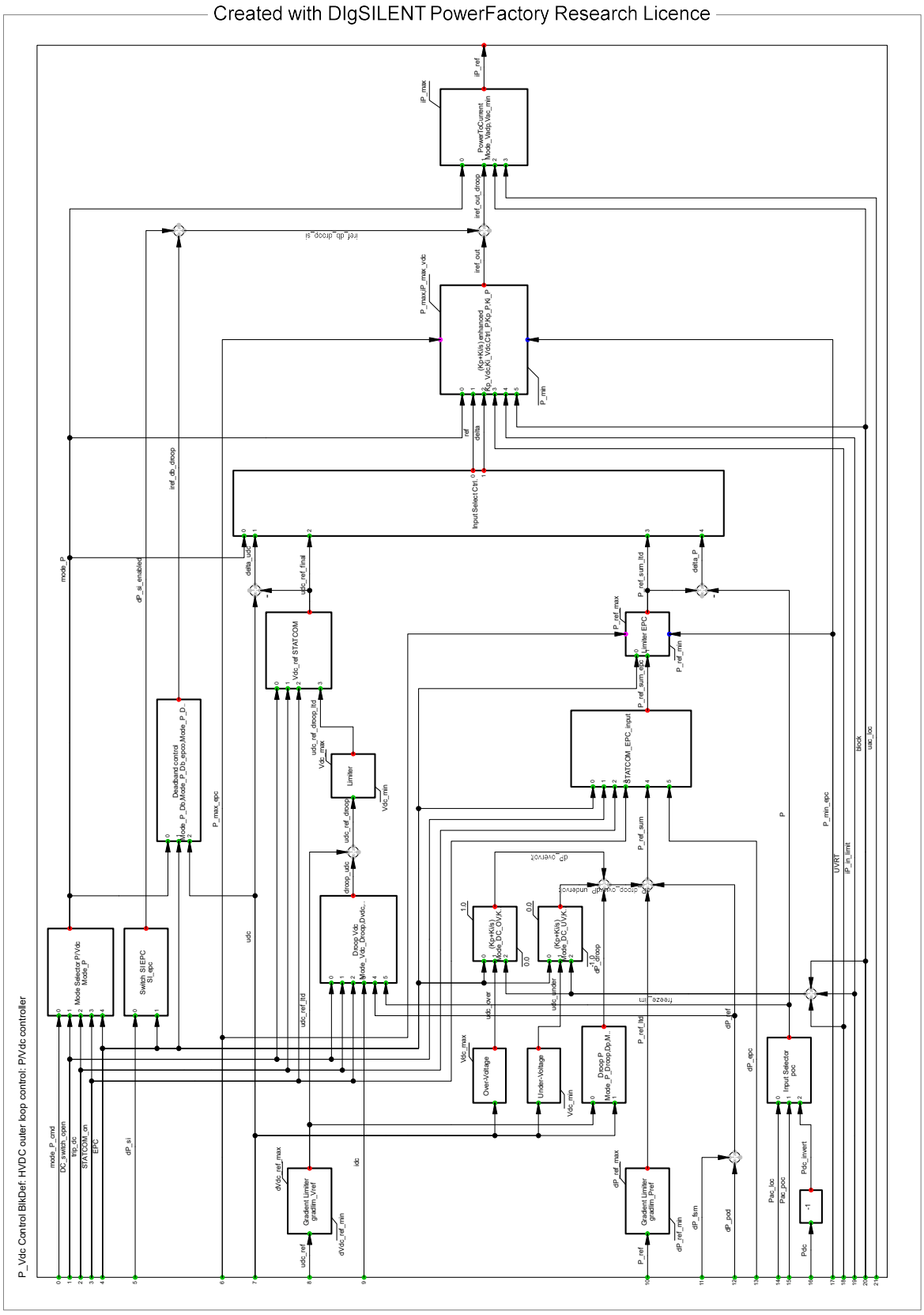

Figure B.11: Common model P/Vdc Control

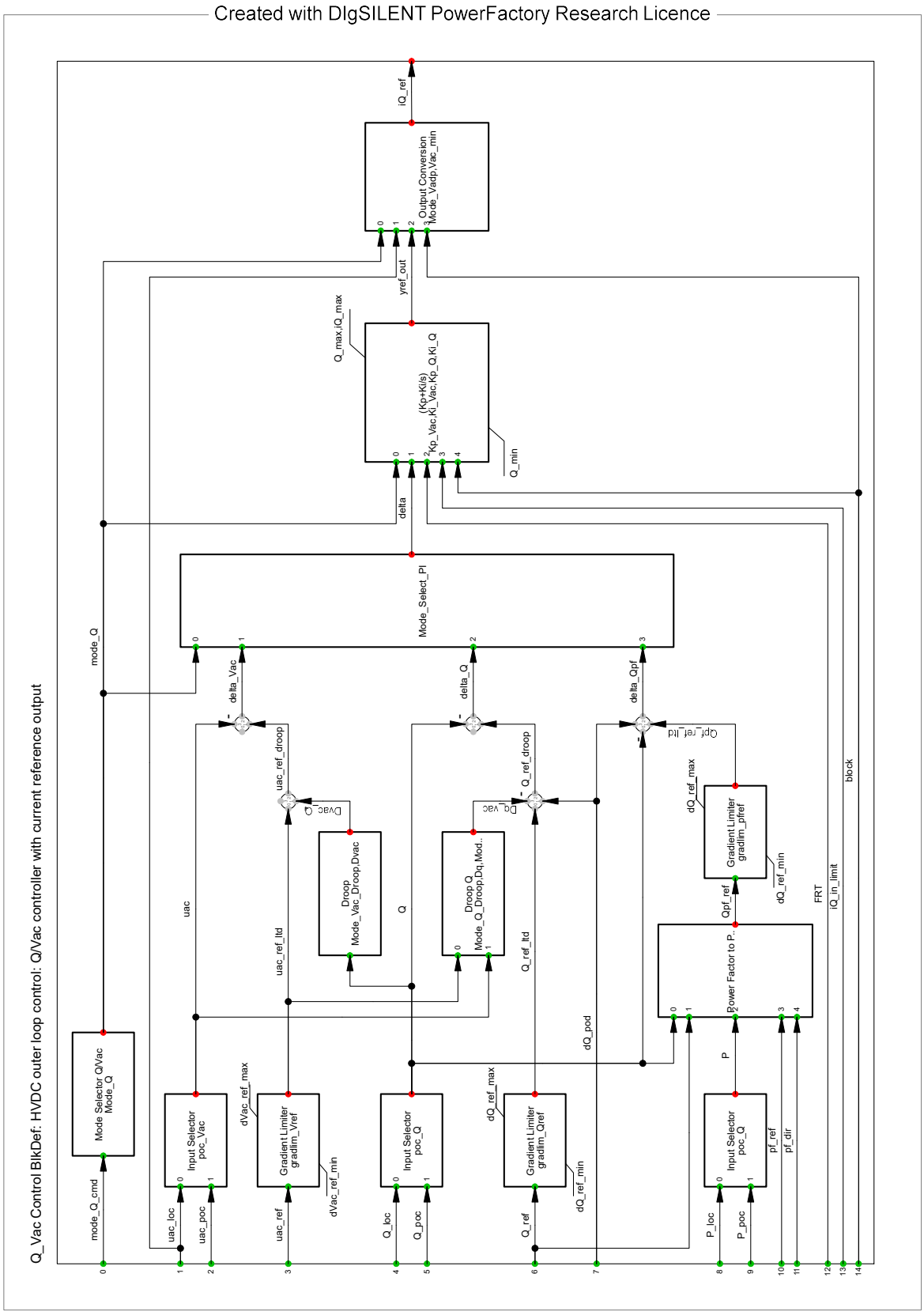

Figure B.12: Common model Q/Vac Control

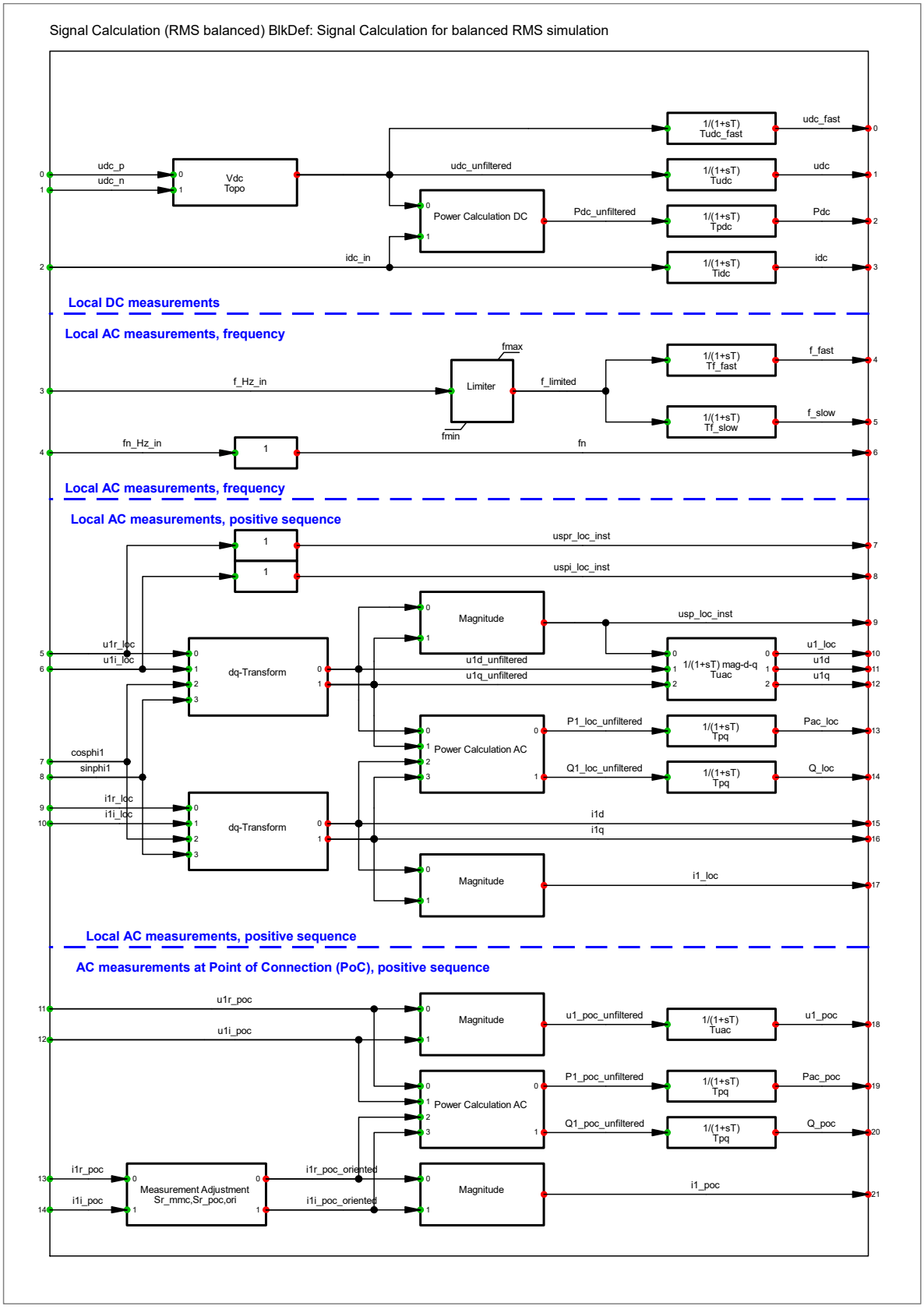

Figure B.13: Common model Signal Calculation

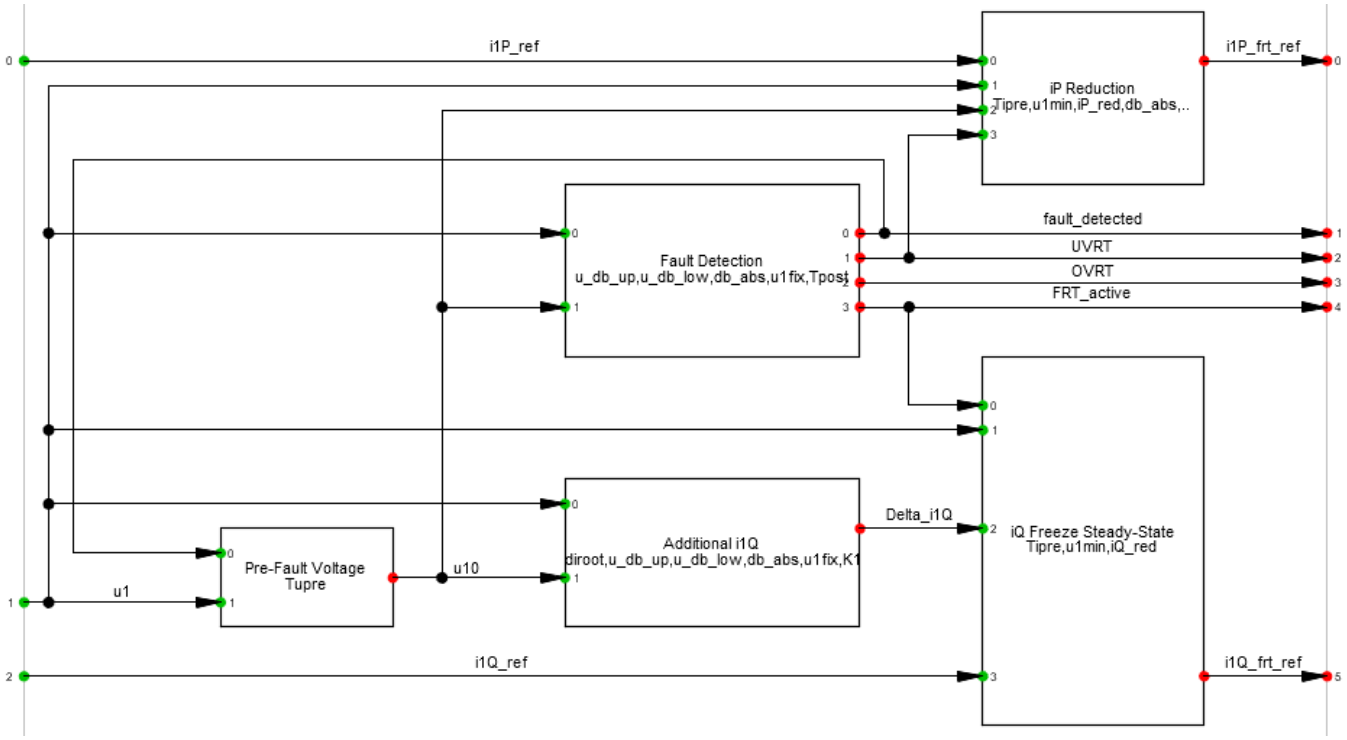

Figure B.14: Common model Fault Ride Through

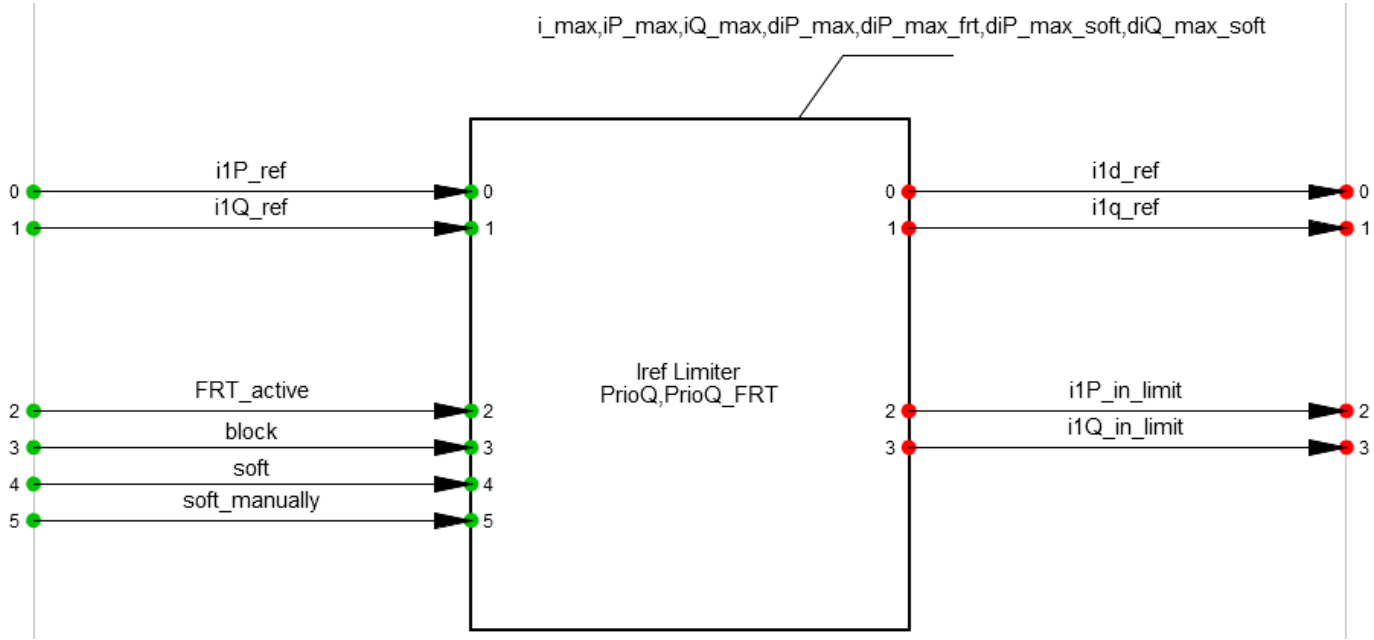

Figure B.15: Common model Current Limiter

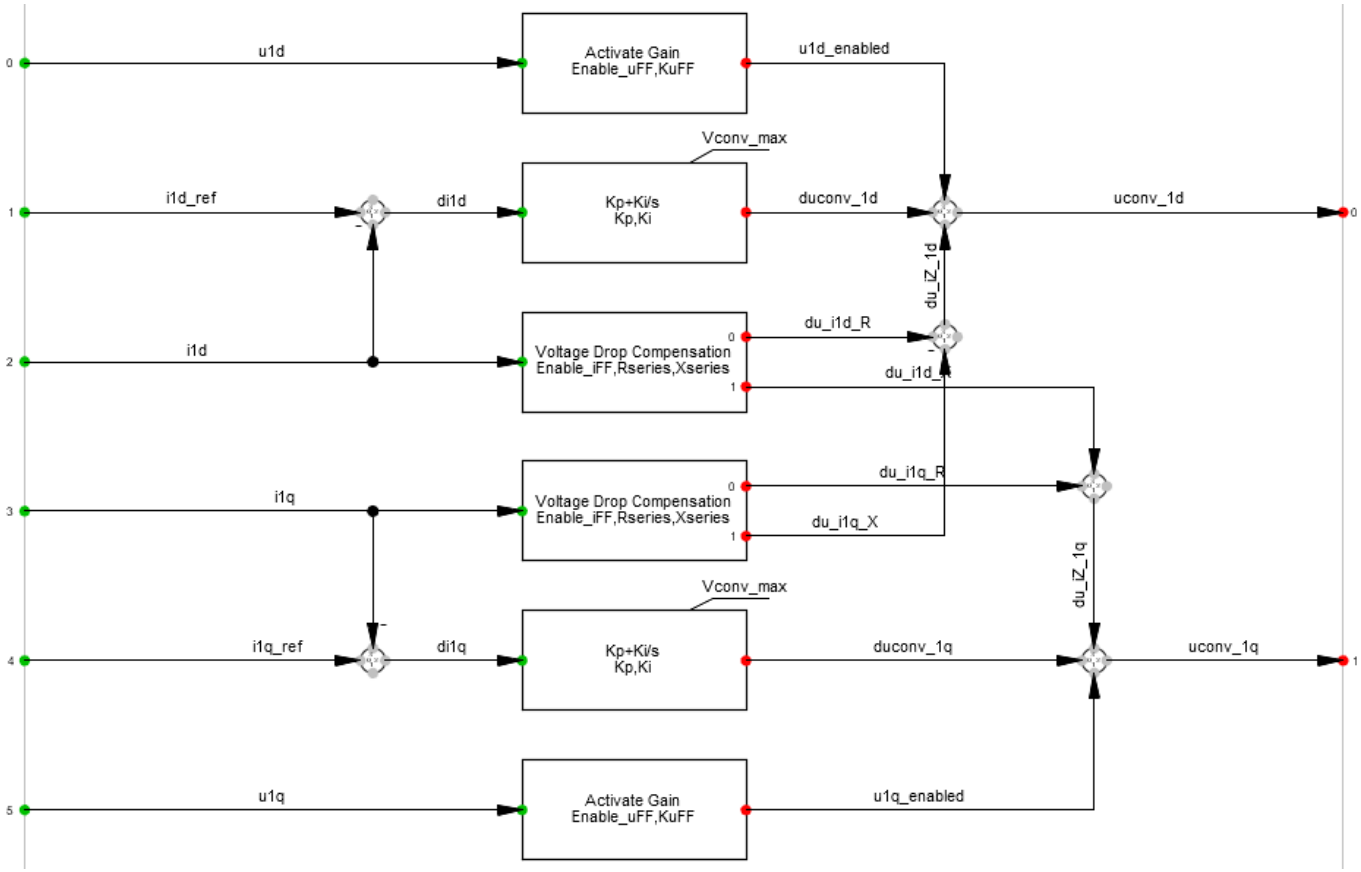

Figure B.16: Common model Current Controller

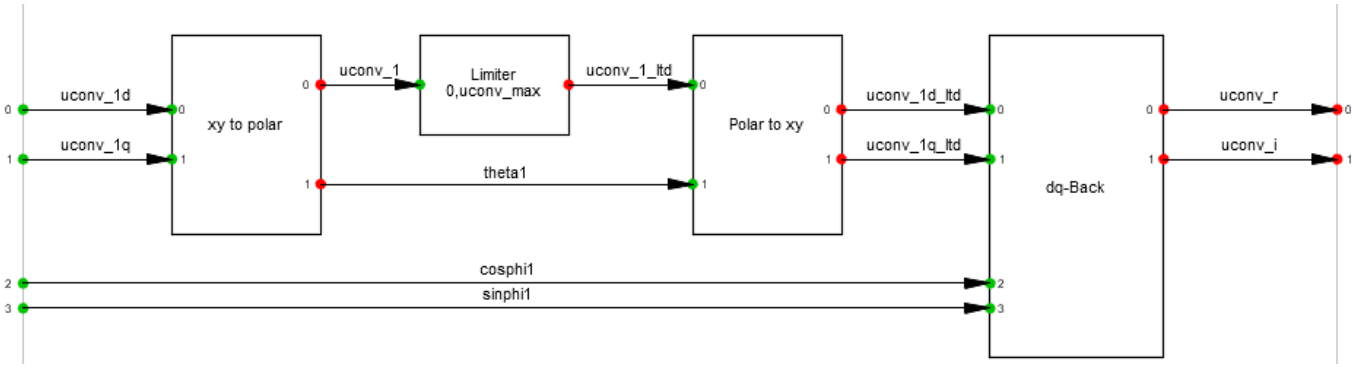

Figure B.17: Common model Output Limiter

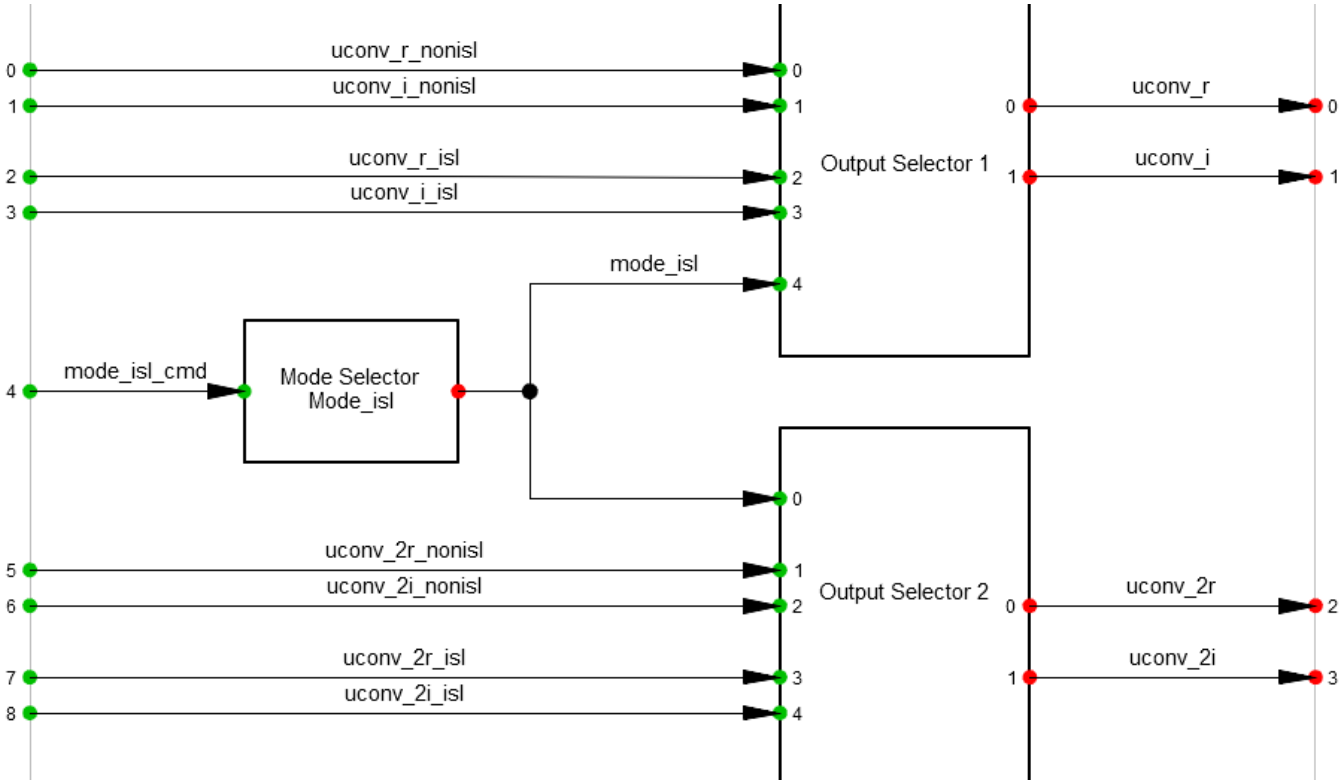

Figure B.18: Common model Operating Mode Selector

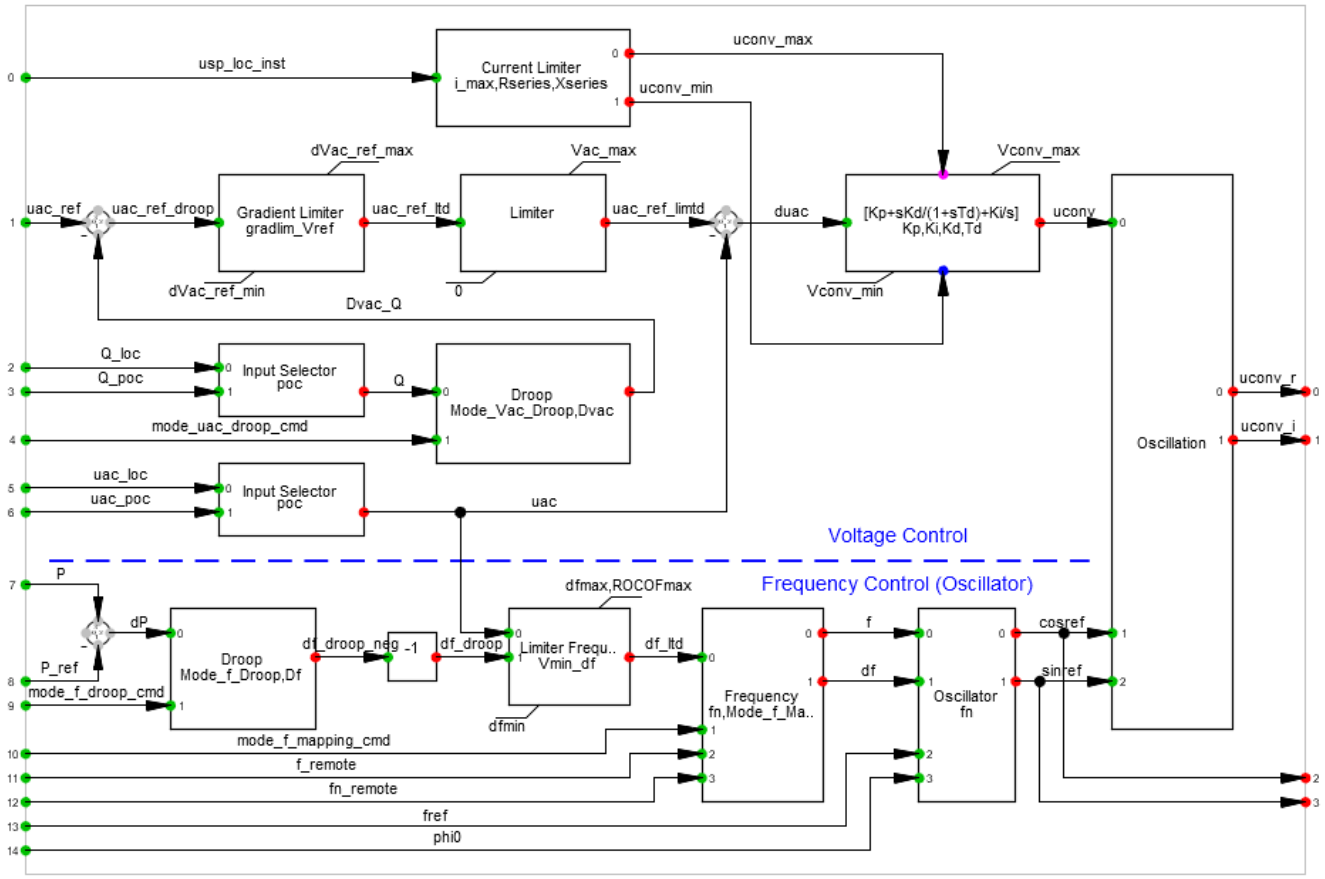

Figure B.19: Common model Island V/f

Delft
University of
Technology

P.O. Box 5031
2600 GA Delft
Tlf. 4525 1700